Single Droplet Microrheology

Victoria C. Harrold

Abstract

The vibration of microlitre sized drops in partial contact with a substrate was used to extract the rheological properties of multicomponent fluids. Sessile and pendant drop vibration was triggered using a short mechanical impulse. Sessile drops were supported on superhydrophobic surfaces and their vibration monitored using laser light, refracted through the drops and focussed on the sensor of a photodiode. Pendant drops were suspended from clean pipette tips and their vibration was recorded using a high speed camera. Time dependent photodiode intensity/centre of mass variations were Fourier transformed to extract the frequency and spectral widths of vibration.

The vibration of aqueous glycerol sessile drops was tracked in real time as the drops evaporated. The changing surface tension and viscosity were extracted using a simple model describing the vibration of a viscous sessile drop. The values of surface tension and viscosity obtained for initial bulk solutions were shown to be in good agreement with literature values, however evaporating drops showed signs of surface contamination after $\sim 300\,\mathrm{s}$.

The vibration of sessile drops of aqueous poly(acrylamide-co-acrylic acid) solutions was used to calculate the shear storage and loss moduli using a simple theoretical model. The resulting rheological properties were found to be in agreement with microrheology measurements of the same solutions. The model was also applied to pendant drops of aqueous poly(acrylamide-co-acrylic acid). The majority of the rheological data measured for the pendant drops agreed with microrheology and sessile drop data. Drop vibration therefore provides an accurate method of quantifying the rheological properties of single drops in short time.

Acknowledgements

My supervisor James Sharp for scientific collaboration and moral support throughout the years.

Financial support from a LeverHulme Trust Research Project Grant (RPG-2012-702, JSS) and an ERC Advanced Grant (340391-SUPRO, MP) for funding the research and my education.

Maxime Paven and Doris Vollmer (from the Max Planck Institute for Polymer Research) for providing superhydrophobic silinated candlesoot surfaces.

Daniel Wesley (from the University of Sheffield) for providing thiol treated surfaces.

Mike Smith for the access to and training for use of the Rheometer, as well as moral support.

Paul Cooling and Boots pharmacy (science building) for access to and training for use of their facilities, including the Zetasizer for microrheology and the new refractometer.

Staff at the University of Nottingham and the NHS for everything they have done to support me throughout my studies.

Contents

CHAPTER 1

Motivation

Understanding how the resonant frequency and oscillation amplitude of capillary waves influence droplet atomisation [1, 2] provides insight into fuel injection [3], spray cooling and coating [4], and nebulization [5]. Drop vibration has also been used in the mixing and demixing of fluids [6, 7], the understanding and manipulation of drop motion (or ratcheting) on surfaces via the overcoming of surface pinning and contact angle hysteresis [8–12], and as a tool for measuring the frequency dependent rheological properties of simple and viscoelastic liquids [13–16].

Conventional techniques for measuring the rheological properties of liquids are often restricted to measuring only one property at a time (e.g. viscosity or surface tension for simple liquids), and require millilitre volumes to be available [16–20]. The vibrated drop method of rheology can quickly and simultaneously measure the mechanical properties of small volumes of fluid ($< 50\,\mu L$) [16]. Levitated viscous [21–24] and viscoelastic drops [15, 25] have been used for drop vibration rheometry, however these are expensive and difficult to set up.

More accessible geometries include substrate supported (sessile) [16, 26–31] and suspended (pendant) [14, 32–34] drops. The rheological properties have been extracted from sessile drops placed on superhydrophobic substrates [16, 30, 35] and pendant drops suspended from pipette tips [32].

Droplet vibration rheometry has the potential to be applied to the analysis of fluids whose composition changes over time, tracking the surface tension, viscosity and viscoelastic properties of droplets with little external influence on

the liquid. As such, the technique has a future in forensic and medical analyses, for example, measuring the coagulation rate of a small sample of blood or the measurement of time dependent changes in the rheological properties of aggregating protein solutions. This work aims to validate this technique as a means of tracking material properties of soft systems in real time. The vibrational behaviour of aqueous glycerol drops was tracked as the evaporating solvent caused the composition (and rheological properties) of the drops to change.

Very few papers have been published discussing the extraction of the rheological properties of viscoelastic drops via the drop vibration technique [15, 33, 34]. The study of vibrating viscoelastic drops can provide further insight into the dynamics of atomic nuclear vibrations [36], crustal deformation of planets [37, 38], and energy relaxation mechanisms in neutron stars [39]. This work aims to show that the drop vibration technique may be applied to extracting the rheological properties from viscoelastic sessile drops on superhydrophobic substrates, as well as from small ($<30\,\mu L$) viscoelastic pendant drops.

CHAPTER 2

Introduction

Rayleigh [40] developed equations to describe the vibration of simple liquid drops as they are ejected from orifices of various shapes. Equation 2.0.1 describes the vibration of drops ejected into a vacuum from a circular orifice,

$$f^2 = \frac{(n^3 - n)\gamma}{4\pi^2 \rho R^3}, \tag{2.0.1}$$

with frequency of vibration f (Hz), resonance mode number n, surface tension γ, density ρ, and drop radius R.

Later, Lamb [41] produced a similar equation (Equation 2.0.2) to describe the capillary vibration of a small fluid drop submerged in an immiscible fluid (such as a water drop in air) in response to a small perturbation:

$$f^2 = \frac{n(n-1)(n+1)\gamma}{3\pi\rho V}, \tag{2.0.2}$$

with droplet volume $V = \frac{4}{3}\pi R^3$. In this equation the density of the surrounding fluid is assumed to be much less than the density of the drop.

Chandrasekhar [42] and Lamb [43] expanded on this to produce equations describing the damping of a spherical drop with arbitrary viscosity (Equation 2.0.3):

$$\Delta f \sim \frac{\eta}{\rho R^2}\,, \tag{2.0.3}$$

where $\Delta f = \frac{1}{\tau}$ is a coefficient of decay (or the width of the vibrational mechanical resonance peak at half height) in the frequency domain, τ is the time constant of decay, i.e. the time for the vibration amplitude to fall to 1/e of the original amplitude (see Figure 2.1), and η is the fluid viscosity.

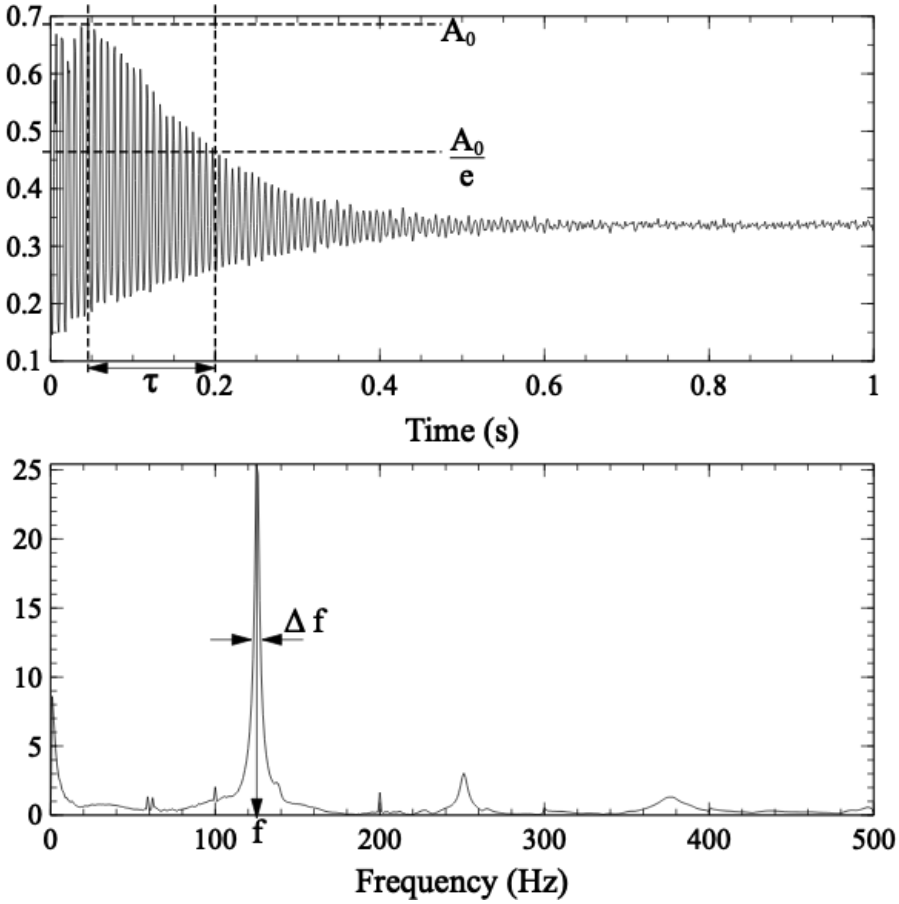

Figure 2.1: The top panel shows the vibration spectrum of a sessile water drop with amplitude A_0 at initial time τ_0 and amplitude $\frac{A_0}{e}$ after decay time τ. The bottom panel shows the corresponding Fourier transform, defining the frequency of vibration as f (position of the peak maximum) with the coefficient of decay in the frequency domain, $\Delta f = \frac{1}{\tau}$, as the width of resonant peaks at half height (full width at half maximum).

In experiments on the applicability of vibrating drops to containerless crystallisation in microgravity, the Rayleigh and Lamb equations have been used to calculate the vibration frequency and damping of simple [22, 23, 44] and viscous [21, 45] levitated drops. Rearranging these equations has allowed researchers to extract the surface tension [46] and viscosity [21] from vibrated levitating drops. The use of drop vibration to measure the surface tension and viscosity of a fluid is not only fast when compared to other methods, such as the drop volume technique [17], but allows the use of significantly smaller volumes of material. Levitated drops do, however, require expensive and complicated equipment. In order to suspend a droplet as if in space the effects of gravity must be mitigated. This is usually done with the use of electrostatic repulsion [47], magnetic levitation of diamagnetic fluids [15], and acoustic levitation [44].

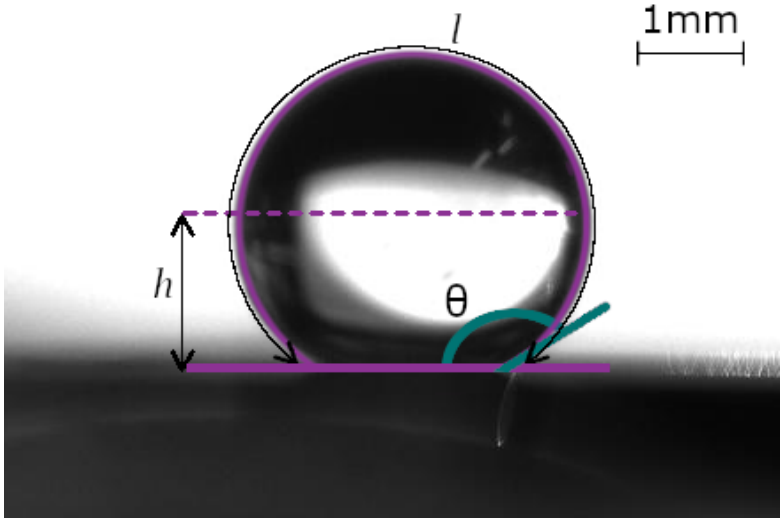

Figure 2.2: A sessile drop of high contact angle θ (defined as the three phase contact angle between the sessile drop and the surface it is resting on) with profile length l. The average height h of the drop, defined by Equation 2.0.6, is (in this case) a little over half the apex height of the drop.

Sessile drops and pendant drops are an attractive alternative. For drops with radius smaller than the capillary length $l_c = \sqrt{\frac{\gamma}{\rho g_{eff}}}$ (where g_{eff} is the effective gravity acting on the drop), surface tension forces dominate and the effects of gravity become negligible. Such small drops have been placed on superhydrophobic surfaces (with contact angle close to 180°, Figure 2.2) in order to

closely mimic the shape of a levitating drop [35], however the vibrational behaviour of the drops has been shown to be impacted by the presence of a substrate [16, 26, 30, 48].

Strani *et. al.* [26] performed a mathematical analysis for the vibration of a simple drop in partial contact with a substrate, representing a bed for crystal growth. They found an additional low frequency mode (when compared to levitated drop modes), which corresponds to centre of mass (CoM) motion from contact-line depinning and drop motion across a substrate (Figure 2.3a) or from fluid compressibility allowing the drop to expand and contract during oscillation 2.3b.

Lyubimov *et. al.* [49] described the vibration behaviour of an ideal hemispherical sessile drop with pinned contact line (see Figure 2.3) using Equation 2.0.4,

$$f^2 = \frac{\gamma \tilde{\omega}_n^2}{6\pi m}\,, \tag{2.0.4}$$

with droplet mass $m = \rho V$, and $\tilde{\omega}_n$ being the roots of

$$F(\tilde{\omega}_n) = \sum_{n=1}^{\infty} \left(\frac{n(4n+1)}{\tilde{\omega}_n^2 - 4n(2n-1)(n+1)} \right) \left(\frac{(2n-1)!!}{2^n n!} \right)^2 = 0.$$

Whilst this equation is very accurate for sessile drops with contact angles lower than 90°, it is not reliable for hydrophobic surfaces [50].

For contact angles > 90°, Mettu *et. al.* [50] found an equation from Noblin to be more accurate. Noblin [51, 52] suggested that the vibration of a small liquid drop (with pinned contact line) at resonance must have a half integer number of wavelengths around the surface of the drop (Figure 2.3), i.e. $n = \frac{2l}{\lambda}$ (profile length l, wavelength λ). To simplify the complex three-dimensional system of waves on a curved surface, Noblin considered the surface vibrations on sessile drops in the form of one dimensional capillary-gravity waves on a bath of

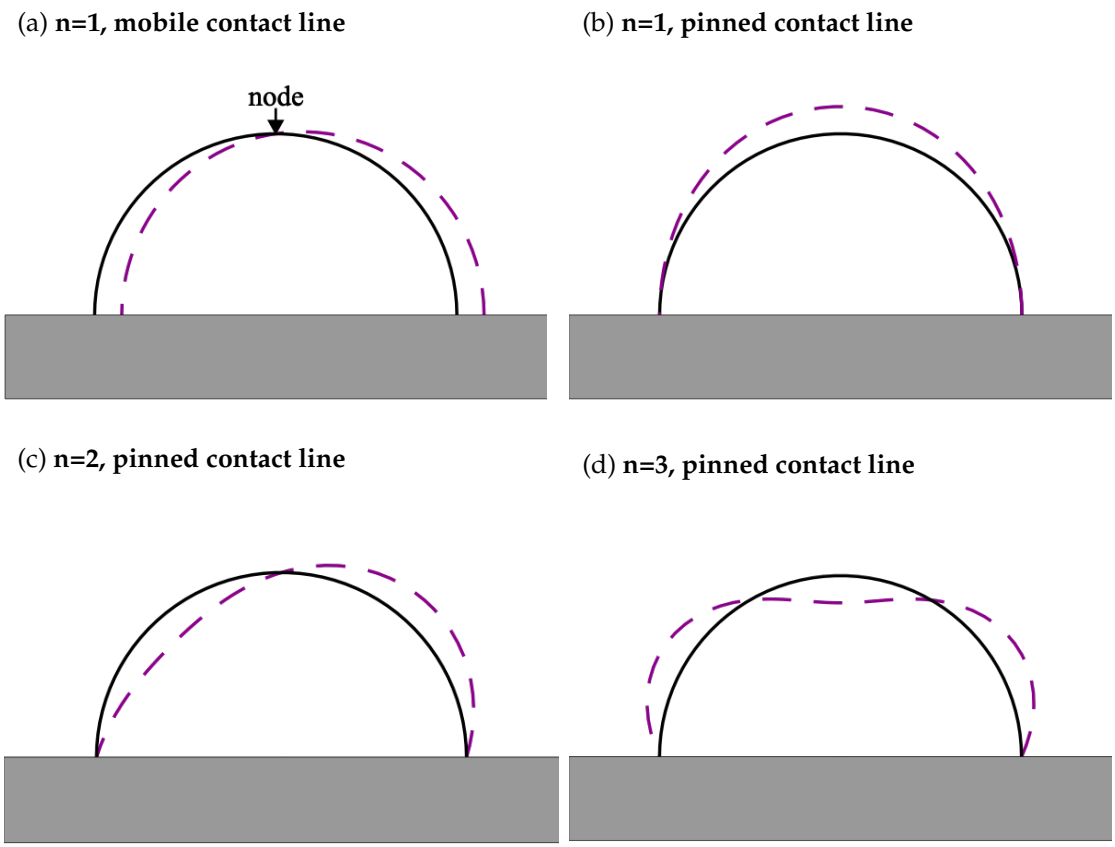

Figure 2.3: Diagrams of vibrating sessile drops with a half integer number of wavelengths around the profile. The panels show the n = 1 (mobile and pinned contact line, top left and top right), 2 (pinned contact line, bottom left), and 3 (pinned contact line, bottom right) modes of oscillation. The oscillation amplitude is 15% of the drop radius.

For the depinned sessile drop in the n=1 mode, the single node occurs at the top of the drop, with antinodes occurring at the mobile contact line between the drop and the surface. The pinned drop in the n=1 mode expands and contracts during oscillation. The n=1 mode demonstrates a moving centre of mass in both situations. The later modes (n = 2 and 3) involve fluid shifting around the drop so that volume is preserved during vibration and the centre of mass remains stationary.

height h. Noblin derived Equation 2.0.5 to describe the frequency of vibration for an ideal sessile drop, with negligible influence from gravity:

$$f^2 = \frac{n^3 \pi \gamma}{4\rho l^3} \tanh\left(\frac{n\pi h}{l}\right), \tag{2.0.5}$$

where h is the average height of the drop at equilibrium, defined by Equation 2.0.6 (Figure 2.2). The average height can be calculated using a weighted average of the heights for all points within the drop.

A contact angle dependent variation of the Noblin equation (Equation 2.0.5) was developed by Sharp *et. al.* [30], who derived an equation for calculating the average height (Figure 2.2) of a pinned sessile drop with radius of curvature R_c and three phase contact angle θ:

$$h = R_c\left(\frac{\sin\theta}{\theta} - \cos\theta\right), \tag{2.0.6}$$

for which $R_c = \frac{l}{2\theta} = \frac{n\lambda}{4\theta}$. For a spherical drop ($\theta = 180°$) the average height would be equal to the drop radius.

The presence of a substrate influences the damping forces acting on a vibrating drop in addition to viscous dissipation effects. Sharp [16] compared the damping of vibration in pinned sessile drops of glycerol in water to theories of energy dissipation resulting from substrate effects [53], surface contamination effects [54, 55] and bulk viscous effects [1, 56, 57]. They found that (over timescales of $\sim$3s) the majority of damping within the vibration of a viscous sessile drop could be described most accurately by bulk damping equations (Δf_{bulk}, Equation 2.0.7), with substrate (boundary layer) damping (Δf_{wall}, Equation 2.0.8) having an increasing influence for contact angles less than $\sim$71°.

$$\Delta f_{bulk} = \frac{2\eta\pi^2 n^2}{\rho l^2}, \tag{2.0.7}$$

$$\Delta f_{wall} = \frac{2}{l}\left(\frac{\pi f \eta}{\rho}\right)^{1/2}. \tag{2.0.8}$$

For drops smaller than the capillary length, the already derived sessile drop equations can be applied to the pendant drop geometry [58]. Temperton *et. al.* [32] applied the Noblin equation (Equation 2.0.5) for the vibrational frequency of a sessile drop and a bulk viscous dissipation coefficient from Landau *et. al.* [56] to the vibration of viscous pendant drops smaller than the capillary length. Using these equations, they were able to calculate surface tension and viscosity values in agreement with literature values.

The vibrational and rheological properties of viscoelastic droplets are also of interest in the study of polymer, biopolymer and protein solutions. Akimoto *et. al.* [59] used an analytical method to calculate the viscosity of levitated viscoelastic drops. The rheological properties of viscoelastic fluids are, however, better described using the frequency dependent shear storage and loss moduli (G' and G'' respectively). Khismatullin *et. al.* [24], investigated the frequency and damping of viscoelastic drop vibration and found both to be influenced by the presence of elasticity. Measurements of the frequency and damping of drop vibration are therefore capable of providing information about G' and G'' for viscoelastic solutions. Temperton *et. al.* [15] used a dispersion relation for surface capillary waves on a semi-infinite viscoelastic medium, derived by Pleiner *et. al.* [60], to describe small amplitude vibration of viscoelastic levitated drops (Equation 2.0.9):

$$4\pi^2\rho(f+i\Delta f)^2 = \frac{4i(f+i\Delta f)(G''(f)-iG'(f))k^2}{f} + \gamma k^3, \tag{2.0.9}$$

with surface wavevector magnitude $k = \frac{2\pi}{\lambda}$.

For vibrating levitating drops, waves are continuous around the surface and an integer number of vibrational wavelengths must fit around the circumference, i.e. $n\lambda = 2\pi R$, where R is the drop radius [15]. Inserting this result into Equation 2.0.9, Temperton *et. al.* [15] derived expressions to extract the frequency dependent shear storage and loss moduli (Equations 2.0.10 and 2.0.11) from vibrating levitated drops:

$$G'(f) = \frac{\pi^2\rho f^2 R^2}{n^2}\left(1 - \frac{\gamma n^3}{4\pi^2\rho R^3(\Delta f^2 + f^2)}\right), \tag{2.0.10}$$

$$G''(f) = \frac{\pi^2 \rho f \Delta f R^2}{n^2} \left(1 + \frac{\gamma n^3}{4\pi^2 \rho R^3 (\Delta f^2 + f^2)}\right). \tag{2.0.11}$$

By varying the size (and hence the resonant frequency, Equation 2.0.1) of vibrated drops, G′ and G″ can be measured at multiple frequencies. Temperton *et. al.* [15] showed that when setting G′=0 in Equation 2.0.10 (simulating purely viscous drops), the corresponding frequency and width equations are consistent with derivations made using the techniques described above [16, 40–42, 51]. In order to simulate purely elastic spheres, Temperton *et. al.* [15] set G″=0 in Equation 2.0.11 and assumed that the effects of surface tension on sphere vibration would be negligible, deriving an estimate for the speed of sound within the sphere that was within a factor of two of the speed of sound through an elastic medium.

Whilst, to our knowledge, no theory exists to accurately describe viscoelastic drops in contact with a substrate, the approximations used to relate near spherical viscous sessile drops to viscous levitated drops can be repeated for viscoelastic drops with small solid-liquid contact area, i.e. sessile or pendant drops. Equations for the shear storage and loss moduli of sessile/pendant drops may be approximated by substituting the relation $k = \frac{2\pi}{\lambda} = \frac{n\pi}{l}$ (from Noblin's sessile drop condition $\lambda = \frac{2l}{n}$) into Equation 2.0.9. These equations do not have a factor accounting for boundary layer damping, however should be a good approximation for sessile drops with high contact angle or for pendant drops, as seen with simple liquids [16, 32].

2.1 Thesis structure

This thesis will first describe the experimental techniques used over the course of this research (Chapter 3). The following chapter (Chapter 4) explores the application of sessile drop vibration on a superhydrophobic substrate to monitoring the surface tension and viscosity of a multicomponent viscous droplet as the composition of the drop changes in real time. Chapter 5 aims to show that the drop vibration technique may be applied to the extraction of the rheological properties from viscoelastic sessile drops on superhydrophobic substrates. The technique is then applied to the rheometry of viscoelastic pendant drops

in Chapter 6, and differences between pendant and sessile drop vibration are discussed. A summary of findings is presented in Chapter 7. Finally, Chapter 8 suggests areas of research that might be explored in the future.

CHAPTER 3

Experimental techniques

3.1 Solution preparation

Solutions were prepared by weight using an analytical balance with draft shield (Ohause Pioneer PX, 0.0001 g precision) and stored at room temperature in glass sample vials wrapped in Parafilm®. Glycerol (ReagentPlus® $\geq$ 99.0%, Sigma, UK) was mixed with deionised water (from an ELGA water purification system) to obtain solutions with concentrations of 1, 5, 25 and 50 wt% glycerol in water with a relative error of 0.02. Poly (acrylamide-co-acrylic acid) powder (PAA, M_w = 5 MDa, Sigma, UK) was dissolved in deionised water and made up to concentrations of 1.1, 2 and 3 wt% PAA in water with a relative error of 0.035. The overlap concentration for this polymer [61] is $\sim$ 0.1 wt% and as such all of the PAA solutions studied contain overlapping chains.

3.1.1 Evaporation rate of glycerol and water

The evaporation rate from a small orifice is given by

$$r = 3.45p\sqrt{\frac{M_w}{T}}\ \mathrm{g\,min^{-1}cm^{-2}}, \tag{3.1.1}$$

where r is the rate of evaporation per unit area, p is the vapour pressure at temperature T (Kelvin) in mmHg, and M_w is the molecular weight relative to hydrogen [62].

In the glycerol-water system, at T = 293 K:

$p = 0.14\,\text{mmHg}$ at 18°C for pure glycerol and $M_w = 92$ [62] so

$$r = 3.45 * 0.14\sqrt{\frac{92}{193}} = 0.3335\ \text{g}\,\text{min}^{-1}\text{cm}^{-2}. \tag{3.1.2}$$

For water $p = 2.3392\,\text{kPa}$ [63] = 17.55 mmHg, $M_w = 18$, so

$$r = 3.45 * 17.55\sqrt{\frac{18}{193}} = 18.4907\ \text{g}\,\text{min}^{-1}\text{cm}^{-2}. \tag{3.1.3}$$

For short (1 s) experiments, only 0.3 g of water would be expected to evaporate from a $1\,\text{cm}^2$ surface.

3.2 Surface preparation

The surface on which a sessile drop rests influences the three phase contact angle (θ, defined by Figure 2.2) and hence the vibrational properties of a sessile drop. Changing the contact angle affects the solid-liquid contact area of drops of a fixed volume, influencing the surface/frictional damping forces acting on the drop vibration.

3.2.1 Glass substrates

Glass slides (Thermo Scientific Menzel Gläser, 76 x 26 mm, 1 mm thick) were sonicated (using a Langford Sonomatic 375 from Agar scientific) in toluene, rinsed in deionised water, and dried using a nitrogen air gun. The glass was then scribed using a glass cutter (Kennedy 130 mm glass and tile cutter, Tungsten Carbide) and split into ~ 20 mm squares. The slides were placed on fresh lens tissues between scribing and splitting to reduce the risk of surface contamination. Dust left on the surfaces by the scribing technique could be removed using a nitrogen air gun and slides stored in slide boxes until used to create superhydrophobic surfaces.

3.2.2 Candlesoot surfaces

Fluorinated candlesoot surfaces were received from Maxime Paven (Max Planck Institute for Polymer Research), having been prepared on glass surfaces in a similar way to that described by Deng *et. al.* [64, 65]. Candlesoot surfaces can be produced by holding a glass slide over a lighted (paraffin) candle flame. Holding a glass slide in the yellow region of the flame ensures an even and well 'bonded' layer of soot is formed. The soot produced is superhydrophobic ($\theta > 160°$, see Section 3.3) but mechanically unstable so it is combined with silica to stabilise the surface [64].

The candlesoot coated slides were placed in a vacuum jar (previously filled with nitrogen to evacuate airborne impurities) with open dishes of 2 mL tetraethoxysilane (TEOS, Sigma-Aldrich, 98%) and the catalyst, 2 mL ammonium hydroxide (VWR, 28%) [64]. The vacuum is turned on briefly to mist the solutions in the dishes, after which it is turned off and vapour deposition occurs over 72 hours at room temperature.

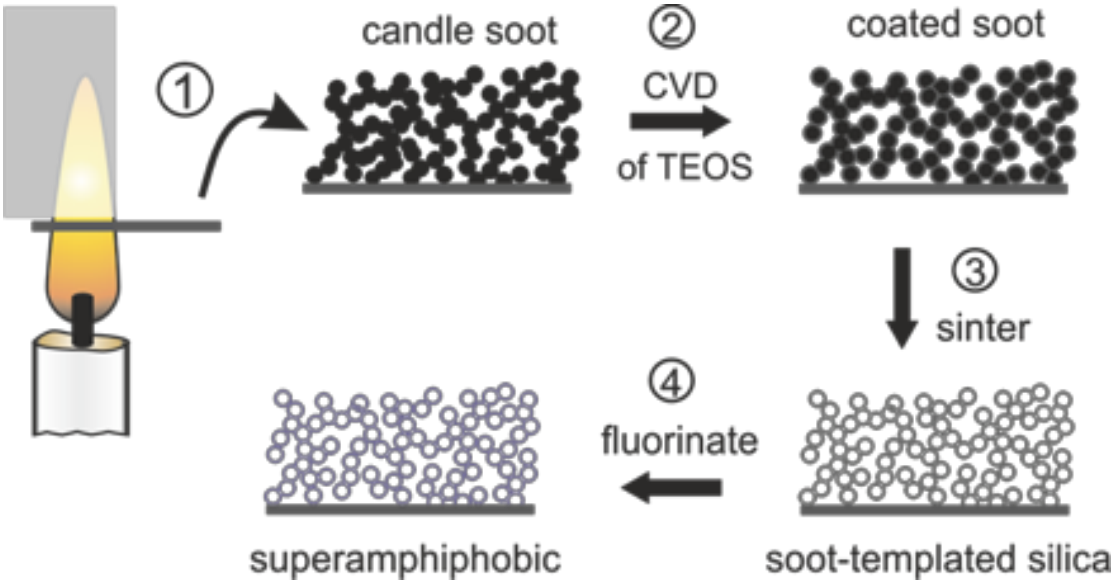

Figure 3.1: Schematic diagram illustrating the sample preparation procedure for superhydrophobic surfaces. (1) Candle soot is collected on a substrate by annealing glass in the flame of a paraffin candle. (2) Silica is deposited via chemical vapour deposition (CVD) of tetraethoxysilane (TEOS). (3) Sintering combusts the soot template leading to soot-templated silica surfaces. (4) Hydrophobization with a fluorosilane results in superhydrophobic surfaces.

After 24 hours, an even ($\sim 20 \pm 5$ nm thick [64]) shell of silane was formed over the candlesoot and did not significantly increase over longer periods of time. The resulting substrates were annealed at 1000°C in the centre of a tube furnace for 3 hours to calcinate the soot and form a fractal-like silica network on the surface (see Figures 3.1 and 3.2). The substrate was returned to a vacuum jar for further chemical vapour deposition of a semi-fluorinated silane, with an open beaker of 0.1 mL (tridecafluoro-1,1,2,2-tetrahydrooctyl)-1-trichlorosilane (Sigma, 97%) for 3 hours, at a pressure of 25 mbar and room temperature [64]. At the end of 3 hours the chamber was evacuated under vacuum for 1 hour to remove any unreacted silane. The resulting substrates had an advancing contact angle of $180 \pm 2°$, a receding angle of $166 \pm 2°$ and a roll-off angle of less than 2° for water [65].

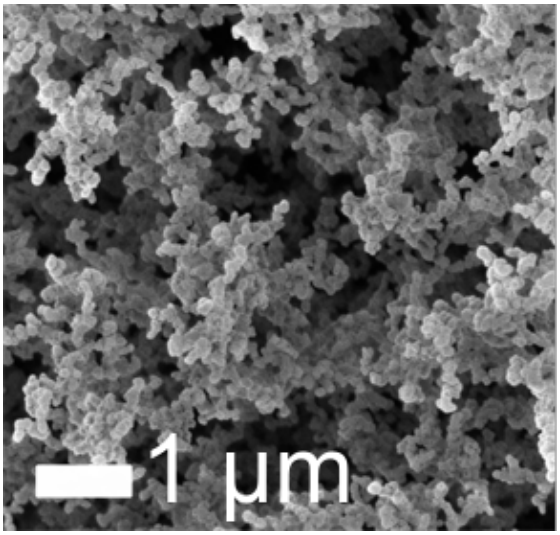

Figure 3.2: A scanning electron microscope image of the surface of a superhydrophobic substrate.

3.3 Vibration of sessile drops

For small (smaller than the capillary length, Chapter 2) drops placed on superhydrophobic surfaces (Section 3.2), with a three phase contact angle of $\sim 180°$ (Figure 2.2), their shape, and therefore behaviour, can be approximated to that of a spherical drop with a small deviation resulting from the presence of a surface [35] and they remain approximately spherical during free vibration. If the drop dimensions are larger than the capillary length, gravitational force

has a significant effect on the drop shape and vertical vibration would become antisymmetric as additional forces act on the drop's downward motion [66].

Although a driving force (or mechanical impulse) may be applied vertically or horizontally, horizontal vibration increases the chance of the drop overcoming contact angle hysteresis and slipping across the surface [9, 66]. This makes its vibration harder to monitor as the drop position changes relative to the camera or laser (Sections 3.6 and 3.7), and changes the dynamics of the oscillating system [16, 30, 32, 48, 65] (see also Section 3.9). The triple phase contact angle is no longer steady around the drop contact line [67], and the frictional forces influencing vibration damping are increased under horizontal vibration. For the purpose of contact angle and stationary contact line analysis (see Section 3.5), it is easiest to work with a pinned drop under purely vertical vibration. Low amplitude vertical vibration allows a drop to remain pinned to the surface [67]. The fundamental frequency for such a drop can be described by the mode number n=2, provided it is incompressible [16, 30, 32, 48, 65] (see also Section 3.9).

Individual sessile droplets were carefully placed onto horizontal candlesoot substrates which had been affixed to an SF-9324 mechanical wavedriver (Pasco Scientific, see Figure 3.3b) using double sided tape. A short vertical mechanical impulse ($\sim 5\,\text{ms}$, $1\,\text{V}$ or $\sim 0.5\,\text{mm}$ amplitude, "top hat" square wave pulse) was applied from below using the wavedriver which was driven using a USB-6211 data acquisition card (National Instruments) via a custom built amplifier, connected to a computer running LabView Software (National Instruments). After this pulse was applied, mechanical vibration was observed on the surface of the drops. In these experiments, the small regions of contact between the droplets and the substrate were observed to remain pinned during drop vibration.

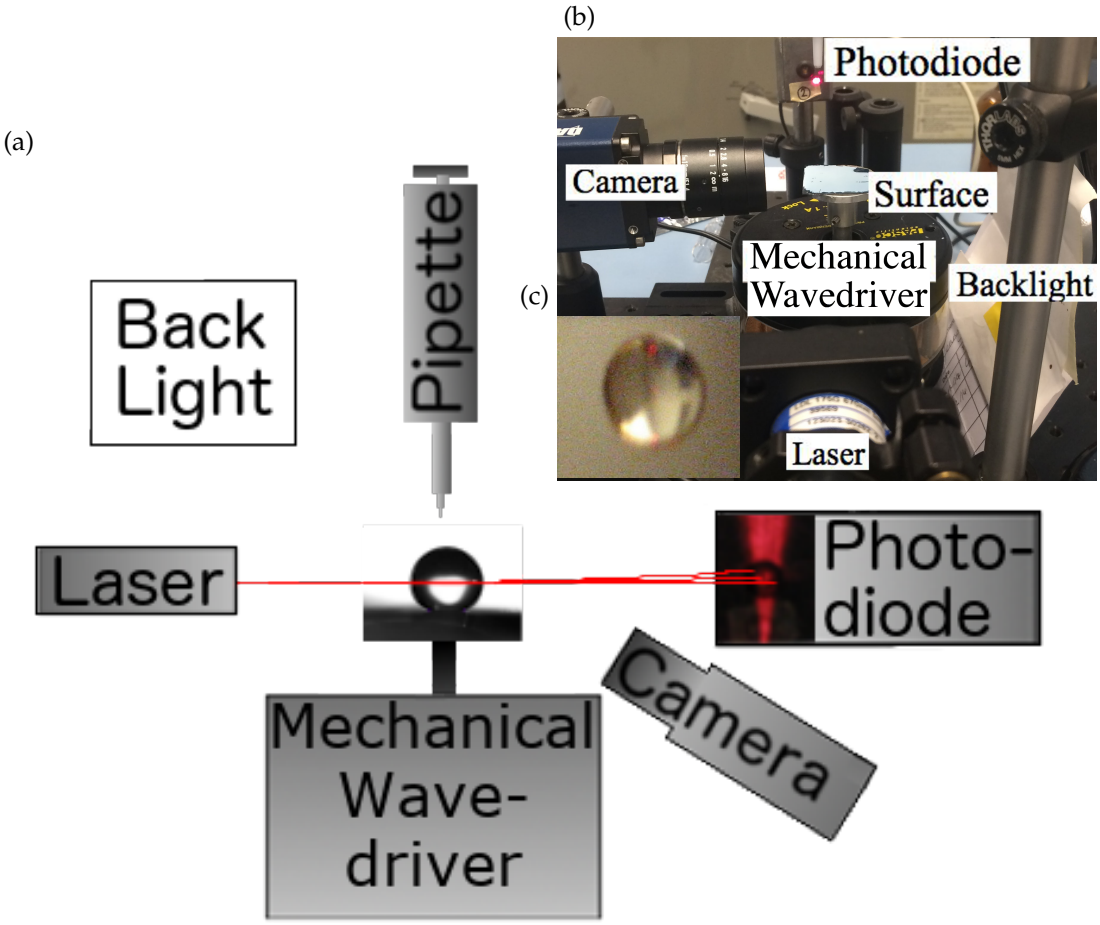

Figure 3.3: Panel (a) shows a diagram of the sessile drop laser optovibrometry setup. A drop rests on a surface on a mechanical wavedriver while a laser sends a beam through the drop and the refracted beam projects onto a photodiode on the opposite side. A camera is set up in front of the drop with a back light beyond. Above the drop a pipette tip is suspended for application of fresh drops. Superimposed on the diagram of the photodiode is a photograph of a fan refraction pattern projected onto the photodiode.

Panel (b) shows a labelled photograph of the same setup from a different angle. The surface is in the centre resting on the mechanical wavedriver, with the laser targeted towards the surface and a photodiode beyond. A camera and a back light are set up on opposite sides to one another across the surface. The inset (c) shows a photo of a sessile drop on a thiol surface from above. The refracted laser beam exits the drop at the top of the image.

3.4 Vibration of pendant drops

If a drop is smaller than the capillary length, the physical system can be considered to be the same whether the surface is above or below the drop (Chapter 2). The pendant drop system involves a similar setup to that of a sessile drop, but in this case a surface or pipette suspends the drop upside down [32, 68]. When a pipette is used, the "surface" on which a drop rests consists of a liquid or gaseous reservoir surrounded by a solid ring, i.e. the pipette tip (Figure 3.4). To minimise the physical impact of the reservoir on drop vibration during these experiments, it was required that the liquid reservoir within the (translucent) pipette tip be deeper than the height of the drops and as consistent in depth as possible between experiments [69].

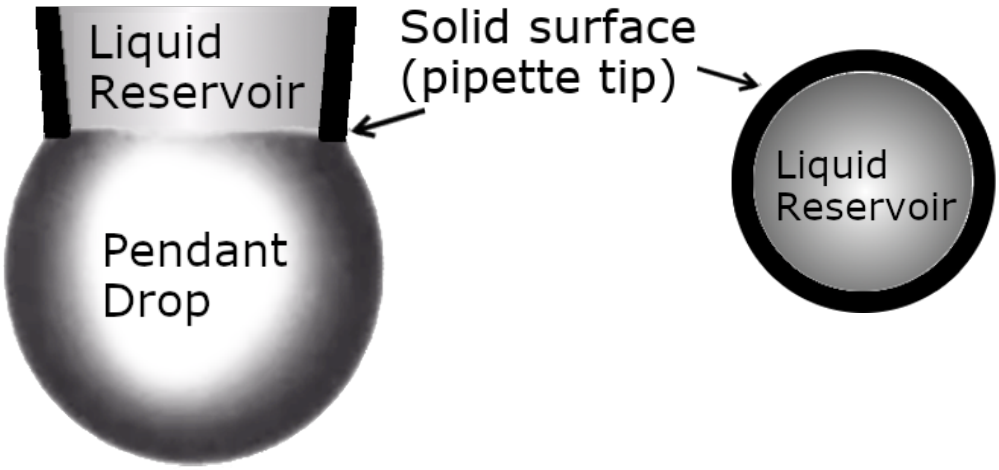

Figure 3.4: A diagram of a reservoir of liquid within a pipette tip from which is suspended a pendant drop. To the right of the image is a diagram of the "surface" from which a pendant drop hangs. The surface consists of a liquid reservoir surrounded by a solid ring formed by the pipette tip.

For the pendant drop experiments (Chapter 6) a retort stand was set up with a clamp to suspend a pipette (Gilson Pipetman, 2 - 20 µL) in front of a diffuse white light source. The pipette tip (Gilson D1000, 1000 µL) passed through a hole in a $\sim$ 1 cm diameter metal bar connected to a mechanical wavedriver (Pasco Scientific SF-9324), at a height that snugly fit the tip (Figure 3.5, 1 - 2 cm from the base of the pipette tip). This wider pipette tip was chosen to increase the maximum size of pendant drops on which the experiment could be carried out without the drops detaching or being drawn up the outer surface of the pipette tip [70, 71]. It was important for this that the tip be firmly attached to the

pipette with no leaks, otherwise the pressure within the tip could vary during experiments. Once a disposable tip had been attached to the pipette, the point of attachment between the tip and the pipette was surrounded by Parafilm® to improve the seal (inset in Figure 3.5). The tip was packed into the metal bar with blu tac to improve tip damping and reduce vertical motion while allowing drops suspended from the end to vibrate. A retort stand clamp was placed at the top of the pipette, and was gently tightened to prevent it from shifting, but kept loose enough to prevent the tip from detaching. A clean pipette tip and syringe were used for each concentration of solution.

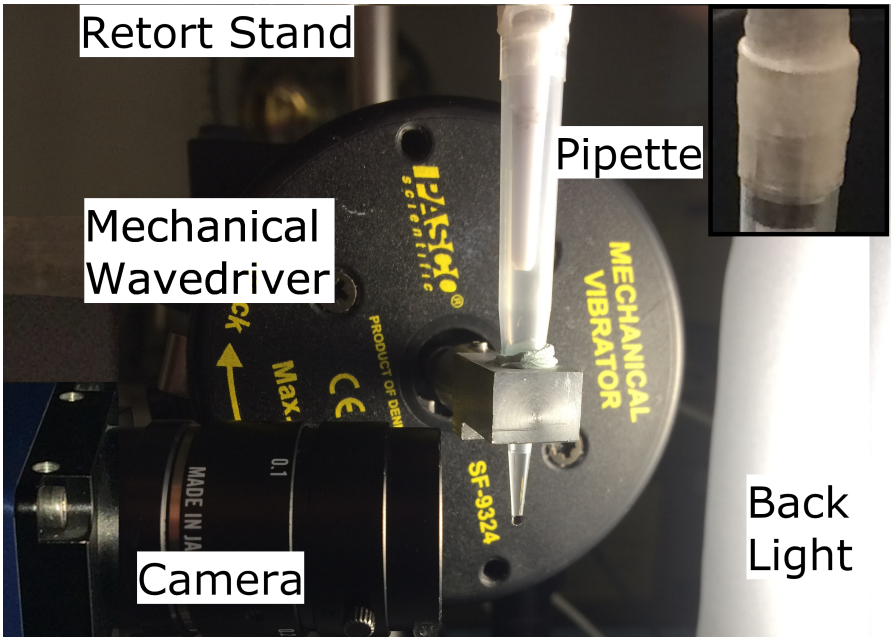

Figure 3.5: A photo of the pendant drop equipment setup. A pipette tip passes through a metal bar connected to a mechanical wavedriver and the end of the tip sits between a backlight and a camera. The inset shows a zoomed in image of the connection between the pipette and the tip, which has been sealed with Parafilm®.

Despite these precautions, drops with higher PAA concentrations had a tendency to be drawn up the inside of the pipette tip or to draw fluid from within the tip into themselves [69]. This resulted in rapidly changing drop sizes that could not be relied upon for accurate measurements. The pipette tip was therefore pre-filled with a 20 µL reservoir of solution (Figure 3.4) and drops were carefully added to the end of the pipette using a fresh syringe (2.5 mL Luer Slip, Terumo) with a needle (BD Microlance™ 3). If a drop was drawn up into the tip, more solution was added until an even pressure distribution between the

fluid within the pipette and the atmosphere outside the pipette was achieved and a consistent drop shape was reached [72]. It was only necessary to perform this initial stabilisation once for each experimental set, after which drops could be carefully removed using lens cleaning tissues (Whatman™) and new drops placed, ready to repeat the experiment. By this method, drops of 1.1%, 2% and 3% PAA in water, with profile lengths ranging from 2 mm to 11 mm were placed with minimal ($\sim$5% volume change) shrinking or growth over the timescales required for the experiments. Mechanical vibration was instigated via a short ($\sim$5 ms, 1 V or $\sim$0.5 mm amplitude top hat pulse) horizontal impulse (using the mechanical wavedriver setup described in Section 3.3) applied to the pipette tip, after which the droplets were observed to vibrate naturally at their resonant frequencies.

3.5 Drop shape parameters

For the droplets studied here, the profile length, l, could have been approximated to the circumference of the drop i.e. $l \sim 2\pi R_c$ (where R_c is the droplet radius of curvature). The analysis described in Section 3.9 could therefore be performed using R_c or the mass of the drop as the parameter which quantifies the size of the drop [16, 30, 32]. However, the profile length was chosen for this work because its relationship to the drop radius of curvature mentioned above only holds for contact angles close to 180°. Use of the profile length allowed deviations in the contact angle to occur away from 180° without them significantly influencing the data analysis. This reduced the uncertainties associated with the measured values of the drop size/profile length.

A Genie HC-640 C camera (Teledyne Dalsa, see Figure 3.3b) with a CCTV lens with variable focal length (Tamron, 1/2" aspherical, Focal length 10 - 40 mm) attached was connected to the computer via an ethernet cable and used to image the drops, which were illuminated from behind by a diffuse white light source. A MatLab program was used to identify the outer edge of the drops and measure their profile length (see Figure 2.2). The images were binarised (converted to black and white) with the luminance threshold chosen to obtain a complete profile of the drop, as close to 0.5 (the threshold used for the calibration images) as possible.

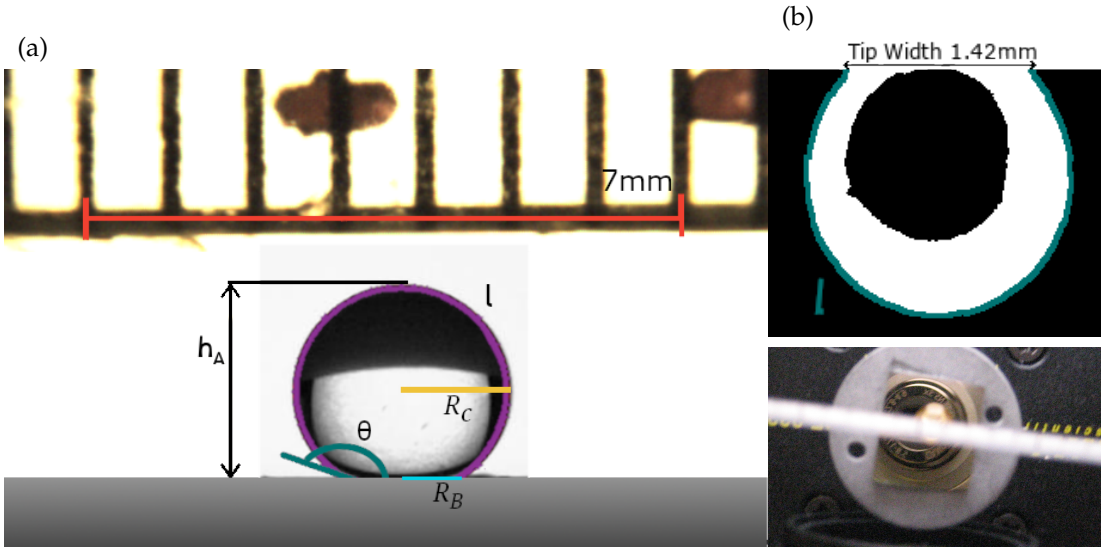

Figure 3.6: Panel (a) shows an image of a ruler suspended in focus above a sessile drop. Several mm markings are visible on the ruler. A red line indicates a 7 mm separation on the ruler. The profile length of the drop (l) is indicated by a purple line around the contour of the drop, the contact angle (θ) is the angle between the substrate and the tangent to the drop as the drop meets the substrate, calculated using Equation 3.5.1. The apex height (h_A) is measured at the top of the drop, the base radius (R_B) is the radius of the drop base and the drop radius (R_c) is the radius of curvature for the drop.

The upper image in panel (b) shows a pendant drop silhouette used to extract the profile length of a pendant drop with known pipette tip diameter, 1.42 mm. The lower image in panel (b) is a photo of the ruler suspended above a sessile drop.

Sessile drop (Section 3.3) images were calibrated (and the number of pixels per mm determined) using a ruler held above the drop (see Figure 3.6). For pendant drops (Section 3.4), the images were calibrated by measuring the pipette tip width using the camera (upper image in Figure 3.6b, the diameter of the pipette tip is known). This method agreed with measurements taken from photos of a ruler placed beneath the tip.

The contact angles for drops with base radius R_B and apex height h_A (See Figure 3.6a) were measured using the relation

$$\tan\theta = \frac{R_B}{R_c - h_A}, \tag{3.5.1}$$

where $(R_c - h_A)$ is the perpendicular distance between the centre of the chord defined by the surface and the centre of the circle describing the drop. Equation 3.5.1 is the tangent equivalent of the equation derived by O'Brien *et. al.* [73] for drops smaller than the capillary length:

$$\theta = \cos^{-1}\left(1 - \frac{h_A}{R_c}\right). \tag{3.5.2}$$

3.6 Laser Optovibrometry

For laser optovibrometry, laser light (3 mW, 670 nm, Edmund Optics) was targeted at a drop suspended from a pipette tip or resting on a horizontal surface (Figure 3.3). The drop acted as a convex lens (Figure 3.7) and the light refracted through the drop projected a refraction pattern [74] (photo overlaid onto photodiode in Figure 3.3a) on a photodiode sensor (custom built, maximum 5 V), beyond the drop. A neutral density filter (ThorLabs, optical density 1.0) was placed over the laser to reduce the light intensity incident on the photodiode. In order to counteract any refraction through the filter, a lens (ThorLabs, plano-convex ⌀1", 150 mm focal length) was also attached to the laser, which had the added benefit of focussing the laser at the drop. Drops were vibrated as described in Sections 3.3 and 3.4.

As the free surface of the drop vibrated, the 'lens' changed shape (Figure 3.8) and the refracted light moved across the photodiode, changing the measured

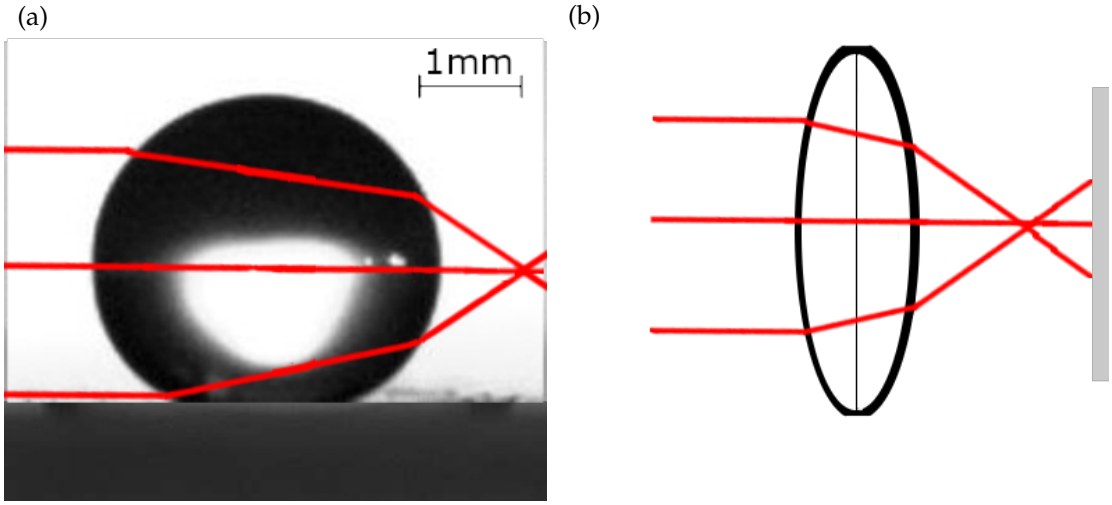

Figure 3.7: Panel (a) shows a photograph of a sessile drop's profile with a diagram of horizontal laser light approaching this drop at different heights and refracting within the drop, causing the light to converge to a focal point beyond the drop. Panel (b) shows an equivalent diagram of light passing through a convex lens. The light again converges at a focal point beyond the drop but in front of a surface onto which the refraction pattern would be projected.

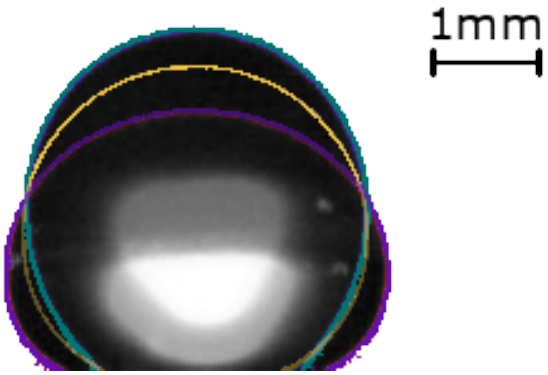

Figure 3.8: Three states of the same mode of the vibration of a sessile drop superimposed over one another, taken shortly after vibration was first triggered (within the first three periods). The top of the drop moves above (teal border) and below (purple border) that for the same drop at rest (yellow border) by approximately one sixth (∼0.4 mm) of the apex height (∼2.9 mm).

intensity. These intensity variations were recorded at a sampling rate of 1 kHz over a 2 - 3 second period using the same data acquisition card used to generate the mechanical impulse. The photodiode's output (Figure 3.9a) was read into LabView and displayed in the form of an intensity vs time curve and its corresponding fast Fourier transform (FFT), giving the mechanical vibrational spectrum of the droplet (Figure 3.9b).

Final processing was performed in MatLab, collecting the frequency and decay of oscillation from this spectrum. This was done by isolating the first peak in the FFT, extracting the peak frequency (referred to as the frequency, f) and measuring the full width of the peak at half the maximum height (FWHM, also referred to as the [peak] width, Δf), shown in Figure 3.9b. These frequencies and widths were used to calculate the rheological properties of the vibrated drops.

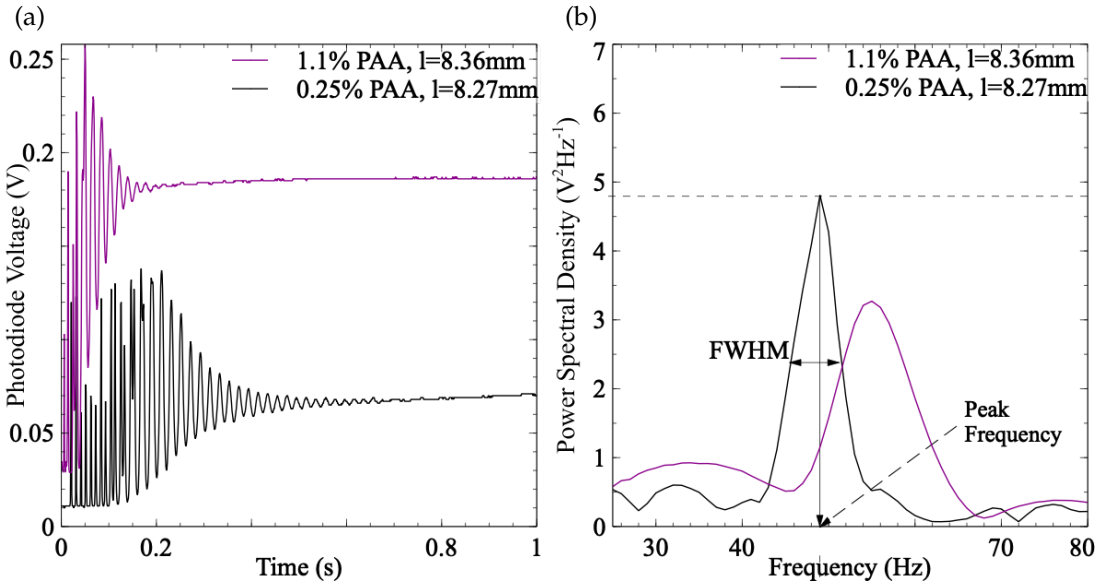

Figure 3.9: Panel (a) shows a plot of the light intensity on the photodiode vs time (s) for drops of 0.25% PAA in water (black line, below) and 1.1% PAA in water (purple line, above) with profile lengths of 8.27 mm and 8.36 mm respectively. The vibration amplitude of 1.1% PAA is damped much faster than that of 0.25% PAA (within 0.2 s rather than 0.6 s). Panel (b) shows a portion of the fast Fourier transform of the data in panel (a) with a diagram to show how the peak frequency and the full width at half maximum (FWHM) of said peak are calculated. The peak for 1.1% PAA is at a higher frequency and wider than that for 0.25% PAA.

3.7 Video capture

Another technique used for monitoring drop vibration was to record the motion of the drop using the high speed camera set up described in Section 3.5. The size of the region imaged by the camera was restricted to the area surrounding the drop in order to closely fit it as it vibrated (Figure 3.10). This allowed a much higher frame rate to be achieved than if the image were left at 480 x 640 pixels (A frame rate of 800 fps can be achieved at 280 x 180 px, 700 fps at 280 x 200 px). Drop vibrations were triggered as described in Sections 3.3 and 3.4. The camera was used to record drop vibration for a period of 1 s, at a high frame rate (300 - 800 fps). These videos can be analysed to track drop height (Figure 3.11a), side position or centre of mass (Figure 3.11b).

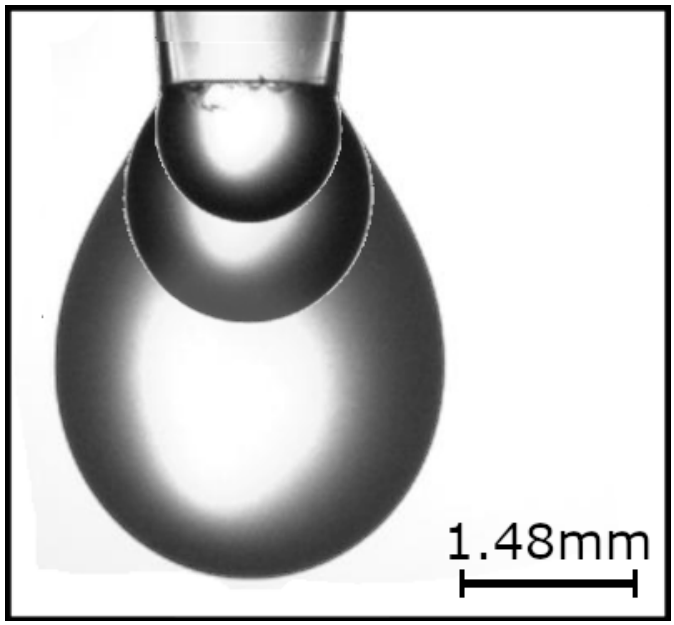

Figure 3.10: Overlayed images of pendant drops of 3% PAA with drop profile lengths 3.2 mm, 5.2 mm and 10.5 mm. The pipette tip has a diameter of 1.48 mm at the base.

From the experiment videos, the position of the centre of mass (CoM) of drops was tracked during their vibration (Figure 3.11b). A "normalised CoM", defined as the displacement of the CoM from the origin (the top left corner of the image), relative to tip position, was obtained by subtracting the tip position from the CoM of the drop. As the majority of drops experienced horizontal vibration (insets in Figure 3.12), the horizontal normalised CoM (nCoMx) was

used in further analysis. The drop vibration behaviour was estimated from the nCoMx by fitting Equation 3.7.1 to the nCoMx with 95% confidence,

$$\begin{aligned} fitcurve = \quad & A_1 e^{-df_1 * 2\pi t} \cos(f_1 * 2\pi t + b_1) \\ & + A_2 e^{-df_2 * 2\pi t} \cos(f_2 * 2\pi t + b_2) \\ & + A_3 e^{-df_3 * 2\pi t} \cos(f_3 * 2\pi t + b_3) + c. \end{aligned} \tag{3.7.1}$$

Here $0 < A_i < 10$ is the vibration amplitude, $0 < df_i < 200$ is the vibration damping coefficient, $0 < f_i < \infty$ is the vibration frequency, $0 < b_i < 2\pi$ is the phase shift of vibration from the origin and $0 < c < 10$ is a constant. The time, t, is the time from start of vibration [16, 75].

(a)

(b)

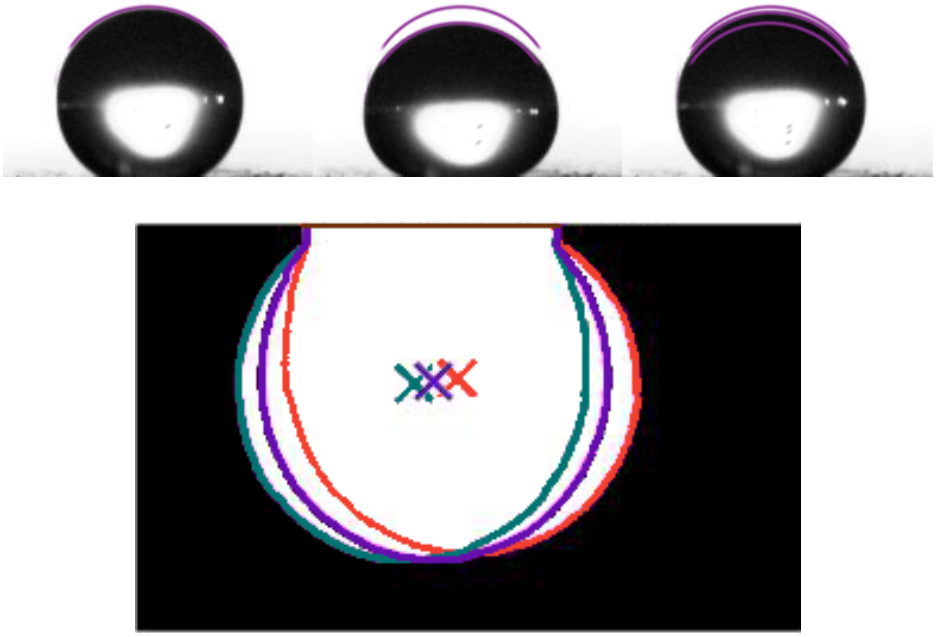

Figure 3.11: The upper panel (a) includes three frames showing the changing shape of a sessile drop of 2% PAA in water as it vibrates. The top is highlighted in each frame and prior drop positions are highlighted in later frames to show the changes in height.
The lower panel (b) shows a black and white image of three superimposed images of an oscillating pendant drop. The drop boundaries are highlighted in purple, green and red. The centre of mass for each image is marked by 'x' symbols of the same colour. The profile length of the purple (central) drop is 5.2 mm.

The decision to fit three harmonic functions was made based on the presence of multiple oscillations resulting from external influences (such as background light intensity oscillation and pipette tip vibration). The value of f_3 was often similar to the other frequencies (f_1 or f_2) or extremely low ($\sim$ 1Hz), and the size (width) of the confidence bounds was significantly (often two orders of magnitude) larger for f_3. Fitting more frequencies would increase the processing time without significantly improving results.

This fitted equation was plotted on top of the nCoMx data (nCoMx displacement vs time) to allow the user to view the level of agreement between the data and the fits (top panel in Figure 3.12). This method was found to be less reliable for drops vibrating at multiple frequencies (e.g. drops for which higher resonance modes were not rapidly damped) so the frequency and width of drop vibration were instead extracted directly from an FFT of nCoMx (bottom panel in Figure 3.12, see also Section 3.6), and the fit from Equation 3.7.1 was reserved for use as an error checking tool. Additional oscillations in the environment, such as motion of the pipette tip and changes in overall light intensity, were tracked and the corresponding peaks in the FFT were used to identify sources of noise in the mechanical vibrational spectra.

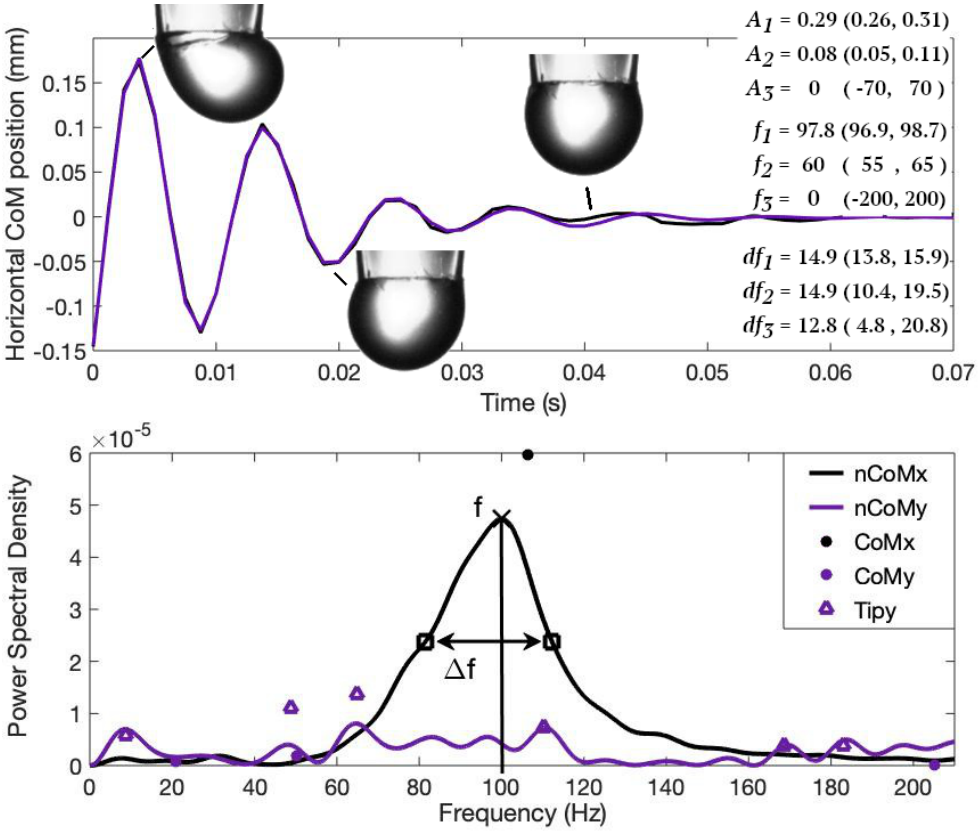

Figure 3.12: The top panel shows the oscillation of the horizontal centre of mass, relative to the pipette tip, (nCoMx, black line) of a pendant drop of 3% PAA in water (with profile length $l \approx 3.6\,\text{mm}$), fitted with the curve from Equation 3.7.1 (purple line, with 95% confidence), with estimated amplitudes $A_1 = 0.29\,(0.26, 0.31)$, $A_2 = 0.08\,(0.05, 0.11)$ and $A_3 = 0\,(-70, 70)$; frequencies $f_1 = 97.8\,(96.9, 98.7)$Hz, $f_2 = 60\,(55, 65)$Hz and $f_3 = 0\,(-200, 200)$Hz; and decay rates $df_1 = 14.9\,(13.8, 15.9)$Hz, $df_2 = 14.9\,(10.4, 19.5)$Hz and $df_3 = 12.8\,(4.8, 20.8)$Hz. Insets show the pendant drop at different stages of oscillation.

The bottom panel shows the Fast Fourier transform (FFT) of the nCoMx data (black line) and defines the full width half maximum (Δf) as the width of the peak at half the maximum peak height. The frequency and width of vibration were measured to be $f \approx 100\,\text{Hz}$ and $\Delta f \approx 30\,\text{Hz}$ respectively. For this drop, Δf is approximately double the estimated values df_i. Also plotted are the FFT of the vertical centre of mass, relative to the pipette tip (nCoMy, purple line), the peak positions of the horizontal (black dots, CoMx) and vertical (purple dots, CoMy) components of the centre of mass without normalisation, and the peak positions of the vertical pipette tip motion (Tipy, purple triangles).

3.8 Surface tension (γ)

The surface tension of the polymer solutions was measured via the pendant drop method (Figure 3.13) [18]. Suspending a drop of solution larger than the capillary length causes the drop to distort under gravity. Measuring the shape of the distorted drop, described by Equation 3.8.1, allows the surface tension to be calculated from the shape parameter (β) [76].

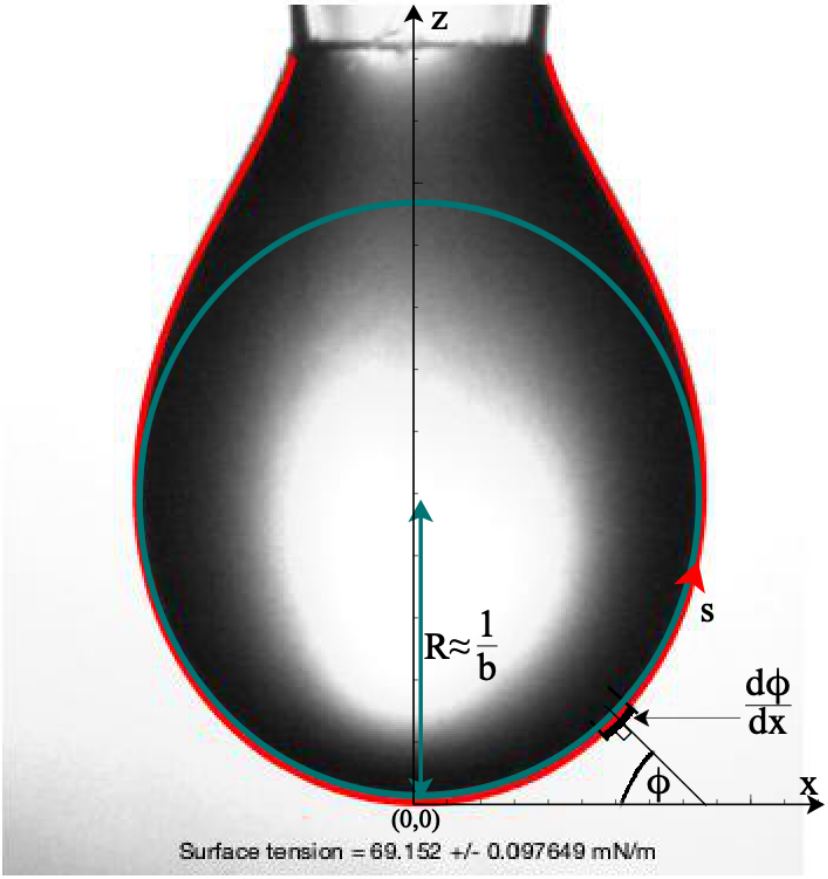

Figure 3.13: A large pendant drop of 1.1% PAA in water distorted by gravity. The drop profile is highlighted in red and the calculated surface tension ($69.152 \pm 0.098\,\mathrm{mNm^{-1}}$) is displayed below the drop. A teal circle, of radius $R \approx \frac{1}{b}$, is fitted to the profile at the base of the drop. The horizontal and vertical axes are defined as x and z respectively, with the origin (0,0) at the base of the drop. s is defined as the arc distance around the drop profile from the origin. For a point along the profile, ϕ is the angle between the normal to the drop curve and the x axis, and curvature, $\frac{d\phi}{dx}$, is defined as the change in angle over changing x.

The shape of a drop under the influence of gravity and surface pressure forces is given by

$$(2 + \beta z) = \frac{d\phi}{ds} + \frac{sin(\phi)}{x}, \tag{3.8.1}$$

where $\frac{d\phi}{ds}$ is the curvature at point (x,z), ϕ is the angle between the normal to the curve at (x,z) and the x axis, s is the arc length between the base of the drop and the point at (x,z), and β is the shape parameter, defined by Equation 3.8.2:

$$\beta = \frac{b^2}{{l_c}^2}, \tag{3.8.2}$$

for which b is the curvature at the base of the drop, and $l_c = \sqrt{\frac{\gamma}{\rho g_{eff}}}$ is the capillary length of the solution [76].

Therefore the surface tension of a pendant drop affected by gravity is given by:

$$\gamma = \frac{\rho g_{eff} b^2}{\beta}. \tag{3.8.3}$$

The densities of solutions were measured by applying a linear fit $m = a + \rho V$ (Figure 3.14) to the masses (m, measured using the balance from Section 3.1) of several volumes (V) of solution (for bulk values between 0.5 and 5 mL, as well as for increasing increments of 0.1 mL from 0.1 to 2 mL), with constant a.

Equation 3.8.3 can then be solved iteratively by fitting a circular arc to the base of the drop (teal line in Figure 3.13) to produce an initial estimate for the curvature, defining an initial surface tension $\gamma_i = 50\,\text{mJm}^{-1}$, and fitting the Young's Laplace differential equation (Equation 3.8.1) to the drop profile in order to obtain β.

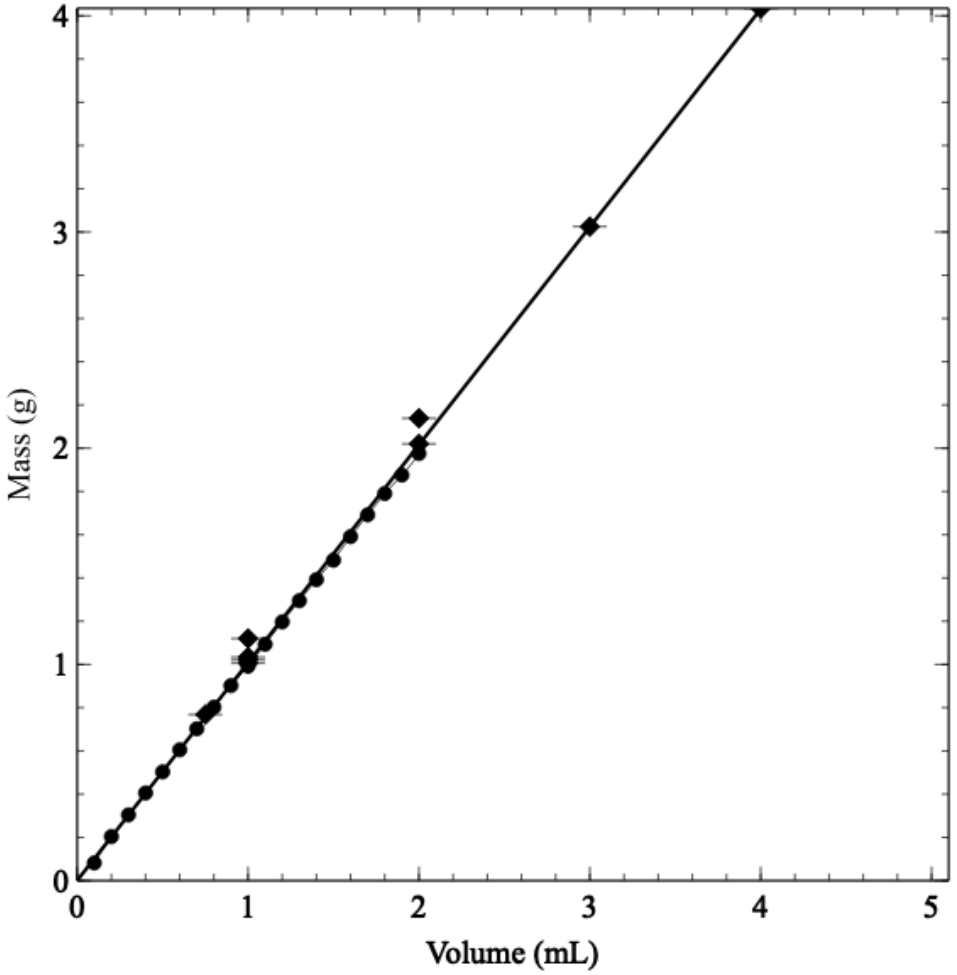

Figure 3.14: Mass vs. volume for 2% PAA in water with a linear fit $m = 0.0009 + 1.0075V$ for which 1.0075 is the density in g/mL. Circles show incremental (in 0.1 mL steps) volume measurements from 0.1 to 2 mL, and diamonds show bulk measurements (for 0.75, 1, 2, 3, 4 and 5 mL).

3.9 Rheological properties

Harrold *et. al.* [65, 77] recently showed that the generalised viscoelastic properties of a vibrating drop supported on a superamphiphobic substrate could be described by considering standing wave states on the surface of the drops. These authors used the dispersion relation for capillary waves on the surface of a viscoelastic fluid (Equation 2.0.9, first introduced by Pleiner, Harden and Pincus [60]) in conjunction with a condition that a half integer number of wavelengths (λ) fit around the profile length of the drops at resonance, i.e. $n\frac{\lambda}{2} = l$, which gave values for the allowed wavevector magnitudes of $k = \frac{2\pi}{\lambda} = \frac{n\pi}{l}$. Inserting this result for k into Equation 2.0.9 and equating real and imaginary parts gave equations for the shear storage (G′, elastic component) and loss (G″, viscous component) moduli of the vibrated sessile or pendant drops:

$$G' = \frac{\rho f^2 l^2}{n^2}\left(1 - \frac{\pi\gamma n^3}{4\rho l^3\left(\Delta f^2 + f^2\right)}\right), \tag{3.9.1}$$

$$G'' = \frac{\rho f \Delta f l^2}{n^2}\left(1 + \frac{\pi\gamma n^3}{4\rho l^3\left(\Delta f^2 + f^2\right)}\right). \tag{3.9.2}$$

As before, ρ is the solution density in $\mathrm{kg\,m^{-3}}$, f is the fundamental vibration frequency in Hz, l is the drop profile length in m, n is the mode number, γ is the surface tension of the solution in $\mathrm{Nm^{-1}}$, and Δf is the full width at half maximum of the fundamental peak in Hz.

For the viscoelastic droplet solutions studied in Chapters 5 and 6, G′ and G″ were calculated by inserting the measured values of l (Section 3.5), f and Δf (Sections 3.6 and 3.7), with surface tension and density values from Table 3.1, into Equations 3.9.1 and 3.9.2.

In assigning the mode number, values of $n = 2, 3, 4, ...$ were used. The justification for choosing n=2 as the lowest vibrational mode is based on the droplet fluid being incompressible and pinned to the surface (having a fixed contact line) [16, 26, 30]. For an incompressible drop, which has constant density, the relation $V = \frac{m}{\rho}$ means that fluid cannot change volume without a change in mass. As seen in Figure 2.3b, for the n=1 mode of vibration to occur for a drop with fixed contact line, the drop must expand and contract, changing volume

PAA Conc.	Surface Tension (mNm^{-1})	Density (kgm^{-3})
0% (water)	72.1 ± 0.4	994.1 ± 0.1
1.1%	70.7 ± 0.3	1003.5 ± 0.1
2%	67.9 ± 0.4	1007.5 ± 0.1
3%	67.0 ± 0.6	1015.6 ± 0.1

Table 3.1: The measured surface tension (see Section 3.8) and density for solutions of poly(acrylamide-co-acrylic acid) (PAA) in water at room temperature, $20 \pm 2°C$.

during vibration. For an incompressible fluid this mode can only occur if the contact line is allowed to move (Figure 2.3a). The n=2 mode, on the other hand, changes shape but preserves volume (Figure 2.3c). The fluid within the drop is able to move between the shape shown in Figure 2.3c and its reflection across the vertical axis. As a result, an incompressible drop with fixed contact line can oscillate in the n=2 mode with no changes in volume.

Sharp *et. al.* [30] confirmed this for sessile drops of water, comparing the shape of an oscillating drop to predictions, and matching mass-frequency behaviour to estimates and previous data from Daniel *et. al.* [9]. Temperton *et. al.* [32] also applied this condition to the analysis of oscillating pendant drops of deuterium oxide, formamide, and 1,1,2,2-tetrabromoethane.

For the simple liquids studied in Chapter 4, Equations 3.9.1 and 3.9.2 were simplified further by setting $G' = 0$ (i.e. no elastic component) and noting that the viscosity of the drops is given by $\eta = \frac{G''}{2\pi f}$ [78, 79]. This gave expressions for the surface tension and viscosity of the form

$$\gamma = \frac{4\rho l^3}{\pi n^3}\left(\Delta f^2 + f^2\right) \tag{3.9.3}$$

and

$$\eta = \frac{\rho l^2}{\pi n^2}\Delta f. \tag{3.9.4}$$

The expressions given in Equations 3.9.3 and 3.9.4 have similar functional forms to those obtained for the corresponding equations (Equations 3.9.5 and 3.9.6 respectively) for levitated drops [23, 40, 42]:

$$\gamma = \frac{\rho l^3}{2\pi\, n(n-1)(n+2)} f^2 \tag{3.9.5}$$

and

$$\eta = \frac{\rho l^2}{2\pi(n-1)(2n+1)} \Delta f. \tag{3.9.6}$$

The expressions derived in Equations 3.9.3 and 3.9.4 are modified slightly due to the requirement that a vibrational node must exist in the contact region with the substrate if the droplets remain pinned during vibration, i.e. $n = \frac{2l}{\lambda}$ [51, 52] – a condition which is not imposed on levitated drops [15] (which are instead confined by $n = \frac{l}{\lambda}$). This additional constraint has the effect of changing the prefactor in Equations 3.9.3 and 3.9.4 when compared to the equivalent expressions for levitated drops (Equations 3.9.5 and 3.9.6 respectively).

Another difference between Equations 3.9.3 and 3.9.4 and those reported for levitated droplets is the addition of the width dependence in the surface tension equation. For inviscid fluids, this term is often neglected as damping is relatively weak and has little effect on the vibrational frequencies of the droplets and the corresponding surface tension values. However, for the fluids studied in Chapter 4 the viscosity could potentially vary over three orders of magnitude. Damping of the droplets will therefore have a significant effect upon their motion. This is particularly true for the higher glycerol concentrations where the increased viscosity is expected to influence the vibrational frequencies of the droplets [50]. The addition of the width dependence in Equation 3.9.3 takes these effects into account and compensates for the effects of shifts in vibrational frequency caused by damping of a mechanically vibrating system [75].

3.9.1 Treatment of uncertainties

In calculating the uncertainties associated with G′ and G″, it is assumed that all the errors are randomly distributed and that the fractional uncertainties in the

physical parameters in Equations 3.9.1 and 3.9.2 can be added in quadrature, e.g.

$$\Delta G' = \sqrt{\left(\left(\frac{\delta G'}{\delta \rho}\right)\Delta\rho\right)^2 + \left(\left(\frac{\delta G'}{\delta f}\right)\Delta f\right)^2 + \left(\left(\frac{\delta G'}{\delta l}\right)\Delta l\right)^2 + ...} \quad (3.9.7)$$

We start with Equation 3.9.1,

$$G' = \frac{\rho f^2 l^2}{n^2}\left(1 - \frac{\pi\gamma n^3}{4\rho l^3(w^2+f^2)}\right) = \frac{\rho f^2 l^2}{n^2}X, \quad (3.9.8)$$

where here, w is the width of the vibrational peaks (note the change of variable name to avoid confusion in calculating uncertainties with the over use of the Δ symbol) and

$$X = 1 - \frac{\pi\gamma n^3}{4\rho l^3(w^2+f^2)}. \quad (3.9.9)$$

Adding the fractional errors in quadrature (using Equation 3.9.7) produces

$$\left(\frac{\Delta G'}{G'}\right)^2 = \left(\frac{\Delta\rho}{\rho}\right)^2 + \left(\frac{2\Delta f}{f}\right)^2 + \left(\frac{2\Delta l}{l}\right)^2 + \left(\frac{\Delta X}{X}\right)^2, \quad (3.9.10)$$

where here Δa represents the uncertainty in each variable, a, and

$$\left(\frac{\Delta X}{X}\right)^2 = \left(\frac{\Delta\gamma}{\gamma}\right)^2 + \left(\frac{\Delta\rho}{\rho}\right)^2 + \left(\frac{3\Delta l}{l}\right)^2 + 4\frac{(w^2\Delta w^2 + f^2\Delta f^2)}{(f^2+w^2)^2} \quad (3.9.11)$$

so that

$$\left(\frac{\Delta G'}{G'}\right)^2 = 2\left(\frac{\Delta\rho}{\rho}\right)^2 + \left(\frac{2\Delta f}{f}\right)^2 + 13\left(\frac{\Delta l}{l}\right)^2 + \left(\frac{\Delta\gamma}{\gamma}\right)^2 + 4\frac{(w^2\Delta w^2 + f^2\Delta f^2)}{(f^2+w^2)^2}. \quad (3.9.12)$$

Inserting typical values of parameters of $f = 50 \pm 0.1\,\text{Hz}$, $w = 20 \pm 0.1\,\text{Hz}$, $l = 8 \pm 0.1\,\text{mm}$, $\gamma = 70 \pm 0.2\,\text{mJm}^{-2}$ and $\rho = 1010 \pm 5\,\text{kgm}^{-3}$ gives values for the fractional error terms of $\left(\frac{2\Delta f}{f}\right)^2 = 1.6\text{x}10^{-5}$, $2\left(\frac{\Delta\rho}{\rho}\right)^2 = 1\text{x}10^{-5}$, $13\left(\frac{\Delta l}{l}\right)^2 = 2\text{x}10^{-3}$, $\left(\frac{\Delta\gamma}{\gamma}\right)^2 = 8\text{x}10^{-6}$ and $4\frac{(w^2\Delta w^2+f^2\Delta f^2)}{(f^2+w^2)^2} = 1.5\text{x}10^{-5}$.

The dominant term (by at least two orders of magnitude) is associated with the uncertainties in the profile length, l, of the drops so that Equation 3.9.12 can be approximated as

$$\Delta G' = \sqrt{13}\frac{\Delta l}{l}G'. \tag{3.9.13}$$

A similar analysis for G″ yields exactly the same form for the uncertainty in this variable, i.e.

$$\Delta G'' = \sqrt{13}\frac{\Delta l}{l}G''. \tag{3.9.14}$$

These formulae were used to calculate the uncertainties of G′ and G″ given in Figure 5.3.

Repeating the analysis for γ and η yields

$$\left(\frac{\Delta\gamma}{\gamma}\right)^2 = \left(\frac{\Delta\rho}{\rho}\right)^2 + 9\left(\frac{\Delta l}{l}\right)^2 + 4\frac{\left(w^2\Delta w^2 + f^2\Delta f^2\right)}{(f^2+w^2)^2} \tag{3.9.15}$$

and

$$\left(\frac{\Delta\eta}{\eta}\right)^2 = \left(\frac{\Delta\rho}{\rho}\right)^2 + 4\left(\frac{\Delta l}{l}\right)^2 + \left(\frac{\Delta w}{w}\right)^2, \tag{3.9.16}$$

with dominant term once again given by the uncertainty in the profile length (by two orders of magnitude for γ and one order of magnitude for η), approximating the uncertainties in γ and η to be

$$\Delta\gamma = 3\frac{\Delta l}{l}\gamma \tag{3.9.17}$$

and

$$\Delta\eta = 2\frac{\Delta l}{l}\eta \tag{3.9.18}$$

respectively.

3.10 Microrheology

Microrheology enables measurement of the rheological properties of low viscoelasticity liquids. Methods include dynamic light scattering (DLS, single scattering), measurement of probe particle mean square displacement (MSD), diffusion wave spectroscopy MSD (multiple scattering) [80] and also single particle tracking techniques such as optical tweezers [81]. The microrheology data in this thesis was collected using DLS microrheology with a Zetasizer nano ZS from Malvern Instruments. The DLS technique is commonly used with liquids of known rheological properties to obtain the size of particles (or spheres) in a solution [82]. However the Zetasizer can be run for solutions with known sphere size to find the rheological properties of the liquid. This simply requires an adjustment of which parameters it considers constant and which are variable.

Selecting sphere material, size and concentration can be challenging. The material must be selected to reduce interactions with the solution. The size must be large enough (or have a high enough refractive index difference between the sphere and the solution) to dominate light scattering over the polymers within the solution, whilst being small enough to be unaffected by gravity and avoid distorting the polymer chains. Finally the sphere concentration must be appropriate to maintain the single scattering regime (indicated by an initial correlation coefficient > 0.8 [83]). The suitability of selections can be confirmed by using the Zetasizer to measure the size of the microbeads in a solution with estimated rheological properties.

Nano- or micro-sized spheres (microbeads) of polystyrene (PL-Latex, Agilent) particles with a range of sizes (100 - 300 nm diameter) were suspended in solutions prepared as in Section 3.1. To prevent the microbeads from aggregating or large particles (such as dust) from contaminating the solutions, these suspensions were refridgerated (for use within one month) in Parafilm® wrapped small glass sample vials which had been cleaned in a sonicator, dried in vacuum and repressurised with nitrogen. Prior to measurements, samples were brought close to room temperature and sonicated to encourage even microbead distribution and remove air bubbles [84, 85]. Cuvettes (DTS0012 polystyrene cuvettes, Malvern) containing these suspensions were placed in the Zetasizer,

which used non-invasive back scattering at 173° to characterise the solutions in a temperature controlled environment (20°C and 25°C, ± 0.1°C). Time dependent changes in scattered light intensity were recorded as the thermal motion of the molecules in the solution jostled the microbeads [86].

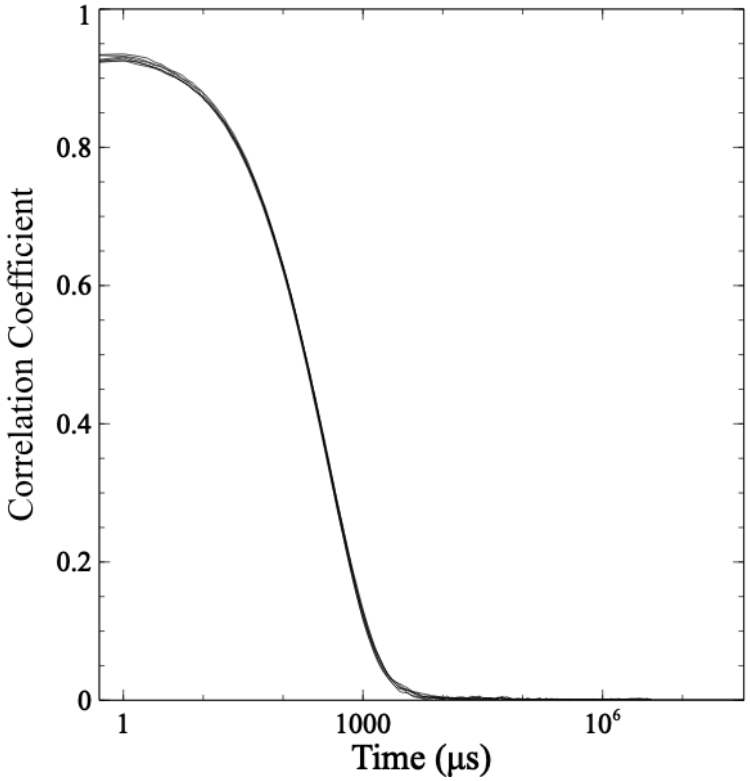

Figure 3.15: The autocorrelation data collected from the Zetasizer for 1.1% PAA in water with 0.05% PL-Latex 50nm microbeads. Logarithmic decay from the y-intercept (correlation coefficient above 0.9) is followed by exponential decay (towards a correlation coefficient of 0).

After a sample had been tested, the Zetasizer returned an autocorrelation function, $g_1(\tau)$, as a function of correlation time τ (see Figure 3.15). For correlation times $\tau \gtrsim 1\,\text{ms}$, the autocorrelation curve follows an exponential decay of the form

$$g_1(\tau) = g_1(0) \exp\left(-\frac{q^2}{6}\left\langle \Delta r^2(\tau)\right\rangle\right), \tag{3.10.1}$$

where $g_1(0)$ is the autocorrelation function at initial time $\tau = 0$, $\left\langle \Delta r^2(\tau) \right\rangle$ is the MSD of the microbead as a function of the correlation time, and the scattering vector (q) is defined by

$$q = \frac{4\pi n_i}{\lambda} \sin\left(\frac{\phi}{2}\right), \tag{3.10.2}$$

with fluid refractive index (without microbeads) n_i, light wavelength λ and scattering angle ϕ [80].

Rearranging Equation 3.10.1 to isolate the MSD gives:

$$\left\langle \Delta r^2(\tau) \right\rangle = \frac{6}{q^2} \left(\ln(g_1(0)) - \ln(g_1(\tau)) \right). \tag{3.10.3}$$

Defining time t such that $t = \tau / 2\pi$, Mason *et. al.* [86] showed that substituting $\tau = 2\pi t$ into Equation 3.10.3 and performing a power law expansion around $t = \frac{1}{f}$ (where f is a frequency to be evaluated in Hz) leads to:

$$\left\langle \Delta r^2(t) \right\rangle \approx \left\langle \Delta r^2 \left(\frac{1}{f}\right) \right\rangle (ft)^{\alpha(f)}, \tag{3.10.4}$$

where

$$\alpha(f) = \left. \frac{d \ln \left\langle \Delta r^2(t) \right\rangle}{d \ln t} \right|_{t=\frac{1}{f}}. \tag{3.10.5}$$

Mason *et. al.* applied a Fourier transform to Equation 3.10.4 and used the result, $if\mathcal{F}_u \left\{ \left\langle \Delta r^2(t) \right\rangle \right\} \approx \left\langle \Delta r^2 \left(\frac{1}{f}\right) \right\rangle \Gamma\left[1 + \alpha(f)\right] i^{-\alpha(f)}$, to estimate the complex shear modulus (G^*) of a viscoelastic fluid in the form of the Generalised Stokes-Einstein theorem [86]:

$$|G^*(f)| = \frac{k_B T}{\pi a \left\langle \Delta r^2(\frac{1}{f}) \right\rangle \Gamma\left[1 + \alpha(f)\right]}, \tag{3.10.6}$$

With Gamma function $\Gamma\left[1 + \alpha(f)\right] \approx 0.457(1+\alpha)^2 - 1.36(1+\alpha) + 1.90$ [86]. Using Euler's equation $e^{ix} = \cos x + i \sin x$, the storage (Equation 3.10.7) and

loss (Equation 3.10.8) moduli can be taken from the real and imaginary parts of Equation 3.10.6 respectively:

$$G'(f) = |G^*(f)| \cos\left(\frac{\pi\alpha(f)}{2}\right), \tag{3.10.7}$$

$$G''(f) = |G^*(f)| \sin\left(\frac{\pi\alpha(f)}{2}\right). \tag{3.10.8}$$

3.10.1 Refractive index

The refractive index of solutions used in the microrheology experiments was measured using a refractometer from Anton Paar (Abbemat 200), which employs the critical angle measurement technique. A prism was coated with a few drops of solution and the system was temperature-controlled during measurements. The refractive index was measured at 20°C and 25°C to allow for the effects of inconsistent ambient room temperature during drop vibration experiments. A laser beam was passed through the prism at different angles until the critical angle for the system was reached and a shadow covered a CCD sensor as light was completely directed away from the sensor. The refractive index of the sample could then be calculated from the equation:

$$\theta_c = \sin^{-1}\left(\frac{n_2}{n_1}\right), \tag{3.10.9}$$

where θ_c is the critical angle for total internal reflection, n_2 is the refractive index of the sample, and n_1 is the refractive index of the prism [87].

3.11 Rheology

A Kinexus rheometer (Malvern) in the cone-plate geometry (using a 50 mm diameter cone with angle 1°) was used to analyse our samples in oscillation mode. For the cone-plate geometry, a torque is applied to the cone, producing shear stress and shear strain in the sample. The resulting torque in the sample can be used to extract the shear stress and the shear strain, which can be used to calculate the elastic shear moduli, loss moduli and viscosity. A normal force

sensor in the lower plate allows elasticity to be measured from the sample's response to the applied rotational force.

It is possible to perform measurements keeping either the shear stress or the shear strain constant. Viscosity measurements are more accurate for high shear rates in constant stress measurements. Below a "yield value" of rotor speed, mechanical (equipment) inertia may dominate over the response of the solution and the torque sensor may record internal resistance before the fluid has begun to deform. High rotor speed on the other hand can cause turbulence rather than the laminar flow required for accurate analysis [88].

The accuracy of measured torque impacts the accuracy of shear stress/strain measurements and relies on equipment sensitivity, which decreases for low assigned torques as equipment error increases (e.g. from bearing friction). Low viscosity fluids require high rotor speeds or a large cone surface area to obtain significant torque signals with insignificant equipment error [89]. This limits the maximum shear rate or frequencies accessible to the system as well as the range of shear storage and loss moduli that can be measured [88].

CHAPTER 4

Tracking changes in the surface tension and viscosity of glycerol/water drops

4.1 Introduction

Droplet vibration has been studied for some time as a means of trying to extract physical properties such as the surface tension and viscosity of fluids [14, 16, 21–23, 30, 32, 51]. Much of the early work in this field concentrated on the study of levitated droplets of single component liquids [46], whose properties could be extracted using theories based upon the theoretical models developed by Rayleigh [40] and Chandrasekhar [42]. These authors showed that the vibrational frequencies and damping coefficients associated with the vibration of a free liquid globe (essentially a levitated liquid drop) could be related independently to the surface tension and viscosity of the fluid using a simple set of equations (Chapter 2).

Confirmation of the results predicted by Rayleigh came when the technology to levitate small liquid droplets became available in the form of acoustic [22] and magnetic levitation devices [23]. Much of the initial work in this area seems to have been motivated by the desire to perform containerless crystallisation studies on pure liquids in microgravity environments [7, 26]. Later work turned to the use of this technique for extracting the physical properties of the

drops and a number of authors were able to demonstrate the viability of drop vibration as a means of extracting surface tension [14, 45] and viscosity [14, 21].

Another method of extracting these properties is to vibrate substrate supported (sessile) or pendant drops. The ease with which a drop can be placed on a substrate, or suspended from a pipette and vibrated makes this approach more attractive and more accessible than magnetic levitation. There are, however, a number of challenges in interpreting the drop vibration data for substrate supported drops. Firstly, the presence of a substrate (or pipette) influences the drop shape and has an influence on the vibrational frequency [16, 30, 32]. Gravity can also play a role in changing the frequencies of vibration if the droplets exceed a critical size. This size is set by the capillary length of the fluid, l_c, above which gravitational effects dominate the shape of the drop and below which surface tension tends to dominate [16, 30, 32]. In the surface tension dominated regime, sessile drops assume the shape of a spherical cap in attempt to minimise their surface area, while in the gravity-dominated regime the drops become flattened.

The contact of the substrate with the free surface of the drop also introduces additional energy dissipation mechanisms that are not present in levitated drops. These energy dissipation mechanisms affect the damping coefficients associated with the time dependent decay of the oscillations. The increased damping also causes an increase in the width of the peaks in the mechanical vibrational spectra of the drops [16].

One way to circumvent the difficulties associated with the presence of the substrate interface is to use non-wetting substrates such as superhydrophobic or superamphiphobic materials [64]. When drops are placed on these surfaces, the energetics of the interaction between the fluid and the substrate are such that the drops bead up and form spheres with three phase contact angles that are close to 180°. In this way the drops assume shapes that are reminiscent of levitated drops and much of the physics of vibration can be described by using similar models.

McHale *et. al.* [35] demonstrated the feasibility of this approach in studies of vibrating liquid marbles – liquid droplets stabilised by the adsorption of small particles on their surface. They showed that the vibrational frequencies of the liquid marbles could be described using expressions similar to those

used for levitated droplets. However, the particles were found to dominate their properties, giving this particular approach limited application in the measurement of surface tension and other (e.g. viscoelastic) properties.

Much of the work on drop vibration to date has concentrated on pure liquids or on viscoelastic systems where the concentration of added solute does not change significantly with time. Here the idea is proposed that drop vibration can also be used to track the surface tension, viscosity and viscoelastic properties of droplets supported on superamphiphobic substrates when the composition of the drops is changing with time. An automated combined light scattering and imaging technique is described for measuring the size, frequencies and spectral widths of vibrating drops of multicomponent fluids. These quantities are related to the surface tension and viscosity of the multicomponent fluid using a simplified model developed for extracting the properties of viscoelastic droplets on the same substrates (Chapter 2, [65]). A series of experiments using drops containing different initial compositions of glycerol and water are used to test the validity of the vibration technique for studying the kinetics of changes in surface tension and viscosity as the droplets evaporate.

The use of the simple system described here and the development of the experimental and theoretical protocols required to extract surface tension and viscosity enable us to validate this technique as a means of tracking material properties of soft systems in real time.

4.2 Method

Glycerol and water were used as a model system for these experiments because they are miscible in all proportions, the viscosity of their mixtures varies over three orders of magnitude (1 mPas - 1 Pas [90]) and glycerol is non-volatile at room temperature [91]. Microlitre droplets containing glycerol/water mixtures with compositions in the range 1 - 50 wt% (0.008 - 0.44 volume fraction, Section 3.1 [65]) were placed on the surface of the superamphiphobic substrates (prepared as described in Section 3.2 [64, 65]) and vibrated as described in Section 3.3. Drop vibration was monitored using laser light refracted through the droplets (see Section 3.6). Both the frequencies, f, and widths, Δf, of vibration

were found to depend upon the size and composition of the drops for each vibrational mode. Experiments were performed using these solutions within 4 months of manufacture (<1 month for 1 and 5%, and <4 months for 25 and 50%).

The profile length, l, and contact angle, θ, of the drops were measured using the technique described in Section 3.5 (Figure 3.6a). The drops studied had radii smaller than the capillary length of the fluids and as such had shapes that are close to that of a perfect sphere when deposited on the superamphiphobic substrates with contact angles close to 180° (Chapter 2).

For each drop, the experiment was repeated several times over the course of 2500 s, during which the drops shrunk as water evaporated (see Section 3.1.1). As the drops evaporated, Equations 3.9.3 and 3.9.4 (Section 3.9) were used to calculate the surface tension and viscosity respectively of the glycerol/water solutions. The minimum time resolution of the measurement and analysis process was three seconds and allowed changes in surface tension and viscosity to be tracked in real time. All measurements were performed at room temperature which was maintained at 20 ± 2 °C. The relative humidity in the room was measured to be 50 ± 5% during the measurements. Independent measurements of the density, ρ, and the surface tension, γ, of the glycerol solutions were obtained using the techniques described in Section 3.8.

4.3 Results and Discussion

Figure 4.1 shows examples of data collected for four drops of similar starting size that had different initial glycerol/water compositions. As the droplets evaporated, the size (profile length) of the drops was observed to decrease and both the frequency and width of the lowest vibrational mode increased with time. The increases in the latter two parameters occurred as a result of the shrinking dimensions of the drops and due to changes in the surface tension and viscosity. Smaller liquid drops have higher vibrational frequencies and experience more damping [16, 32]. In addition, the mass-loss over time of one or more of the droplet components is expected to cause changes in the material properties of the mixture.

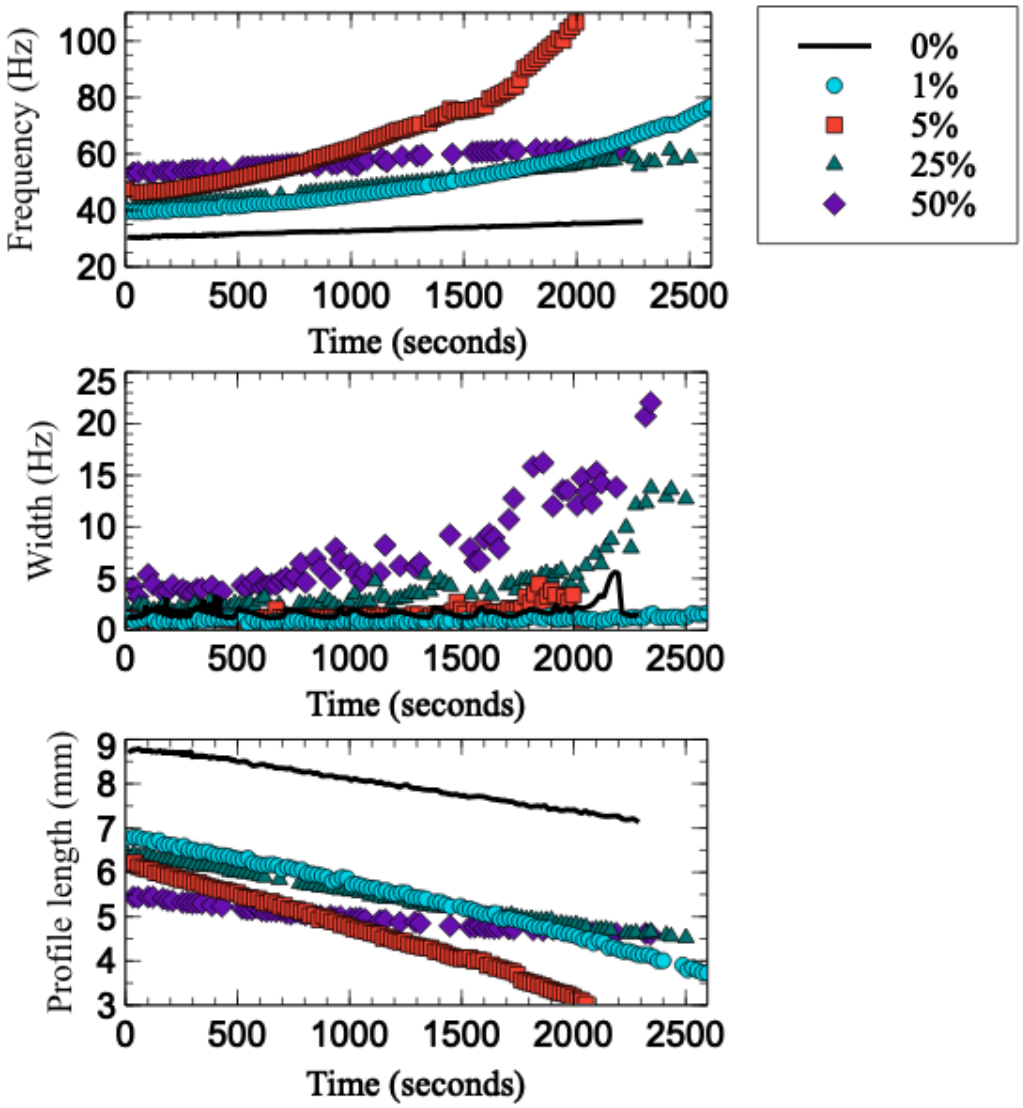

Figure 4.1: The panels show how the vibrational frequency (top), spectral width (middle) and profile length of droplets varies with time. Data are shown for four droplets of similar starting size having initial compositions of 0 wt% (black line), 1 wt% (cyan circles), 5 wt% (red squares), 25 wt% (teal triangles) and 50 wt% (purple diamonds) of glycerol. The initial compositions correspond to glycerol volume fractions of 0, 0.008, 0.04, 0.209 and 0.44 respectively. The frequency and width increase with time, while the profile length decreases with time. The width increases as the starting concentration of glycerol is increased; the frequency behaviour corresponds to the profile length of the drops.

When interpreting the data for the binary mixtures used in these experiments it was assumed that the dominant source of mass loss occurred as the result of evaporation of water (Section 3.1.1). This assumption was supported by the observation that pure glycerol droplets did not evaporate on the time scales of the experiments ($\sim$2000 s). However, microlitre droplets of pure water were observed to undergo significant mass loss as a result of evaporation over similar time scales.

Figure 4.2 shows the time dependent variation of the surface tension obtained for the droplet data shown in Figure 4.1. The measured values of f, Δf and l in Figure 4.1 were used to calculate γ and η at each time point using Equations 3.9.3 and 3.9.4. A value of n=2 was used for the lowest mode of vibration as has been discussed previously for vibrating drops with pinned contact regions [16, 30, 32, 48, 65].

The changing composition of the drops meant that their density varied somewhere in the range between 998 kgm^{-3} (pure water [90]) and 1260 kgm^{-3} (pure glycerol [90]) during the experiments. At each time point, the volume of the drop was calculated using the equation, $V(t) = \frac{l^3}{6\pi^2}$, derived from the equation for the volume of a sphere, $V = \frac{4\pi R^3}{3}$, with its circumference approximated to the profile length, $l \sim 2\pi R$. The volume fraction of glycerol was then calculated by assuming that mass loss occurred purely as the result of the evaporation of water. This gave an equation for the volume fraction of glycerol in the drop, $\phi(t)$, such that

$$\phi(t) = \phi_0 \frac{V_0}{V(t)} \,, \tag{4.3.1}$$

where ϕ_0 and V_0 are the initial glycerol volume fraction and volume of the drop respectively. Values of the density of the drops were then calculated using a fit to data obtained by Sheely [90] for bulk glycerol/water solutions (see Figure 4.3). This fit gave the result that the density of the drops varied according to the equation $\rho = 988 + 270\,\phi(t)$. Insertion of the volume fraction dependence of the density in Equations 3.9.3 and 3.9.4 allowed the correct surface tension and viscosity values to be extracted for the evaporating droplets at each time point.

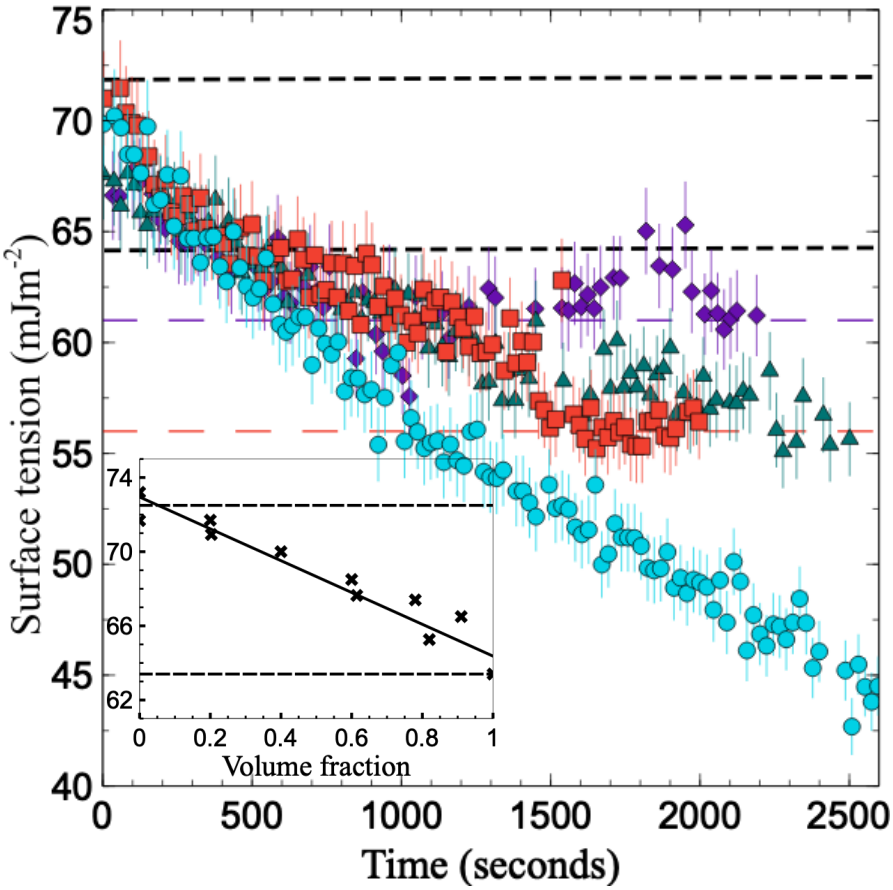

Figure 4.2: A plot of the time dependence of the surface tension of evaporating glycerol/water solutions. Data are shown for four droplets of similar size having initial compositions of 1 wt% (cyan circles), 5 wt% (red squares), 25 wt% (teal triangles) and 50 wt% (purple diamonds) of glycerol in water. The initial compositions correspond to glycerol volume fractions of 0.008, 0.04, 0.209 and 0.44 respectively. The dashed horizontal lines at $\gamma = 72\,\mathrm{mJm^{-2}}$ and $\gamma = 64\,\mathrm{mJm^{-2}}$ correspond to the surface tensions of pure water and pure glycerol respectively. The surface tension of all droplets rapidly drops below that of pure glycerol, plateauing around $56\,\mathrm{mJm^{-2}}$ for 5 wt% and 25 wt%, and around $61\,\mathrm{mJm^{-2}}$ for 50 wt%. The surface tension of 1 wt% decreases to $44\,\mathrm{mJm^{-2}}$ without plateauing in the 2500 s timescale. The inset shows the expected surface tension of different volume fractions (concentrations) of pure glycerol in water. The surface tension decreases as the concentration of glycerol increases. Data from Takamura *et. al.* [92] and The Glycerine Producers' Association [93].

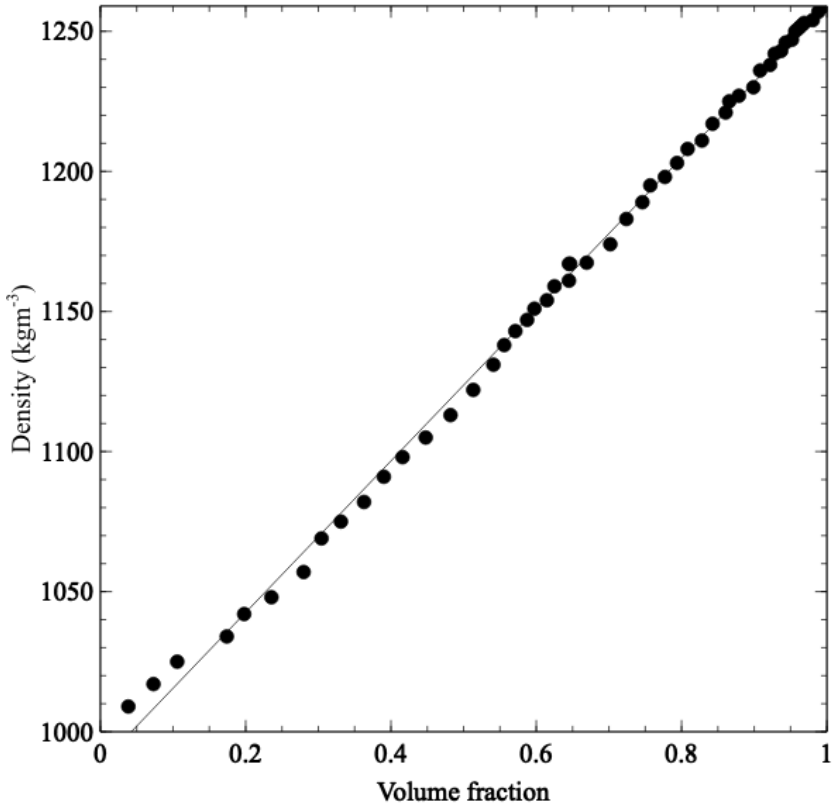

Figure 4.3: Plot showing the density of glycerol/water mixtures as a function of the glycerol volume fraction. This relation holds because the mass, and as a result of incompressibility, the volume, of glycerol do not change over the timescales of these experiments, so $\phi_1 V_1 = \phi_2 V_2$. Data were taken from Sheely [90] and measured at 20°C. The solid line is a linear fit to the data which has the equation $\rho = 988 + 270\phi$, where ρ is the density of the mixture and ϕ is the volume fraction.

Figure 4.2 shows that the surface tension of the drops varies with time in a manner that is almost independent of the drops' initial composition. Moreover, the surface tension varies over a range of values that is larger than that expected for glycerol/water solutions (Inset in Figure 4.2). If the changes in surface tension were caused purely by a change in composition of the drops then the surface tension values should vary in a range somewhere between that of pure water ($72\,mJm^{-2}$ [54]) and pure glycerol ($63\,mJm^{-2}$ [54]). The final values of the surface tension obtained from these experiments were as low as $\sim 40\,mJm^{-2}$. Given that the drop vibration technique has already been shown to be a viable method of determining surface tension [14, 32, 45], this would seem to suggest that some contamination of the surface of the drops is occurring during the experiments. The fact that the kinetics associated with the changes in surface tension are similar for all the droplets studied regardless of their initial compositions is also consistent with the presence of surface contamination.

Contamination of the drop surface could have occurred either as a result of contact with the substrate or as a result of deposition of airborne contaminants. There was no visible evidence of surface contamination of the surface by soot particles from the substrate. However, submicron sized fragments of soot, TEOS or the fluorinated silane that was used to coat the candle soot could potentially have migrated across the surface of the droplets during the experiments. A series of simple tests were performed to determine whether this type of surface contamination was occurring. These simple tests were performed by filling a clean 20 cm diameter glass beaker with water and gently dusting the surface with talc. Fine syringe needles were either dipped in the silane of interest, or used to mechanically scrape some of the candle soot residue off the surface of the substrates being used. These syringe needles were then gently pushed through the talc coated water surface at the centre of the glass beaker.

In the case of both TEOS and the fluorinated silane, a hole formed in the talc layer and was observed to grow to the diameter of the glass beaker in less than one second. This gives a lower bound for the spreading rate of these molecules of around $10\,cm\,s^{-1}$. Spreading of TEOS or the fluorinated silane across the surface of the drops was therefore not responsible for the surface contamination observed in the drop vibration experiments. The time

scale associated with the contamination of the microlitre drops studied would be ~ 0.03 seconds for a drop with a profile length of $\sim 6\,\text{mm}$. This is at least four orders of magnitude smaller than the timescale associated with the surface tension changes shown in Figure 4.2 and indicates that the candle soot substrates contain no free surfactant like molecules that could contaminate the surface. However, there was still a possibility that particles of soot were able to break off from the surface of the substrate and contaminate the drop surface. A similar test, repeated with mechanically scraped soot from the substrate showed no discernible change in the talc layer over a period of 2000 s i.e. no hole was observed to form. While not entirely perfect, these simple tests suggest that the superamphiphobic substrates used in this work were mechanically and chemically stable on the timescales associated with the experiments and that they were not responsible for contaminating the drop surface. This would suggest that airborne contamination of the droplets surfaces is a more likely candidate for the surface tension changes observed in Figure 4.2.

Henderson and Miles [94] demonstrated that a clean water surface can become contaminated with low surface tension impurities such as organic deposits from the air on time scales of $\sim 5\,\text{mins}$ (300 seconds). Figure 4.2 shows that the surface tension of the glycerol/water drops changes on time scales of hundreds of seconds and falls below the surface tension of glycerol after ~ 300 seconds for all the compositions studied. Both water and glycerol have relatively high surface tensions compared to organic materials, which typically have $\gamma \sim 40-50\,\text{mJm}^{-2}$ [95]. It is therefore not unreasonable that contamination could occur as a result of the preferential adsorption of species with lower surface tension values on the drop surface. The fact that the surface tensions of the drops approached values similar to those associated with organic materials lends additional support to this argument.

The surface tension data in Figure 4.2 was plotted as a function of the instantaneous volume fraction of glycerol in the drop as shown in the inset in Figure 4.4. The initial values of the surface tension were found to agree with independent measurements of fresh solutions obtained using the pendant drop technique (white squares) before significant exposure to the air had occurred [18]. The agreement between the surface tension values at $t = 0$ and the pendant drop measurements gives us confidence that the technique is capable of measuring

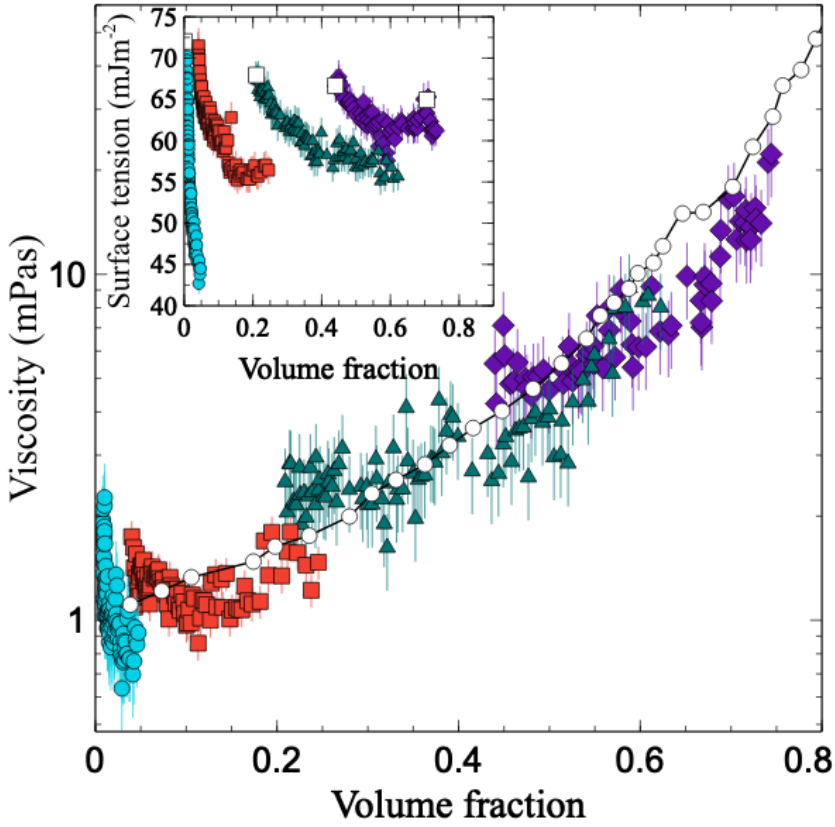

Figure 4.4: Composition dependence of the properties of glycerol/water solutions. The main panel shows the variation of the viscosity of glycerol/water solutions obtained during the evaporation experiments as a function of the glycerol volume fraction. Data are shown for droplets having initial compositions of 1 wt% (cyan circles), 5 wt% (red squares), 25 wt% (teal triangles) and 50 wt% (purple diamonds) of glycerol. The initial compositions correspond to glycerol volume fractions of 0.008, 0.04, 0.209 and 0.44 respectively. The white circles show results for the bulk viscosity of glycerol/water solutions obtained by Sheely [90] at 20°C. The majority of the evaporation data follows the trend of the bulk solution data, with greater deviation for lower concentrations. The inset shows a plot of the surface tension as a function of composition for the same droplets. The white squares in this plot are the results of pendant drop measurements of the surface tension obtained from clean solutions, prior to contamination from the air (see text). While the initial surface tension of the evaporating solutions correspond with bulk measurements, as evaporation occurs the surface tension significantly deviates from these values.

the correct surface tension values for the initially uncontaminated drops. However, as time progresses and the exposure to air increases, the surface tension values obtained during the drop vibration experiments deviate from those obtained for clean solutions.

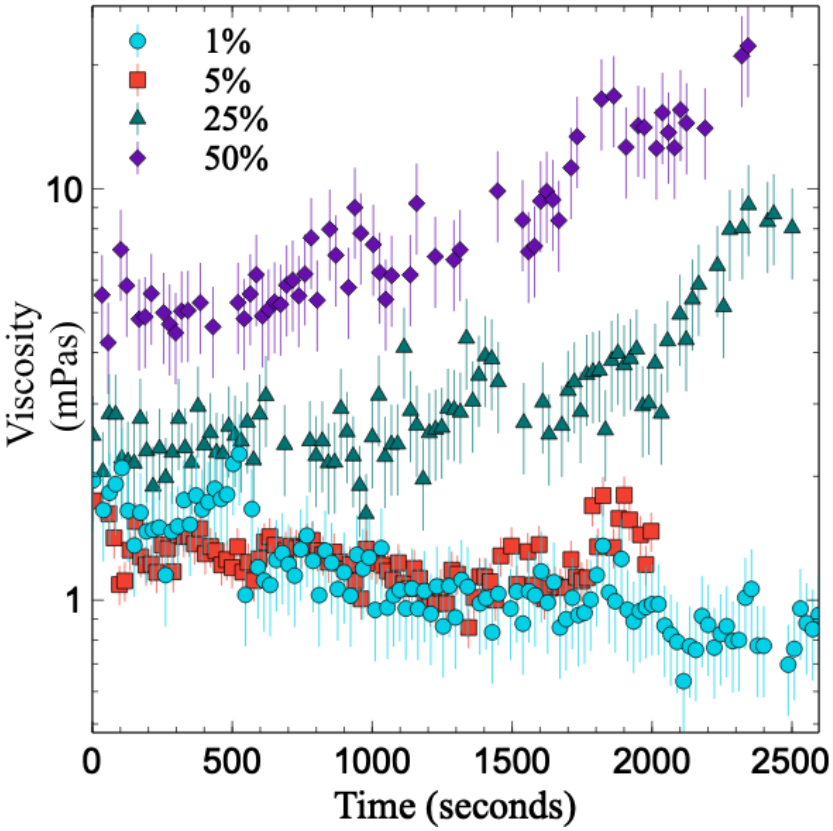

Figure 4.5: A plot of the time dependence of the viscosity of evaporating glycerol/water solutions. Data are shown for four droplets of similar size having initial compositions of 1 wt% (cyan circles), 5 wt% (red squares), 25 wt% (teal triangles) and 50 wt% (purple diamonds) of glycerol. The initial compositions correspond to glycerol volume fractions of 0.008, 0.04, 0.209 and 0.44 respectively. The viscosity increases as starting concentration increases. Over time the viscosity of the 25 wt% and 50 wt% solutions increases, whereas that of 1 wt% decreases and 5 wt% exhibits very little change.

Figure 4.5 shows how the viscosity of the droplets varies as a function of time. Unlike surface tension, viscosity is a bulk property and should therefore be unaffected by the surface contamination effects discussed above. The plots in Figure 4.5 show that the initial viscosity obtained using Equation 3.9.4 increased

with increasing glycerol composition of the drops. Moreover, for the two highest initial glycerol/water compositions studied (25 and 50 wt% glycerol), the viscosity was observed to increase further as the droplets evaporated and the glycerol composition increased – the range of values obtained being bounded by the viscosities of pure water (1 mPas) and glycerol (1 Pas).

To determine whether the values of viscosity shown in Figure 4.5 are consistent with values expected for the composition of the drops, the same data was plotted in the main panel of Figure 4.4 against the corresponding instantaneous volume fraction of glycerol in the drops. Values obtained from Sheely [90] for bulk glycerol/water solutions at a temperature of 20°C are also shown for comparison (white circles). The majority of droplet data is shown to agree with the bulk solution viscosity data within the limits of experimental uncertainty. Any small deviations of the drop vibration data away from the bulk data are believed to occur as the result of small temperature variations resulting from the environment not being temperature controlled during experiments (due to the air conditioning being turned off to prevent air circulation from inducing additional drop vibrations). Such a drift in temperature is likely to have caused the slight downward drift in viscosity with time observed for the two lowest initial compositions (0 and 5 wt%) shown in Figure 4.5 [96, 97]. The fact that the viscosities obtained for these two compositions are consistent with literature values, within the limits of experimental uncertainty (as shown in Figure 4.4), suggests that these data are representative of the glycerol water mixtures being studied. However, these data suggest that the changes in viscosity measured using the vibration techniques described above are more susceptible to variations in temperature for low glycerol concentrations – pointing to the need for greater temperature control.

Despite the small temperature related effects described above, the level of agreement observed between literature values and the volume fraction dependence of the viscosity shown in Figure 4.4 is encouraging. It demonstrates that the model described above captures the essential physics of drop vibration. It also demonstrates the validity of the assumption that volume changes in the drops are caused by the evaporation of water.

The automated approach to drop vibration described above provides an inexpensive method of simultaneously tracking changes in the surface tension and

viscosity of microlitre liquid droplets – regardless of whether they occur as the result of surface contamination effects or simply as a result of changes in composition of the drops. One limitation of the technique is that the composition dependence of the density is required to obtain the surface tension and dynamic viscosity of the solutions. However, the ratio of these quantities to the density can be obtained directly from the measurements. In the case of viscosity, this ratio is referred to as the kinematic viscosity.

A further limitation of this approach is that the size of the droplet must be smaller than the capillary length of the fluid for the assumptions made in deriving the dispersion relation in Equation 2.0.9 to hold. However, the requirement for a small sample volume is likely to be of benefit for studying expensive samples and samples where volumes are low (such as blood samples).

Caution should also be exercised when applying the results of the simple model derived here to drop vibration studies. The dispersion relation of Pleiner *et. al.* [60] was derived for capillary waves on the surface of an infinitely deep (viscoelastic) fluid. Application of this dispersion relation to curved droplet interfaces is therefore questionable. In the limit where the amplitude of surface deflections of the drops becomes small compared to their size/radius ($< 0.1R_c$) this approximation has been shown to hold. However, for larger amplitude vibrations and in cases where the contact region becomes depinned during vibration, the validity of this approximation becomes significantly weaker [65]. In such cases, more rigorous theories which consider a full expansion of the spherical harmonics associated with surface fluctuations of the droplets should be applied [26, 49, 98–100].

4.4 Conclusion

Automated light scattering measurements can be used to probe changes in the surface tension, viscosity and viscoelastic properties of multicomponent microlitre droplets simultaneously and in real-time. The viscosity and initial surface tension values obtained from drop vibration measurements of evaporating glycerol/water droplets were found to be in good agreement with data obtained from bulk glycerol/water solutions (using Section 3.8 and Figure 4.3). The simple apparatus described here is inexpensive and easy to implement. Its

portability lends it to applications in a broad range of settings including microfluidics devices, ambient, high pressure and ultra-high vacuum (e.g. ionic liquids) environments. Moreover, the ease with which this technique can be implemented lends itself to the study of a range of soft matter systems including (but not limited to) aggregating protein solutions, blood droplet rheology, gelation reactions, self-healing materials, viscoelastic polymer solutions and liquid crystals.

CHAPTER 5

Mechanical Vibrations of Viscoelastic Drops on Superhydrophobic Surfaces

5.1 Introduction

Mechanical vibrations of viscoelastic drops hold significant potential as a method of determining the frequency dependent flow (or rheological) behaviour of microlitre volumes of non-Newtonian fluids such as polymer solutions. Drop vibration has already been demonstrated as a viable approach to the measurement of simple liquid properties such as surface tension and viscosity in levitated [21–23], sessile [16, 30, 51] and pendant [14, 32] geometries. This was developed in the previous chapter for solutions whose properties change over time, via the continuous monitoring of evaporating solutions of glycerol in water (Chapter 4).

Measurements of the frequency and spectral widths of mechanical vibrational peaks are capable of providing information about the frequency dependent shear storage and loss moduli (G' and G'' respectively) of viscoelastic solutions such as polymer, biopolymer and protein solutions [15, 28, 40, 42, 58]. If the vibrating drop is considered as a damped harmonic oscillator, then the frequency of vibration should be related to its effective spring constant and hence the storage modulus and surface tension of the material. At the same time, the width of the resonance provides information about viscous damping

in the drop which is determined by the loss modulus. The drop size can be varied to probe the mechanical response at different frequencies [51].

A key advantage of using drop vibration (rather than conventional rheometry) is that it provides access to higher frequencies for weakly viscoelastic materials. In conventional rheometry, inertial effects associated with the instruments tend to dominate the measurements at high frequencies and it becomes difficult to extract G' and G''. Although higher frequencies can be accessed using techniques such as microrheology [101] and piezorheometry [19], the low cost, low sample volume, portability and ease of implementation of the drop vibration technique make it much more attractive.

This chapter demonstrates that the frequencies and widths of the mechanical vibrations of viscoelastic drops supported on hydrophobic substrates can be used to extract values of the frequency-dependent storage and loss moduli. This study is the first combined experimental and theoretical study of the vibration of sessile viscoelastic drops. As such, it represents a significant step forward in our understanding of the drop vibration phenomenon and our ability to measure the rheological properties in small sample volumes ($\sim$ µL to mL) – as is often the case with biological samples.

5.2 Method

Microlitre drops of poly(acrylamide-co-acrylic acid) (PAA) in water (prepared at concentrations of 1.1, 2 and 3 wt% using the technique described in Section 3.1) were placed individually on to superhydrophobic substrates (Section 3.2 [64]) and vibrated as described in Section 3.3. Laser light was used to monitor drop vibration (see Section 3.6) and extract the frequency, f, and width, Δf, of the fundamental mode of vibration. The resonant frequencies and widths of vibration were found to depend on the size of the drops and their physical/mechanical properties. These experiments took less than one second to perform, so the drops would lose $\ll$1 g to evaporation over these timescales (see Section 3.1.1). These experiments were performed within 3 months of solution manufacture.

The physical dimensions of the drops – in particular their profile lengths, l, were measured using the technique described in Section 3.5 (Figure 3.6a). The density, ρ, and surface tension, γ, of the PAA solutions were measured as described in Section 3.8 and are shown in Figure 5.1.

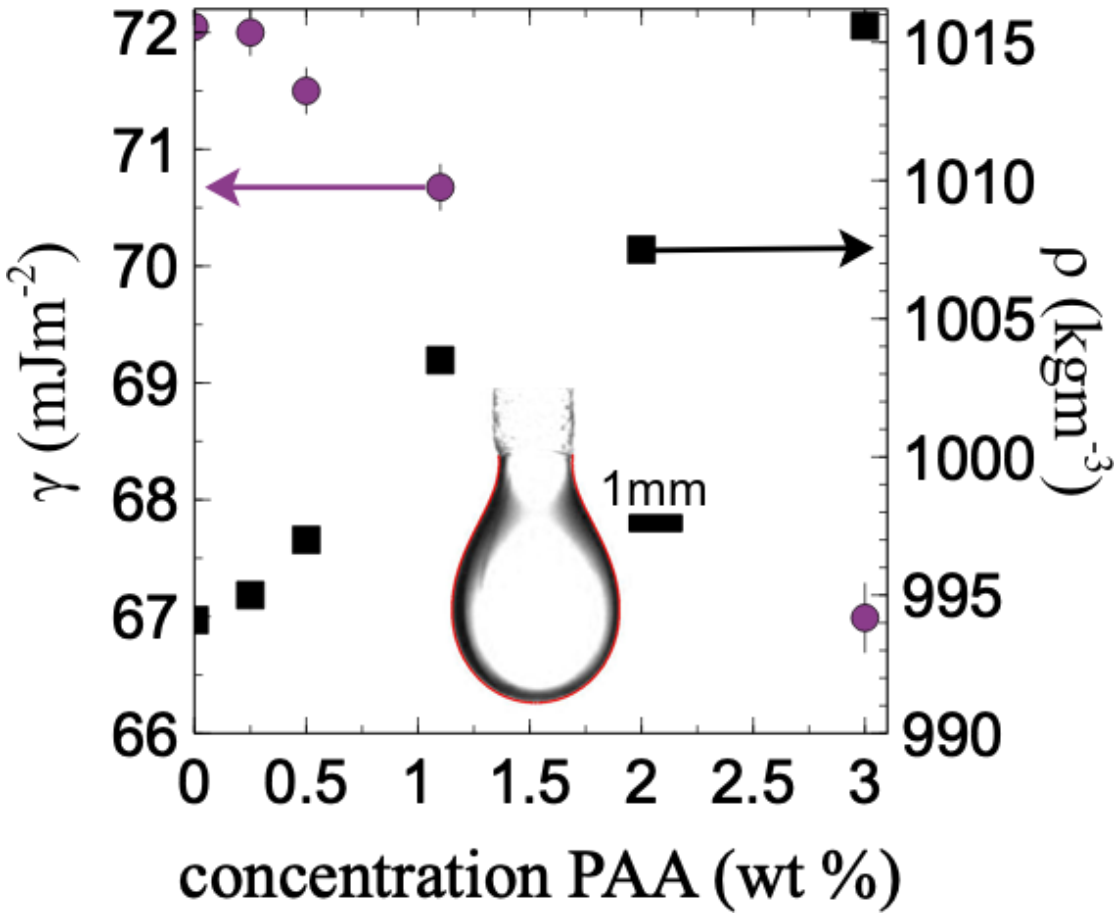

Figure 5.1: Concentration dependence of the surface tension (purple circles) and density (black squares) of the viscoelastic solutions. The inset shows an image of an elongated pendant drop that was used to determine the surface tension of the viscoelastic fluids using axisymmetric drop analysis [18]. The red line on this image is the fit obtained when extracting the surface tension.

5.3 Results and Analysis

Figure 5.2 shows plots of the frequency and width of the lowest frequency vibrational peak obtained in the drop vibration experiments. These data are

shown as a function of the drop profile length for PAA solutions with concentrations in the range 1.1 - 3 wt% , corresponding to drop volumes ranging from 1 to 20 µL. As the polymer concentration is increased, both the frequency and width of all the vibrational peaks increases. This is consistent with an increase in stiffness (from both viscous and elastic sources [102]) and a greater viscous damping in the drops with increasing polymer concentration. This stiffening occurs despite the decrease in surface tension and points to the fact that other material properties are influencing the vibrational response. It is therefore important to extract the shear storage and loss moduli of a solution to fully understand its vibrational response.

In order to interpret the data shown in Figure 5.2 in a more quantitative manner, it is necessary to relate the frequency, f, and width, Δf, of vibrational peaks to the drop size as well as to G' and G''. This was done using the simple model of viscoelastic drop vibration described in Section 3.9 (Equations 3.9.1 and 3.9.2 respectively). Figure 5.3 shows plots of the values of G' and G'' obtained from the drop vibration data using these expressions – the G' and G'' values are plotted against the vibrational frequencies of the drops as this sets the frequency of the measurement probe. For these pinned drops, a value of n=2 was assigned to the fundamental mode of vibration [16, 26, 30].

Microrheology measurements of the same PAA solutions used in the drop vibration experiments were collected as described in Section 3.10 [86, 101, 103]. These microrheology measurements were used to obtain an independent measure of the G' and G'' values (solid lines in Figure 5.3) over the same frequency range used in the drop vibration experiments (10 - 300 Hz) – a range that is not accessible for these weakly viscoelastic solutions using conventional rheological techniques. In each case, the G' and G'' values were found to agree for each particle size studied (see Figure 5.3). The G' and G'' values obtained using different particle sizes were averaged to obtain the final values for each PAA concentration.

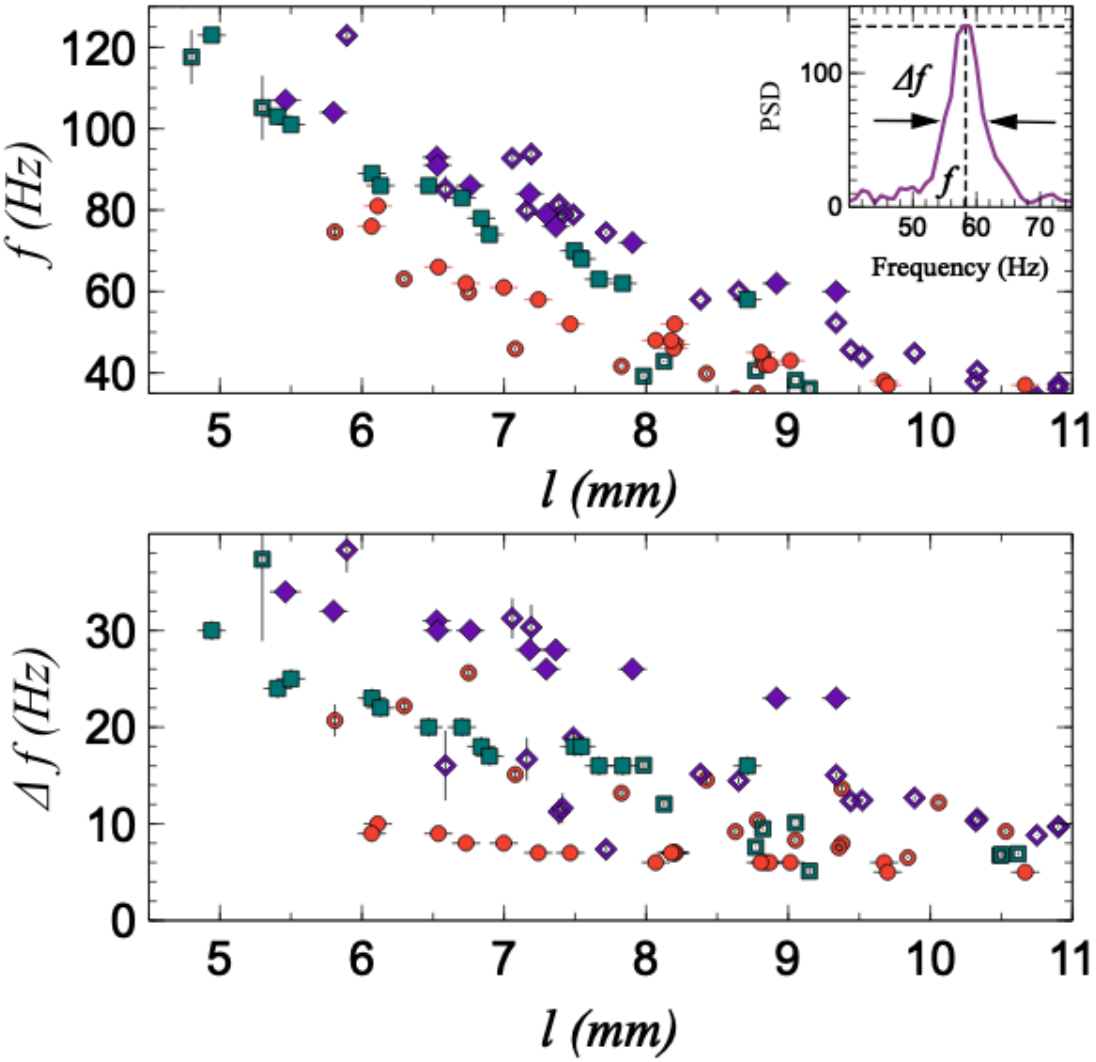

Figure 5.2: Plots of the vibrational frequency (f) and spectral width (Δf) as a function of the drop profile length (l). Data are shown for the lowest vibrational mode of drops of 1.1 wt% (red circles), 2 wt% (teal squares) and 3 wt% (purple diamonds) PAA in water. The inset in the top panel shows how f and Δf are defined. The frequency and width of vibration both decrease as drop size increases. Overall, the frequency and width of vibration increase as the concentration of PAA increases.

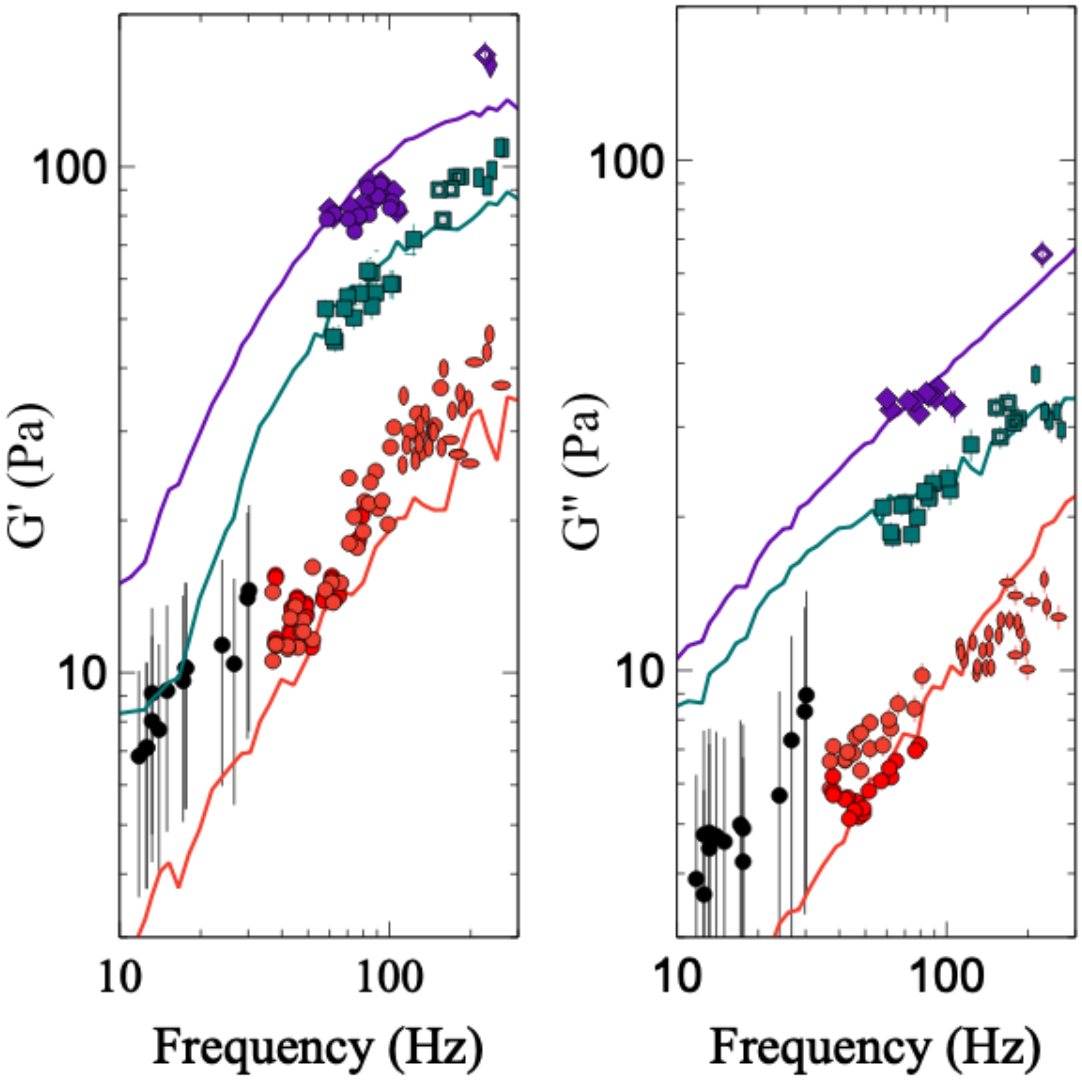

Figure 5.3: Rheological properties of vibrating drops. Values of G′ (left panel) and G″ (right panel) were calculated by inserting measured values of f, Δf, l, ρ and γ in Equations 3.9.1 and 3.9.2 (Chapter 3). The values of G′ and G″ are plotted against the vibrational frequency for ∼10 - 12 drops per concentration. Data are shown for 1.1 wt% (red circles), 2 wt% (teal squares) and 3 wt% (purple diamonds) PAA in water and represent the average taken from 2 - 3 measurements per drop. The different modes of vibration are plotted as separate symbols. These are $n = 2$ (solid), 3 (hollow), 4 (vertically stretched symbols) and 5 (horizontally stretched symbols). The black circles show results obtained from magnetically levitated drops of 1.1 wt% PAA similar to those described by Temperton *et. al.* [15]. The solid lines are the results obtained from microrheology studies of the PAA solutions.

5.4 Discussion

The plots in Figure 5.3 demonstrate agreement between the drop vibration technique and microrheology. This agreement is better for higher concentrations of PAA than for the 1.1 wt%. The values obtained are also in agreement with previous results obtained from levitated drop studies of PAA solutions similar to those described by Temperton *et. al.* [15] (see Figure 5.3). However, despite the level of agreement, it is worth stressing that the model applied to describe the drop vibration phenomenon is simplified as curvature and the finite size of the drop may modify the dispersion relation (Equation 2.0.9) used to describe drop vibration. The simplified model used may account for the differences between the drop vibration data and microrheology in e.g. the slope of the G″ data for the 1.1 wt% PAA data in Figure 5.3.

The use of the semi-infinite medium assumption for the drop can, in part, be justified because the radius of the drops was typically an order of magnitude larger than the observed amplitudes of vibration (amplitudes of vibration were measured to be <16% of the drop radius). Also, the fact that very little of the interfacial area is in contact with the substrate means that the near spherical drops experience little substrate damping [16]. For larger amplitude vibrations (approaching the size of the drops) and or shallower three phase contact angles, the validity of this approximation is likely to break down. A rigorous theory of drop vibration would require correct expansion of the spherical harmonics of the drop and the application of appropriate boundary conditions associated with the presence of the drop interfaces.

The theory described above is also valid for droplets with radii that are smaller than the capillary length $l_c = \sqrt{\frac{\gamma}{\rho g}}$ (~ 2.7 mm for the solutions studied here, where γ is the surface tension of the drop, ρ is the solution density and g is the acceleration due to gravity). For drops larger than l_c an additional term of the form $\rho g k$ (where k is a wavevector magnitude) would need to be added the right hand side of Equation 2.0.9 to account for the effects of gravity on the drops [51]. In addition, there are limits on the values of G′ and G″ that can be measured with this technique. As both G′ and G″ depend upon f, Δf and l, there is some scope for choosing an appropriate drop size that will enable these quantities to be determined. However, practical considerations,

such as the time resolution of the data collection, mean that there are limits on the sampling frequency that can be used to measure the drop vibrations, and the level of damping that can be present in the drops before the oscillations become critically damped, i.e. damped faster than can be measured. The range of frequencies that can be accessed is limited by the size range of the drop (due to the relation $l = \frac{n\lambda}{2} = \frac{nv_\lambda}{2f}$, where v_λ is the wavespeed on the drop) and external noise impacting photodiode measurements. Camera and calibration resolution limit the smallest drop size that can be measured to approximately 1 mm.

For the experimental setup used here, the highest frequency of vibration that could be measured is around 500 - 1000 Hz depending on the sampling frequency used, and whether multiple modes of drop vibration were observed. When only the fundamental mode could be isolated, the practical limit was reduced by difficulties exciting vibrations on the surface of small sessile drops, as well as noise from environmental oscillations becoming more difficult to distinguish from the rapidly damped high frequency drop vibrations. Assuming that the drop has the largest radius possible before gravitational effects start to become important i.e. $R = l_c$, the corresponding profile length would be $l \sim 2\pi l_c$. This gives an upper limit for G′ of order ~ 70 kPa for fluids of this kind according to Equation 3.9.1. However, this could be extended further if higher sampling rates and larger drops were used while accounting for the effects of gravity as discussed above.

In the case of G″, the limiting factor is the droplet damping as it becomes difficult to measure the width of the resonant peaks when damping becomes too large. Larger drops tend to give better results as small drops tend to have larger spectral widths (shorter damping times) – a result that is consistent with measurements of the dynamics of liquid air interface oscillations in microbubbles [104] and simple liquids [16, 30, 32].

In obtaining an approximation to the upper limit for G″, the width of the peak has been set to be comparable to the vibration frequency of the drop i.e. $f \sim \Delta f$ such that the peak becomes very broad and almost indistinguishable as a peak. According to Equations 3.9.1 and 3.9.2, this should give a similar theoretical upper limit for $G'' \sim 70$ kPa to that obtained for G′ when using the setup described here. However, caution must be exercised when analysing data

from very broad vibrational peaks, as both G′ and G″ may vary strongly over the range of frequencies spanned by such peaks and the simple dependence described by Equations 3.9.1 and 3.9.2 will therefore be invalid.

Previous measurements of drop vibration in glycerol/water mixtures [16] and other simple liquids [32] have been used to extract viscosities between $1\,\text{mPas} < \eta < 1\,\text{Pas}$ with relative ease at frequencies up to 100 Hz ($G'' = 2\pi f \eta \sim 0.63 - 630\,\text{Pa}$). Hence the upper limiting value of G″ is expected to lie somewhere in the range 1 - 70 kPa for the experimental setup described here.

5.5 Conclusions

In the absence of a complete theory of viscoelastic drop vibration, the heuristic approach adopted here provides a reasonable description of the rheological properties of viscoelastic solutions; even for µL sized droplets. The fast, simple and non-invasive technique described lends itself to the measurement of liquid and viscoelastic properties in a range of different environments (ambient, high pressure, ultrahigh vacuum e.g. ionic liquids) and avoids the need for complex, bulky levitation apparatus. In contrast to Chapter 4, the drops were not observed to be contaminated on the shorter timescales involved in these experiments.

CHAPTER 6

Video Capture of Oscillating Pendant Drops

6.1 Introduction

In previous chapters, the vibrational properties of evaporating viscous drops and stable (not evaporating) viscoelastic drops on superhydrophobic surfaces were studied. While these experiments were an improvement on levitated drops (which require expensive equipment to produce) they still present their own problems because of the need for a superhydrophobic substrate. These substrates are not readily available and can be difficult to produce (Section 3.2) [64]. One way to circumvent these difficulties is to use sessile drops on surfaces with contact angles $<180°$. However previous work has shown that using drops with small contact angles introduces additional damping mechanisms and extracting the rheological properties is extremely difficult [16, 30]. A potentially more attractive way of accessing rheological properties involves the use of pendant drops, where a drop is suspended from a pipette, and a relatively small proportion of the drop is in contact with a solid surface, the rest of the "substrate" being a liquid reservoir within the pipette tip (Figure 6.1, see also Section 3.4). This results in less energy dissipation from the solid-liquid interface than if the entire substrate were a solid, and vibrational behaviour similar to that for levitated drops [32]. In this geometry, large pendant drops can also be used to extract the surface tension (Section 3.8) of the fluids at long times, and provide this important parameter for use in the equations that are used in the calculation of the shear storage and loss moduli (G' and G''

respectively) of the viscoelastic solutions (Equations 3.9.1 and 3.9.2). These equations were derived for levitated spherical drops, but provide a useful starting point for pendant drops, for which additional damping factors (due to the presence of the pipette tip) may need to be taken into account (Chapter 2).

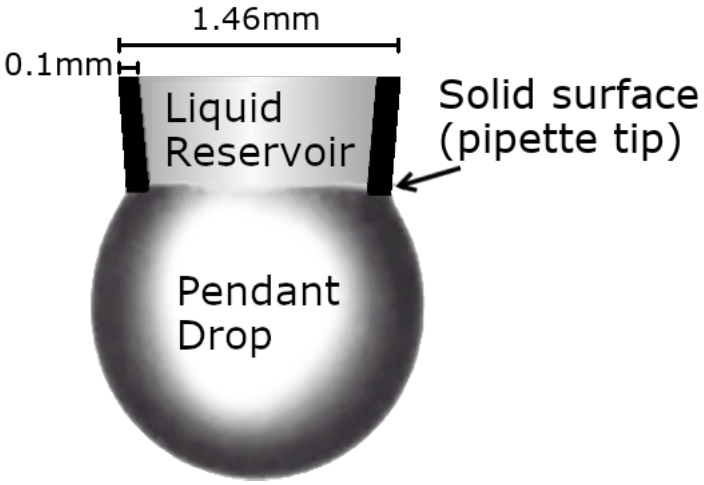

Figure 6.1: The image shows a cross-section of the "surface" from which a droplet of 2wt% PAA in water (with profile length 4.4mm) hangs. The surface consists of a liquid reservoir surrounded by solid walls formed by the pipette tip. The pipette tip diameter is $\sim$1.46mm, with tip walls $\sim$0.1mm wide.

In this chapter, pendant drops of poly(acrylamide-co-acrylic acid) solutions were suspended from polypropylene pipette tips, and their vibrational motion tracked using a camera. The resulting motion of the drops was used to extract the vibrational frequency and damping of drop motion. These parameters were used in a similar method to that previously described (Section 3.9) in an attempt to extract the rheological properties of the fluid. Images of elongated drops of the same fluids were also used to extract the surface tension.

6.2 Method

Using the technique described in Section 3.1, solutions of poly(acrylamide-co-acrylic acid) in water were made up to concentrations of 1.1, 2 and 3wt%. Droplets were suspended from a pipette tip and vibrated using the techniques described in Section 3.4. Drop vibration was monitored as described in Section

3.7. These experiments took less than one second to perform, so the drops would lose $\ll 1\,g$ to evaporation over these timescales (see Section 3.1.1). Two batches of solutions were prepared for these experiments. Experiments were performed on the first batch, which was the same batch used for Chapter 5, over the course of 12 months. The second batch was used within 2 months of manufacture.

The profile lengths, l, of the drops were measured using the technique described in Section 3.5 (Figure 3.6b). The density, ρ, and surface tension, γ, of the PAA solutions were measured as described in Section 3.8. For these pendant drop experiments, the surface tension measurements could be taken without setting up any additional equipment.

The measured frequency, f, and width, Δf, of vibration were used to calculate the shear storage, G', and loss, G'', moduli as described in Section 3.9 (Equations 3.9.1 and 3.9.2 respectively) using the surface tension and density values shown in Table 3.1.

These equations are approximations, valid for semi-infinite viscoelastic layers, and large spherical droplets as explained previously in Chapter 2. Given the previous successful use of these equations (Section 5.3), it is informative to determine how well they might predict the viscoelastic properties of pendant drops. The G' and G'' data obtained using Equations 3.9.1 and 3.9.2 were plotted as a function of oscillation frequency of the individual drops and compared to microrheology data (Section 3.10) for the solutions studied here.

The pipette tip was noted to continue to vibrate at low amplitudes $< 0.05\,mm$ (after the initial impulse) and low frequency ($< 10\,Hz$) during these experiments. Drop position measurements were therefore taken relative to the tip position (as described in Section 3.7) rather than relative to the camera.

6.3 Results and analysis

6.3.1 Vibration Data

Figure 6.2 shows plots for the frequency and width of the lowest vibrational peak obtained in the pendant (solid markers) and sessile (hollow markers)

drop vibration experiments (Section 5.3). These data are shown as a function of the drop profile length for PAA solutions with concentrations in the range 1.1 - 3 wt%. Using the relationships $f \propto Al^{-\frac{3}{2}}$ from the Noblin equation (Equation 2.0.5) and $\Delta f \propto Al^{-2}$ from Sharp (assuming bulk viscous damping dominates [16], Equation 2.0.7), the lines in Figure 6.2 show fits calculated with 95% confidence applied to the sessile (thick lines) and pendant (thin lines) drop data. Table 6.1 shows the fits acquired for the sessile and pendant drop frequency data. Table 6.2 shows the fits acquired for the sessile and pendant drop width data.

Conc.	Sessile Frequency fn.	Pendant Frequency fn.
1.1%	$f = 1.3+1105\,l^{-1.5}$	$f = -10.8+547\,l^{-1.5}$
2%	$f = 11.3+1183\,l^{-1.5}$	$f = -10.2+579\,l^{-1.5}$
3%	$f = 20.0+1151\,l^{-1.5}$	$f = -15.4+759\,l^{-1.5}$

Table 6.1: Fit functions (calculated with 95% confidence) for the dependence of sessile (obtained in Section 5.3) and pendant drop frequency (f) data on profile length (l) for 1.1, 2 and 3 wt% PAA in water.

Conc.	Sessile Width fn.	Pendant Width fn.
1.1%	$\Delta f = 2.8+208\ l^{-2}$	$\Delta f = -1.0+280\,l^{-2}$
2%	$\Delta f = 6.6+541\,l^{-2}$	$\Delta f = -0.7+243\,l^{-2}$
3%	$\Delta f = 16.2+553\,l^{-2}$	$\Delta f = -3.9+459\,l^{-2}$

Table 6.2: Fit functions (calculated with 95% confidence) for the dependence of sessile (obtained in Section 5.3) and pendant drop width (Δf) data on profile length (l) for 1.1, 2 and 3 wt% PAA in water.

As the polymer concentration was increased, the frequency of the fundamental mode increased, although at a different rate than that observed for sessile drops of the same solutions in Section 5.3. This behaviour is consistent with an increase in stiffness of the drops, either as a result of increasing surface tension or bulk elastic effects. Given that the surface tension is known to decrease with increasing PAA concentration (see Table 3.1), this increased stiffness is likely to arise from changes in the bulk rheology of the fluid.

The data obtained for the width of the vibrational peaks increases between 2% and 3%. However the 1.1% width has a wide spread and overlaps both the 2%

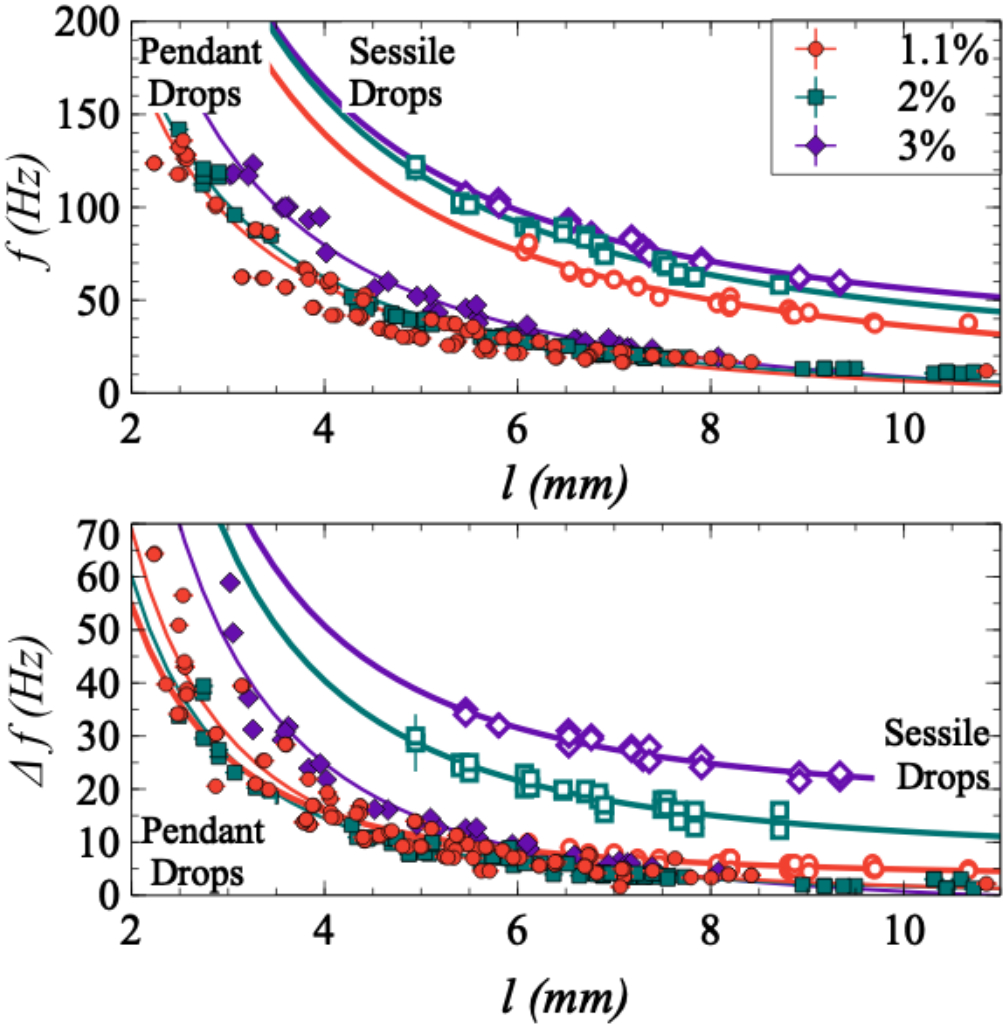

Figure 6.2: The upper panel shows a plot of the vibrational frequency, (f), of pendant drop vibration as a function of the drop profile length, l. The lower panel shows a plot of the spectral width, (width, Δf), of pendant drop vibration as a function of the drop profile length, l. Data are shown for the lowest vibrational mode of drops of 1.1 wt% (red circles), 2 wt% (teal squares) and 3 wt% (purple diamonds) PAA in water. Hollow markers show the sessile drop data obtained in Section 5.3, which are approximately three times greater in f and in Δf than the pendant drop data for all data apart from the 1.1% width data. Fits (Tables 6.1 and 6.2) are shown for the sessile (thick lines) and pendant (thin lines) drop data.

and 3% data. This is contrary to expectations of rising width with increasing concentration (Section 3.6).

The sessile drop vibration frequency and width data from Chapter 5 were approximately three times higher (3, 3.4, and 3.6 times higher for 1.1%, 2% and 3% respectively) than the pendant drop frequency and width data for all concentrations apart from the 1.1% width data, which was the same magnitude as the corresponding sessile drop data (Figure 6.2). Alternatively, the profile length for sessile drops could be considered to have a multiple of two (1.9, 1.94, and 1.78 times higher for 1.1%, 2% and 3% respectively) difference in the calibration from that for pendant drops. Performing either of these adjustments has a similar impact on the data, with a slightly greater change of shape (compared to the sessile drop data) from a profile length adjustment. Evaluating Equations 2.0.5 and 2.0.7, this common factor of three difference may indicate an error in the profile length calibration, perhaps because of the higher likelihood for sessile drops to move from the calibrated position, or that a lower vibrational mode (n=1) could be present in the case of pendant drops. Since the pendant drops were observed to remain pinned during experiments and the PAA solutions were considered to be incompressible, the frequency and width data were extracted from what was initially believed to be the peaks corresponding to the same vibrational mode as that studied for sessile drops in previous chapters (n=2).

The anomalous behaviour of the width of the 1.1% pendant drops is unusual, and suggests that these samples may have experienced an additional damping mechanism that was not present for 2% and 3% pendant drops or for any of the sessile drops measured in Chapter 5. Sharp [16] discussed several sources of damping within sessile drops of glycerol in water. They examined the effects of bulk viscous damping, solid-liquid boundary layer damping, and damping caused by drop surface contamination. Bulk viscous damping occurs as a result of energy dissipation due to velocity gradients within a viscous fluid [56]. Solid-liquid boundary layer damping is caused by the no-slip/pinning condition at solid-liquid boundaries, which requires that fluid velocity must go from a finite value at the surface of the drop to zero at the substrate. More rapid decay of fluid velocities in a drop (relative to the bulk fluid) attached to a surface gives higher energy dissipation. Drop surface contamination produces an additional

energy dissipation mechanism at the liquid-air surface of the drop, and energy dissipated due to "friction" in adsorbed layers of molecules produces similar, but stronger, damping effects to boundary layer damping [16].

For drops with sizes smaller than the capillary length ($l_c \sim 2.7\,\text{mm}$ for the PAA solutions studied here), the pendant drop geometry is expected to be very similar to that obtained for sessile drops (see Sections 2.0 and 3.4) i.e. drop shape is not influenced by gravity [15, 32]. However, in contrast to a sessile drop, where much of the base of the drop is in contact with a substrate, only a small proportion of a pendant drop was in contact with a solid surface (Figure 6.3). As a result, boundary-layer damping effects should have a much smaller impact on pendant drop motion than Sharp [16] found for sessile drops. Temperton *et. al.* [32] found the damping effects on (viscous) simple liquid pendant drop vibrations to be similar to those for levitated drops and used bulk damping to successfully describe decay of oscillations.

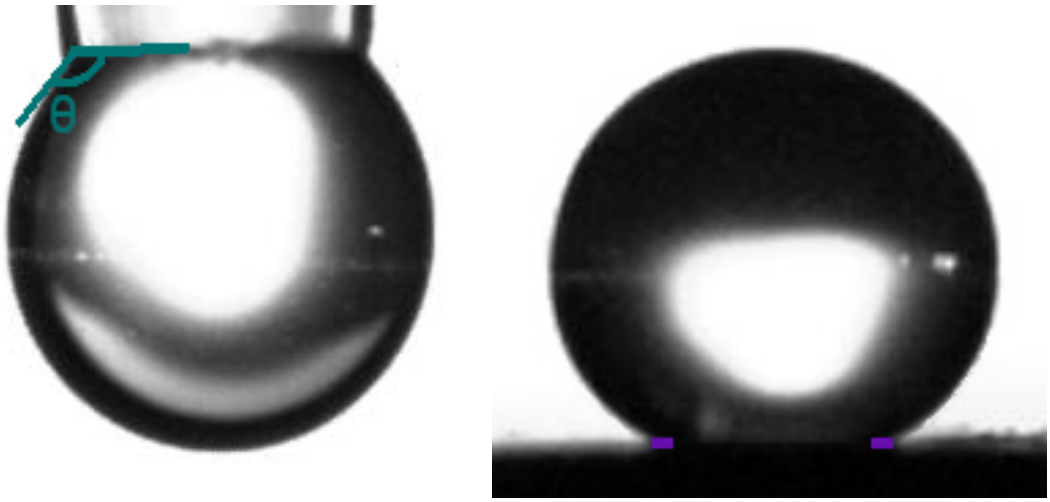

Figure 6.3: Images of 2% PAA in water as a pendant drop (first panel) and a sessile drop (second panel) on a candlesoot substrate [64]. Both drops have profile length of 5.4 mm. Purple marks indicate the equivalent position of the pipette tip walls. The solid-liquid contact area for the sessile drop is ~4.5 times that for the pendant drop. The contact angle, θ, of the pendant drop is defined as the angle between the pipette tip base and the tangent to the drop profile at the tip surface, as indicated by the teal lines.

It is unlikely that the spread in the spectral width of the lowest order vibration mode of 1.1% PAA is due to boundary-layer damping. The presence of the liquid reservoir increases the volume over which bulk viscous damping may

act beyond that of just the drop, i.e. fluid velocities can continue to decay into the pipette, giving something which looks much more like bulk damping of capillary waves on an infinitely deep liquid bath [32]. In this system, fluid velocity gradients are able to decay over larger distances and so are smaller. This reduces energy dissipation when compared to a sessile drop where velocity gradients are much steeper because of the presence of the substrate. Increasing the viscosity should increase the dominance of bulk damping.

Sharp [16] found that boundary layer damping dominates at contact angles lower than $\sim 38°$, but only for low viscosities ($\eta \leq 10.07\,\text{mPas}$). At higher viscosities bulk damping dominated regardless of the contact angle. Pendant drops have a high contact angle ($\sim 133°$, as defined in Figure 6.3 and Section 3.5) and drops of low viscosity (1.0, 3.3 and 9.7 mPas) were found by Temperton *et. al.* [32] to behave in a similar way to levitated drops, meaning that they were unaffected by boundary layer damping.

Previous experiments with glycerol in water (Chapter 4) indicated contamination of the drop surfaces with organic compounds over timescales of $\sim 5\,\text{mins}$ (300 seconds). Henderson and Miles [94] demonstrated $\sim 300\,\text{s}$ to be the time scale over which a clean water surface can become contaminated with low surface tension impurities such as organic deposits. The pendant drop experiments were performed in the same environment as the glycerol in water experiments. If the pendant drops were contaminated, it would be expected to be by the same contaminants as those which contaminated the glycerol in water drops, and the surface tension would be expected to drop to the same value as for glycerol in water. Drops were replaced between each experiment, leaving them exposed to the air for a maximum of 3 minutes, with measurements being taken within the first minute. Significant surface contamination is therefore unlikely to have occurred over the timescales of these experiments. The surface tensions of the PAA solutions were measured after the experiments (Table 3.1) and were found to be within $4\,\text{mNm}^{-1}$ of those measured previously for sessile drops of similar solutions (see Figure 5.1 in Section 5.3). This indicates a lack of surface contamination.

6.3.2 Shear storage and loss modulii

The frequency and width data in Figure 6.2 were converted to the shear storage (G') and loss (G'') moduli using Equations 3.9.1 and 3.9.2 (Figure 6.4), with surface tension and density values taken from Table 3.1, starting with the assumption that the peak observed in the vibrational spectrum corresponds to the n=2 mode, as for pinned sessile drops (Section 3.9), and that the profile length was correctly calibrated. It was found that the majority of the G' data was negative (first panel in Figure 6.4), and the non-negative values were ~ 10 times lower than the G' results for sessile drops (on superhydrophobic candle-soot substrates) and microrheology data (Section 5.3, Figure 5.3). Negative G' values are unphysical as a positive stress-strain response is expected for the solutions used [15].

The G'' data (second panel in Figure 6.4) clustered closely together and followed a steeper gradient, but were of a similar order of magnitude to the values obtained from microrheology data. The 1.1% solution data was higher than both the 2% and 3% data. Considering Figure 6.2, it is expected that the G'' result was significantly influenced by the anomalous width data for the 1.1% solutions according to Equations 3.9.1 and 3.9.2.

As discussed in Chapter 2, Equations 3.9.1 and 3.9.2 are approximations based on a semi-infinite liquid bath (i.e. without the presence of a solid-liquid boundary) and had previously only been applied to levitating spheres [15]. Sharp [16] showed that the presence of a surface can have significant impact on the damping of a vibrating drop, particularly for liquids with low viscosity. It might follow that the G' and G'' relations (Equations 3.9.1 and 3.9.2) would need to be adjusted to account for the additional damping mechanisms resulting from the presence of the surface and the size of the solid-liquid contact area relative to the drop size and viscosity. The presence of these additional damping mechanisms is likely to have greater impact on the accuracy of Equation 3.9.2 due to its stronger dependence on Δf which is a direct measure of vibration damping.

However, it is first beneficial to understand the source of the negative G' data, and to re-examine some of the initial assumptions above. Examining Equation 3.9.1, in which all the variables are positive, the term in the brackets must be the source of the negative G' values, i.e. $\frac{\pi\gamma n^3}{4\rho l^3(\Delta f^2+f^2)} > 1$. This suggests that

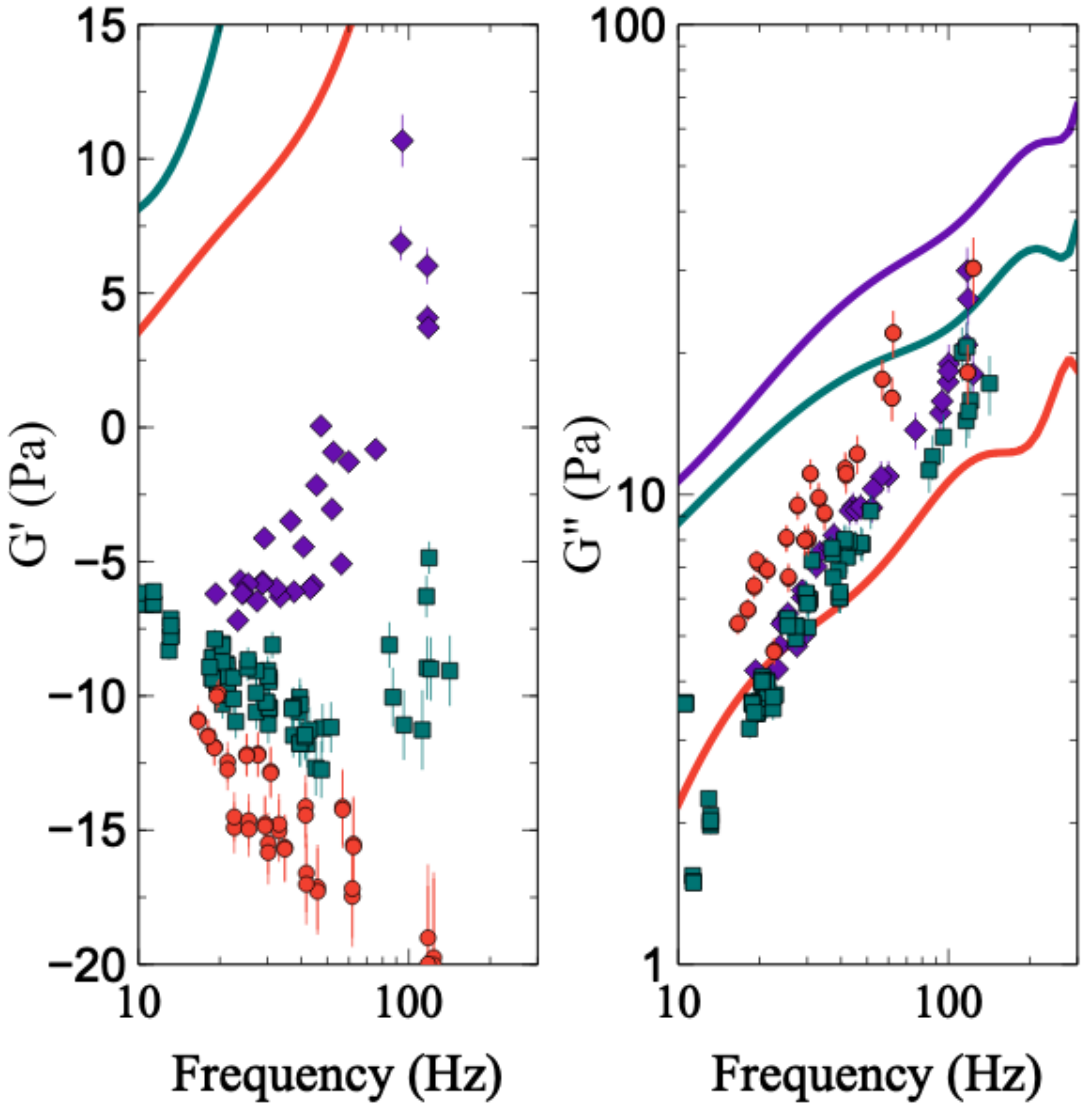

Figure 6.4: Rheological properties of vibrating pendant drops of 1.1 wt% (red circles), 2 wt% (teal squares) and 3 wt% (purple diamonds) PAA in water. Values for the shear storage (G′, left panel) and loss (G″, right panel) moduli (calculated by inserting measured values of f, Δf, ρ and γ into Equations 3.9.1 and 3.9.2, for the mode number n=2) for different concentrations of pendant drops of PAA in water vs oscillation frequency. Thick lines indicate fits to microrheology data obtained in section 5.3.

The majority of the G′ data are negative, with the exception of 3% data for frequencies > 100 Hz. G″ increases with frequency. 3% and 2% data are clustered together, with 1.1% above them.

either the surface tension values or the mode number assigned to the peak in the vibration spectrum are incorrect, or that the equations require significant reworking to describe the system.

The surface tensions were remeasured for these solutions and found to be in agreement with the values measured for sessile drops (Figure 5.1) so it is unlikely to be the surface tension values that are not correct. While sessile drops are able to migrate across a superhydrophobic substrate and the ruler (Section 3.5, Figure 3.6) must be carefully positioned accordingly, pendant drops remained pinned on the pipette tip and could be calibrated relative to the width of the tip. Image calibration is therefore assumed to have been more accurate for pendant drops than for sessile drops, but it was the pendant drop data which produced negative G'. An alternative solution presents itself in the form of the description of the drop motion. It is possible that using n=1, corresponding to centre of mass motion (top two panels in Figure 2.3), may improve the agreement with the sessile drop data. After all, the motion of the drops was observed to involve centre of mass motions and the majority of frequency and width data were lower for pendant drops than sessile drops in Figure 6.2. We discuss this possibility in further detail in the following section.

6.3.3 Compressibility

In the case of sessile drops, the n=1 mode was forbidden due to the incompressibility condition and pinning constraints [16, 26, 30] placed on the drop motion by the presence of the substrate. However, the pendant drops experienced compressibility within the system, as evidenced by the up and down motion of the liquid within the pipette tip, particularly if there was air trapped above the fluid within the pipette.

In the video analysis (see Section 3.7), the centre of mass oscillations of drops was used to extract the vibration of the pendant drops, so it is likely that the n=1 mode, which corresponds to centre of mass oscillations, was present. The n=1 mode may also involve volume changes, which were observed for some drops which moved into the pipette tip during vibration. However, the volume changes observed resulted in only a 5% error in the profile length.

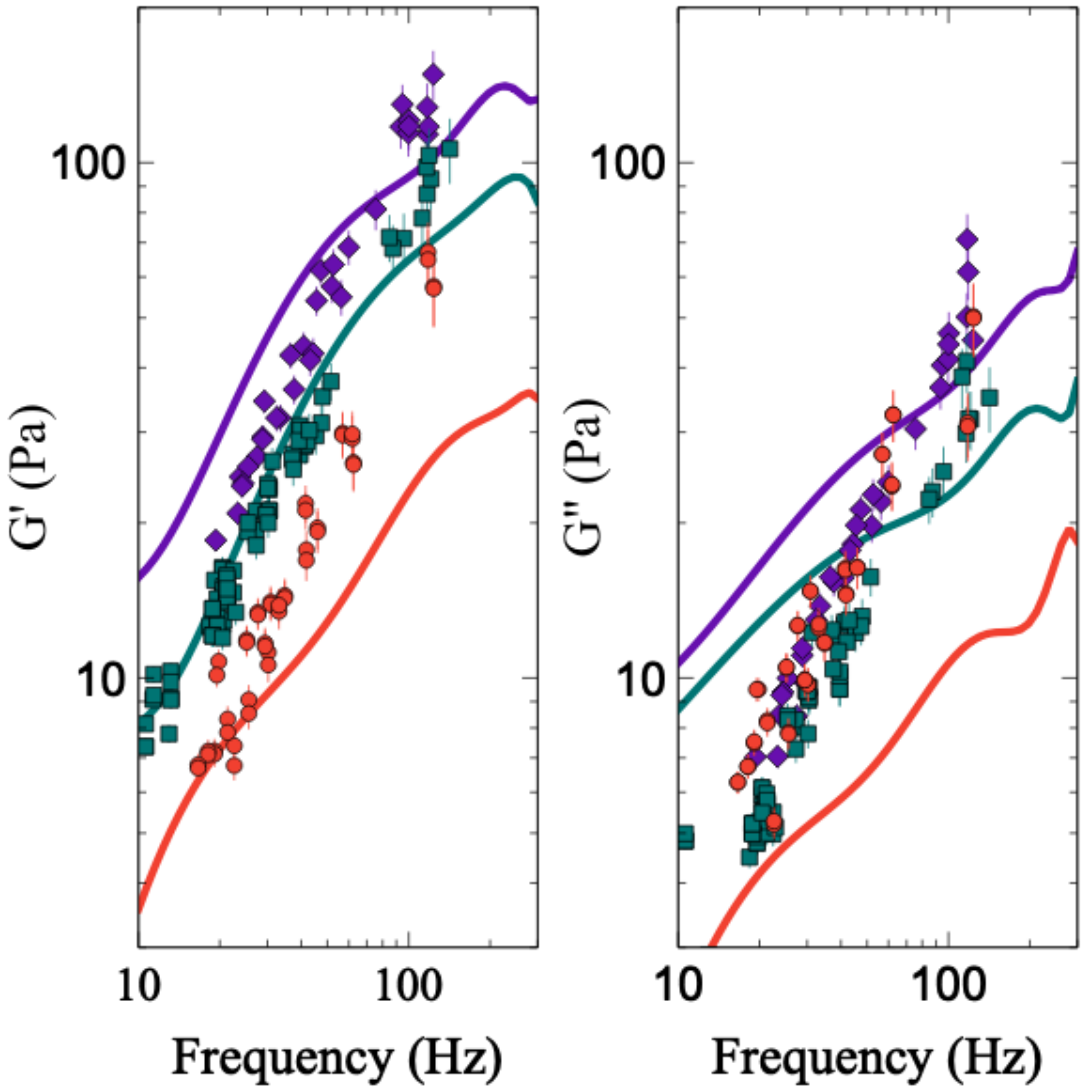

Figure 6.5: Rheological properties of vibrating pendant drops of 1.1 wt% (red circles), 2 wt% (teal squares) and 3 wt% (purple diamonds) PAA in water, with the mode number, n, set to 1. Values for the shear storage (G′, left panel) and loss (G″, right panel) moduli (calculated by inserting measured values of f, Δf, ρ and γ into Equations 3.9.1 and 3.9.2 with n=1) for different concentrations of pendant drops of PAA in water vs oscillation frequency. Thick lines indicate fits to microrheology data obtained in Section 5.3.

Setting n=1 in Equations 3.9.1 and 3.9.2, improved agreement significantly for G' (first panel in Figure 6.5) and removed all negative data. The order of magnitude for the G'' data was in agreement with the microrheology data obtained in Section 5.3 (second panel in Figure 6.5), however the data continued to follow the steeper gradient seen previously (second panel in Figure 6.4) than the data from microrheology experiments. The concentration data were clustered very close together, with that for 1.1% PAA overlapping both 2% and 3%.

There is still disparity between the pendant drop data and the microrheology data, particularly for 1.1% PAA. The factor of 3 difference observed in the 1.1% width in Figure 6.2 is presumed to be the result of additional damping mechanisms. Equations 3.9.1 and 3.9.1 both have a Δf dependence, so this factor of 3 is expected to impact both G' and G'' (although it is expected to have a greater impact on the G'' values). For Figure 6.6, the 1.1% width data was divided by a factor of 3 and input into Equations 3.9.1 and 3.9.2 with n=1 and all other data, including the 1.1% frequency, input as measured. The 2% and 3% G' and G'' data were used from Figure 6.5.

Figure 6.6 shows an improvement in the agreement between the 1.1% data and the microrheology data as well as a clearer separation between the different concentrations. Repeating the above analysis with the profile length multiplied by a factor of ~ 2 for the n=2 mode returns similar G' and G'' data, with the same damping factor present for 1.1%, however image calibration errors are assumed to be unlikely in the case of pendant drops. This suggests that the difference in magnitude between the pendant and sessile drop data was primarily the result of the different oscillation modes in each case, however the 1.1% width data highlights the presence of potential additional damping mechanisms that need to be accounted for. The pendant drop rheology data are not in perfect agreement with microrheology measurements, particularly for 3% PAA, however this is likely the result of the assumptions used to derive Equations 3.9.1 and 3.9.2 (Chapter 2).

Possible sources of damping that may impact 1.1% PAA but not 2% or 3% include bulk solution contamination, pipette contamination, reservoir surface contamination and increased dominance in reservoir damping.

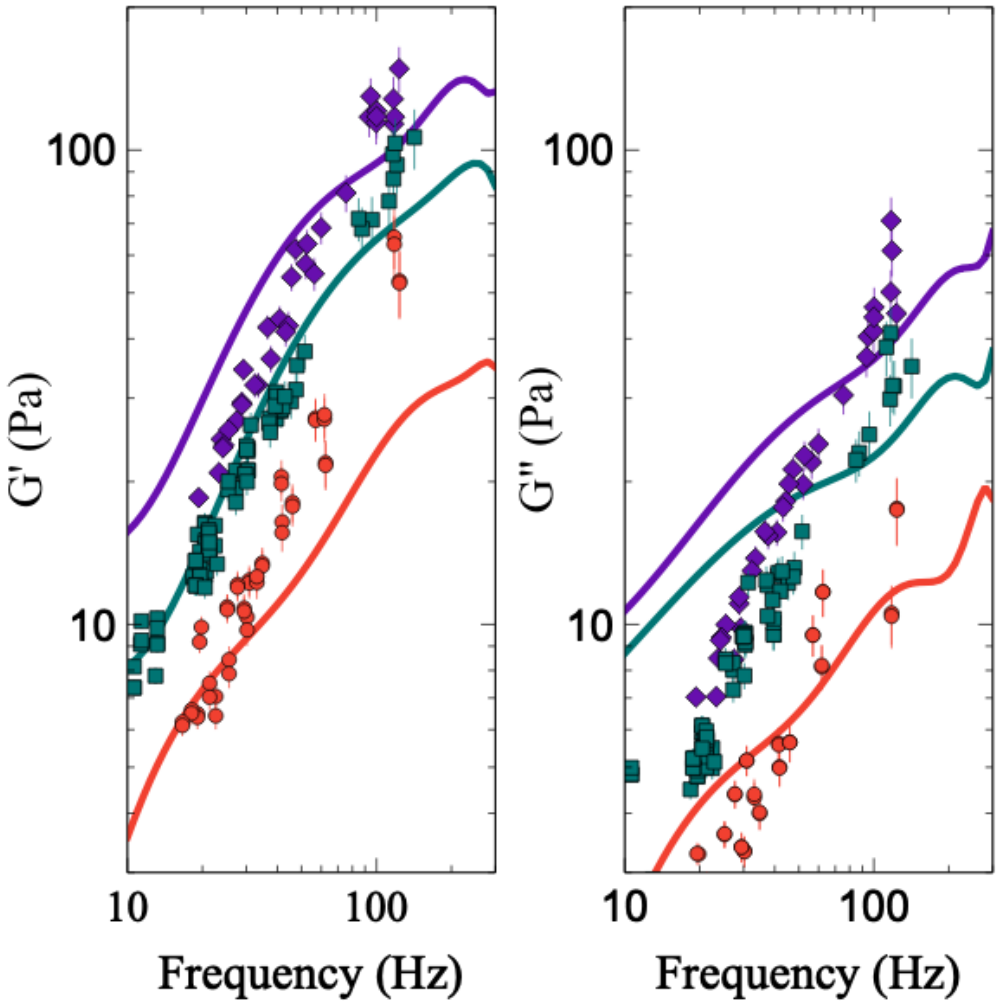

Figure 6.6: G′ and G″ calculated for n=1 with the 1.1% width data divided by 3 to fit the factor of 3 difference identified for all other frequency and width data. The fit is improved.

Bulk solution contamination would be expected to impact the frequency and surface tension of solutions, as well as the width. These experiments were carried out with both fresh and old solutions, and the surface tensions of both were measured. If both sets of solutions were impacted, the contaminant would be expected to also influence the 2% and 3% solutions, which were produced under the same conditions and within a day of one another.

Pipette tip surface contamination could result in contamination of the drop surface. Although contamination from air sources takes ~ 300 seconds [94], migration of contaminants from the pipette tip is likely to be faster. Tests were previously carried out (see Section 4.3) on the spreading rate of contaminants (TEOS, fluorinated silane, and candlesoot residue) over the surface of water. TEOS and the fluorinated silane were found to spread very rapidly (timescales of $\sim 0.03\,\mathrm{s}$ for a drop with a profile length of $\sim 6\,\mathrm{mm}$). If the pipette tips were contaminated, it is likely that the pendant drops would have been contaminated before measurement could begin (the duration of the pulse applied to the drops prior to measurement was $1\,\mathrm{s}$). At least 3 pipette tips were used for each concentration so such contamination would have to have affected multiple tips, in which case 2% and 3% would also be impacted.

Reservoir surface contamination may have been possible since the reservoir of fluid inside the pipette remained throughout experiment sets (3 sets of ~ 24 drops per concentration) and came into contact with the air between each drop ($< 15\,\mathrm{s}$ for the majority of drop changes). However, this should have resulted in the contamination increasing (and the agreement decreasing) as more drops were measured (and more opportunities were provided for reservoir contamination). Drop sizes were placed at random yet all of the 1.1% width data were affected, meaning that contamination did not increase between drops. This is an unlikely source of contamination unless the contaminant saturated the surface of the reservoir before the first drop was placed (within $30\,\mathrm{s}$). These timescales would also impact the drops and should be drop size dependent i.e. impact smaller drops faster/more strongly than larger drops. However the damping for 2% and 3% drops behaved as expected for these solutions, suggesting that they were unaffected by any such contaminants despite their high water content. The pipette tips were also taken from the same box, so prior contamination of the pipette tips themselves would be

expected to have influenced all experiments, some of which were made (for all concentrations) within the same day. This seems to be an unlikely solution to the problem.

Contamination of the liquid-air interface at the top of the reservoir may be more likely since the top of the reservoir was in contact with the air within the tip for ~ 30 minutes at a time. Once the reservoir was produced, the pipette was left alone, so the air inside the pipette was not subjected to changes in pressure and contamination should occur over timescales of 5 minutes [94] and should have a noticeable impact by the 6th drop. The pipette should be air tight in order to function, so contamination would be from air already in the pipette. Damping effects from the presence of any contaminants at the top of the reservoir are unlikely to have propagated through the reservoir to impact the vibration of the drop, unless the penetration depth for the solution was at least 5 times the radius of the drop.

The lower viscosity of 1.1% PAA in water, compared to 2% and 3%, increases the penetration depth (δ) of shear waves into the reservoir. As a result, the solid-liquid contact area and associated energy dissipation of 1.1% would be higher than for 2% and 3%. However, Temperton *et. al.* [32] successfully extracted the rheological properties of low viscosity (1, 3.3 and 9.7 mPas) drops with no evidence of boundary layer damping. The most notable difference (aside from the presence of elasticity) in the PAA pendant drops compared to Temperton's experiments is the presence of centre of mass motion resulting from the compressible air bubble above the reservoir. If the penetration depth were high enough, drop vibration might be influenced by the surface at the top of the reservoir and by boundary layer damping within the pipette tip.

The tips used in these experiments had an inner diameter $D_{in} \sim 1.26$ mm and tip wall thickness 0.1 mm. The solid-liquid contact area for penetration depths smaller than the drop radius (r) should be the area of the ring at the base of the tip, or 0.4 mm^2. As the penetration depth increases, the contact area "seen" by the vibrating drop should increase by $\pi D_{in}(\delta - r)$, i.e. 4 mm for every 1 mm increase in δ. This would result in a very rapid increase in boundary layer damping if the penetration depth was larger than the drop size.

Penetration depth is defined as the position for which wave amplitude is e^{-1} of the amplitude at the surface [105]. For viscous liquids, this is defined by

Equation 6.3.1 [56, 106]. Using this equation, the penetration depth of surface waves at frequencies 30 and 50 Hz were estimated for a 1.1% PAA solution with density 1004 kgm^{-3} (from Table 3.1), and viscosity $\sim$20 mPas. The penetration depth was estimated to be 0.46 mm at 30 Hz and 0.36 mm at 50 Hz. For these frequencies, drops had profile lengths over 3.5 mm (over 4.5 mm for 30 Hz), corresponding to radii over $\sim$0.7 mm (using $l/2\theta = r$ for $\theta = 144°$). These penetration depths are comparable to the drop sizes and waves may penetrate a short distance into the pipette tip, increasing the influence of boundary layer damping,

$$\delta = \sqrt{\frac{2\eta}{2\pi\rho f}}, \tag{6.3.1}$$

where δ is the penetration depth (m) for waves of frequency f (Hz), η is the solution viscosity (Pas) and ρ is the solution density (kgm^{-3})[56, 106]

The additional damping for 1.1% may be the result of boundary layer damping, however this has not been confirmed. Other possibilities have presented themselves, many of which can be tested by performing experiments in controlled environments and comparing results.

6.4 Conclusion

The pendant drop vibration technique was capable of measuring the vibrational properties of viscoelastic pendant drops of poly(acrylamide-co-acrylic acid) in water. These measurements were however, difficult to achieve. The pipette tip did not always provide a stable surface to "pin" a drop to. Care had to be taken to ensure that drop sizes remained consistent during experiments. The pipette tip was prone to vibrating as a result of the mechanical impulse applied to trigger drop vibration, and without sufficient damping would interfere with drop vibration measurements. The motion of the tip needed to be tracked separately from the drop in order to isolate the drop vibrational frequencies.

A factor of $\sim$3 difference in the frequency and full width half maximum (width) data, or a factor of $\sim$2 calibration error in the profile length data, was observed between pendant and sessile drop vibration, for all but the 1.1% PAA width

data. Image calibration errors are assumed to be more likely in the case of sessile drops than pendant drops due to calibration techniques (Section 3.5), however assumptions that the pendant drop data was correct lead to a negative (unphysical) shear storage modulus (G'). This indicated that the pendant drops vibrated predominantly in the n=1 mode, rather than the n=2 mode measured for sessile drops, and that an additional damping mechanism was present for 1.1% drops.

The shear storage and loss (G'') moduli, calculated from Equations 3.9.1 and 3.9.2 (using the measured surface tension and density for the solutions used and assuming the measured mode of vibration was n=1), was of the same order of magnitude as microrheology data (Section 5.3) used for comparison. The G' versus f data had similar gradients to sessile drop and microrheology comparison data and followed the expected trend of increasing G' with increasing concentration. The separation in G' between the different concentrations was lower than for the sessile drop and microrheology comparison data. The G'' versus f data clustered close together with a steep gradient, behaving similarly to the full width half maximum (Δf) of frequency peaks. Dividing the 1.1% width data by 3 resulted in G'' estimates that sat closer to the sessile drop and microrheology comparison data. The additional damping mechanism observed for 1.1% PAA was suggested to be the result of boundary layer damping from the inner walls of the pipette tip, however this remains unconfirmed.

Differences between the pendant drop results and microrheology/sessile drop technique results indicated that the model used to extract the rheological properties (G' and G''), which assumes a spherical levitated drop, needs to be adapted to account for differences in the pendant drop system. Of particular interest is the compressibility of the system resulting from the presence of an air bubble above the reservoir within the tip, as well as impact of the reservoir on the bulk viscous and boundary-layer damping.

CHAPTER 7

Conclusion

Optovibrometry techniques were used to extract rheological properties from sessile drops of glycerol in water and poly(acrylamide-co-acrylic acid) (PAA) in water as well as from pendant drops of PAA in water. Vibrations were triggered on the surface of microlitre droplets using a mechanical impulse. The frequency and full width at half maximum (width) of the resonant vibrations were used to examine the applicability of this technique to solutions whose properties change in real-time as well as to viscoelastic droplets.

A range of drop sizes (profile lengths between 2 and 11 mm) were used in order to access multiple frequencies. For all of the drops studied here, the frequency and width of vibration decreased as the drop size increased, and increased as the polymer concentration increased.

Superhydrophobic surfaces provided by Deng *et. al.* [64] were used to produce sessile drops with high three phase contact angles (advancing contact angle of $180 \pm 2°$, a receding angle of $166 \pm 2°$ and a roll-off angle of less than $2°$ for water [65], Figure 2.2). The vibrational behaviour of the sessile drops were extracted using light scattering techniques described in Section 3.6.

Viscous sessile drops of glycerol in water were vibrated several times over the course of ~ 2000 s (Chapter 4). As the water evaporated from the drops, the changes in vibrational behaviour and drop size (profile length, tracked via a camera) were recorded. The surface tension and viscosity for these solutions were calculated using Equations 3.9.3 and 3.9.4 respectively.

As the concentration of glycerol was increased, the viscosity increased and the surface tension of the solutions decreased. The initial surface tension and viscosity values obtained from drop vibration measurements of evaporating glycerol/water droplets were found to be in good agreement with data obtained from bulk glycerol/water solutions. As the water evaporated from the drops (and the glycerol concentration increased as the drops shrank), the agreement with bulk (near time t = 0) solutions steadily decreased (see Figure 4.4), particularly for surface tension measurements (from Equation 3.9.3), although viscosity measurements (from Equation 3.9.4) also deviated noticeably at low volume fractions ($\phi < 0.2$).

The surface tension of the glycerol/water drops changed on time scales of hundreds of seconds and fell below the surface tension of glycerol after ~ 300 seconds for all concentrations studied (see Figure 4.2). This is comparable to the time scales over which a clean water surface can become contaminated with low surface tension impurities such as organic deposits from the air on time scales of ~ 5 mins (300 seconds) [94].

The optovibrometry technique successfully measured the surface tensions and viscosities of aqueous glycerol solutions at short experimental times. For measurements on longer timescales, the technique was able to identify surface tensions indicative of contamination via low surface tension (~ 40 - $55\,\mathrm{mJm^{-2}}$ from Figure 4.2) impurities, such as organic materials, which typically have $\gamma \sim 40$ - $50\,\mathrm{mJm^{-2}}$ [95].

After confirming the technique's ability to extract rheological data from viscous sessile drops, the method was applied to viscoelastic sessile drops of PAA in water on short timescales (Chapter 5).

The shear storage (G') and loss (G'') moduli were calculated by inputting the measured frequency and width data, along with surface tensions and densities measured for the bulk solutions, Equations 3.9.1 and 3.9.2 respectively [15, 65]. As the concentration of PAA was increased, the G' and G'' values both increased, and were found to be in good agreement with data collected for the same solutions via dynamic light scattering microrheology (see Figure 5.3) [86]. The values obtained are also in agreement with previous results obtained from levitated drop studies of PAA solutions similar to those described by Temperton *et. al.* [15] (see Figure 5.3).

Pendant drops, suspended from a polypropylene pipette tip, were recorded using a high speed camera (Dalsa Genie HC-640), and their (2D) centre of mass tracked as they vibrated (Figure 3.11b). Due to tip oscillations, it was necessary to also track the motion of the pipette tip. A vibration spectrum was created from the drop position relative to the pipette as a function of time (see Section 6.2).

The technique was then applied to pendant drops of PAA in water with sizes smaller than the capillary length (~ 2.7 mm for the PAA solutions studied). These pendant drops of PAA in water experienced centre of mass oscillations indicative of the n=1 vibrational mode (rather than the n=2 mode observed for the sessile drops). The majority of the rheological data measured for the pendant drops agreed with microrheology and sessile drop data, however 1.1% PAA displayed increased damping. The source of additional damping for 1.1% PAA was suggested to be boundary layer damping from the inner walls of the pipette tip, however this remains unconfirmed.

The optovibrometry technique is a promising method for extracting the rheological properties from viscoelastic fluids and for monitoring the changes to these properties in real time. The agreement between the technique and conventional rheometry measurements has room for improvement, since the model is oversimplified and does not account for boundary layer damping or large amplitude vibrations. The technique is inexpensive compared to conventional rheometry techniques and requires much smaller volumes of liquid (µL vs mL or cL), however it is vulnerable to external influences such as vibrations, air convection and (in the case of the laser scattering technique) external light sources.

The measurement range of this technique is limited by the size range of the drop (i.e. by the capillary length), damping and by equipment resolution. The upper limit for G' was estimated to be 70 kPa, and for G'' was narrowed down to a range between 1 (from previous successful measurements [16, 32]) and 70kPa (at which $f \sim \Delta f$ is considered to produce a very broad and almost indistinguishable peak).

CHAPTER 8

Future work

The optovibrometry technique shows promise as a method for obtaining the rheological properties of small (microlitre) volumes of fluid for lower viscosities than can generally be accessed by conventional rheometry. Conventional techniques, such as microrheology, typically require millilitre volumes of fluid.

The small drop size requirements would be beneficial to the rheology of airway fluid in the human respiratory system, which has limited volume availability and a large viscosity range [107]. The technique also provides an alternative way to test for dry eye disease (keratoconjunctivitis sicca). Only a single tear would be required to measure the viscosity of tears, which is often lower in individuals with dry eyes [108]. In situations where the grade of lubricant being used is vital to ensuring efficient operation (such as with machine and clock oil) the drop vibration technique may quickly establish the viscosity of a single drop prior to application, thus preventing unnecessary breakdowns and delays. A feature that makes this technique useful to such applications is the ability to measure fluid properties without destroying the sample.

The technique has successfully estimated the rheological properties for both viscous and viscoelastic liquids [15, 32]. A greater range of incompressible viscoelastic drops should be investigated and used to improve the accuracy of the model describing the viscoelastic sessile drop system. This should include experiments at different temperatures, as well as the isolation of the contact angle dependence of the vibrational frequency and width of sessile drops discussed by Farmer *et. al.* [30], which is closely linked to boundary layer damping, particularly for fluids with high penetration depth. The unexpected damping source for 1.1% PAA pendant drops should also be investigated,

particularly the impact of boundary-layer damping from the reservoir within the pipette tip.

Once the contact angle dependence of the frequency and width have been established, changes to drop vibration (for a known fluid) may be used in surface characterisation, as a tool to identify the contact angle or potentially the damping properties of a substrate from the relationship between the solid-liquid contact area, the contact angle and the width. The effect of surface elasticity on drop vibration may be analysed, and vibrating drops or drop impacts may be used to observe film oscillations with a greater understanding of the drop side of the interaction [109].

With enough information about the impact of temperature, ambient air flow and substrate composition, it is possible that a model may be put together to estimate when drops of fluid will drip off of a plant's leaves or remain to be absorbed or evaporate. This may be used in agriculture to optimise the use of fertilisers and pesticides by selecting the conditions, droplet (spray/atomisation) size and fluid composition to encourage the active ingredients to remain on the leaves or drip down to the roots.

The ability of the technique to monitor changes in properties over time (shown in Chapter 4) indicates a promising way to measure blood coagulation rates using only a small volume of blood (microlitres vs millilitres) and not reliant on selecting appropriate sample tubes [110, 111], a very important factor when dealing with low clotting risk patients, animals, and forensic situations in which limited volumes are available. However, for this to be a viable technique for measurements on timescales longer than 300s (the contamination timescale for a water drop [94]), work needs to be done to eliminate/reduce contamination risks (such as through controlled air flow and filters or through additional air monitoring).

To better understand the sources (and impacts on drop vibration) of contamination, experiments can be carried out in a clean or controlled environment and contaminants deliberately added to the substrate (or pipette tip), air within a pipette (upper surface of the reservoir, Figure 6.1), drop surface, and bulk fluid independently to track their influence on drop vibrations. The changes in measured rheological properties for a single component drop, tracked over a period of time, can be used to identify the presence of contaminants in the environment

and estimate their rheological properties relative to the uncontaminated drop. This could be done prior to testing valuable fluids or performing sensitive tests in order to reduce the risk of contamination or to calibrate the results to the presence of a contaminant. The rate of contamination may also be used to estimate the saturation of airborne contaminants in the environment. This may be adapted to the deliberate contamination of drops to improve the self cleaning properties of superamphiphobic substrates [112, 113].

Knowledge of the relationship between contaminants and drop vibration may be of use in the field evaluating global dimming [114, 115]. The impact of particulate type or size on (water) droplets [116] may indicate the conditions required for a contaminated cloud to precipitate and suggest techniques to trigger rainfall, dislodge drops from particulates or deliberately bind a drop to particulates to cleanse the air.

It would be beneficial to investigate the centre of mass oscillations observed in pendant drops of poly(acrylamide-co-acrylic acid) (PAA) in water and their impact on the model used to describe the relationship between drop vibration and rheological properties (Section 3.9), which assumes incompressibility and small vibration amplitude compared to drop size (Chapter 2). Compressible drops have not been thoroughly investigated using this technique, although the success of setting n=1 for the pendant drops (Section 6.3) suggests that the corrections required may be small. The vibrational properties of compressible fluids and bubbles should be investigated to improve understanding of fluid and thin film mechanics [117], as well as yield stress in small (microlitre) volumes [118]. The drop vibration technique may be used to research the behaviour of different gas bubbles trapped in a large volume of fluid [34] or in a thin film membrane. This may provide greater insight into gas properties and the impact of much lower "fluid" densities and varying film thickness on vibration.

Applying thin viscoelastic layers to the surface of a liquid drop, while difficult, may provide useful insight into the vibration of immiscible multi-component fluids. Some techniques for the manufacture of these layered drops include drop surface contamination (observed in Chapter 4), self assembly of a barrier from components within the drop [116, 119], the creation of a bubble filled with fluid rather than gas. The effects of layer thickness, multiple layers of different

materials [120], and layer viscoelasticity on vibration may be investigated and applied to models of complex systems such as planets [41] or (particularly if the technique can be applied to drops closer to the nanolitre scale) colloidal spheres.

Investigations into drop vibration can lead to an increased understanding of fluid responses in microfluidic systems [121, 122]. The optovibrometry technique can be used to provide automated analysis of the mechanical properties and/or surface tension of droplets within microfluidic systems. As an expansion on the current uses of microfluidic systems for cell culturing [123], it may be useful to examine the efficacy of a (vibrating) spherical drop for the growth of cells and bacteria while monitoring the mechanical properties of the drop/culture system.

Bibliography

[1] Bojan Vukasinovic, Marc K. Smith, and Ari Glezer. Dynamics of a sessile drop in forced vibration. *J. Fluid Mech.*, 587:395–423, 2007. doi: doi.org/10.1017/S0022112007007379.

[2] Shirley C. Tsai, Patrick Luu, Paul Childs, Asseged Teshome, and Chen S. Tsai. The role of capillary waves in two-fluid atomization. *Phys. Fluids*, 9 (10):2909–2918, 1997. doi: doi.org/10.1063/1.869403.

[3] Fushui Liu, Ning Kang, Yikai Li, and Qing Wu. Experimental investigation on the spray characteristics of a droplet under sinusoidal inertial force. *Fuel*, 226:156 – 162, 2018. doi: doi.org/10.1016/j.fuel.2018.04.008.

[4] Ping Wang, Siddharth Maheshwari, and Hsueh-Chia Chang. Polyhedra formation and transient cone ejection of a resonant microdrop forced by an ac electric field. *Phys. Rev. Lett.*, 96:254502, Jun 2006. doi: doi.org/10.1103/PhysRevLett.96.254502.

[5] C. T. Pan, J. Shiea, and S. C. Shen. Fabrication of an integrated piezo-electric micro-nebulizer for biochemical sample analysis. *J. Micromech. Microeng.*, 17(3):659–669, 2007. doi: doi.org/10.1088%2F0960-1317%2F17%2F3%2F031.

[6] F. Mugele, J. C. Baret, and D. Steinhauser. Microfluidic mixing through electrowetting-induced droplet oscillations. *Appl. Phys. Lett.*, 88:204106, 2006. doi: doi.org/10.1063/1.2204831.

[7] E. D. Wilkes and O. A. Basaran. Forced oscillations of pendant (sessile) drops. *Phys. Fluids*, 9(6):1512–1528, 1997. doi: doi.org/10.1063/1.869276.

[8] Susan Daniel, Sanjoy Sircar, Jill Gliem, and Manoj K. Chaudhury. Ratcheting motion of liquid drops on gradient surfaces. *Langmuir*, 20:4085–4092, 2004. doi: doi.org/10.1021/la036221a.

[9] Susan Daniel, Manoj K. Chaudhury, and P.-G. de Gennes. Vibration-actuated drop motion on surfaces for batch microfluidic processes. *Langmuir*, 21:4240–4248, 2005. doi: doi.org/10.1021/la046886s.

[10] Ashutosh Shastry, Marianne J. Case, and Karl F. Böhringer. Directing droplets using microstructured surfaces. *Langmuir*, 22:6161–6167, 2006. doi: doi.org/10.1021/la0601657.

[11] Susan Daniel, Manoj K. Chaudhury, and John C. Chen. Fast drop movements resulting from the phase change on a gradient surface. *Science*, 291 (5504):633–636, 2001. doi: doi.org/10.1126/science.291.5504.633.

[12] P. Brunet, J. Eggers, and R. D. Deegan. Vibration-induced climbing of drops. *Phys. Rev. Lett.*, 99:144501, 2007. doi: doi.org/10.1103/PhysRevLett.99.144501.

[13] F. K. Hansen. Surface tension by image analysis: Fast and automatic measurements of pendant and sessile drops and bubbles. *J. Colloid Interf. Sci.*, 160(1):209 – 217, 1993. doi: doi.org/10.1006/jcis.1993.1386.

[14] W. Meier, G. Greune, A. Meyboom, and K. P. Hofmann. Surface tension and viscosity of surfactant from the resonance of an oscillating drop. *Eur. Biophys. J.*, 29:113–124, 2000. doi: doi.org/10.1007/s002490050256.

[15] Robert H. Temperton, Richard J. A. Hill, and James S. Sharp. Mechanical vibrations of magnetically levitated viscoelastic droplets. *Soft Matter*, 10: 5375–5379, 2014. doi: doi.org/10.1039/C4SM00982G.

[16] James S. Sharp. Resonant properties of sessile droplets; contact angle dependence of the resonant frequency and width in glycerol/water mixtures. *Soft Matter*, pages 399–407, 2012. doi: doi.org/10.1039/C1SM06916K.

[17] R. Miller, A. Hofmann, R. Hartmann, K.-H. Schano, and A. Halbig. Measuring dynamic surface and interfacial tensions. *Adv. Mat.*, 4:370–374, 1992. doi: doi.org/10.1002/adma.19920040513.

[18] O. I. del Rio and A. W. Neumann. Axisymmetric drop shape analysis: Computational methods for the measurement of interfacial properties from the shape and dimensions of pendant and sessile drops. *J. Colloid Int. Sci.*, 196:136–147, 1997. doi: doi.org/10.1006/jcis.1997.5214.

[19] M. Roth, M. D'Acunzi, D. Vollmer, and G. K. Auernhammer. Viscoelastic rheology of colloid-liquid crystal composites. *J. Chem. Phys*, 132:124702, 2010. doi: doi.org/10.1063/1.3358331.

[20] T. G. Mason and D. A. Weitz. Optical measurements of frequency dependent linear viscoelastic moduli of complex fluids. *Phys. Rev. Lett.*, 74:1250, 1955. doi: doi.org/10.1103/PhysRevLett.74.1250.

[21] I. Egry, G. Lohöfer, I. Seyhan, S. Schneider, and B. Feuerbacher. Viscosity of eutectic $pd_{78}cu_6si_{16}$ measured by the oscillating drop technique in microgravity. *Appl. Phys. Lett.*, 73:462–463, 1998. doi: doi.org/10.1063/1.121900.

[22] C. L. Shen, W. J. Xie, and B. Wei. Parametrically excited sectorial oscillation of liquid drops floating in ultrasound. *Phys. Rev. E*, 81:046305, 2010. doi: doi.org/10.1103/PhysRevE.81.046305.

[23] R. J. A. Hill and L. Eaves. Vibrations of a diamagnetically levitated water droplet. *Phys. Rev. E*, 81:056312, 2010. doi: doi.org/10.1103/PhysRevE.81.056312.

[24] D. B. Khismatullin and A. Nadim. Shape oscillations of a viscoelastic drop. *Phys. Rev. E*, 63:061508, 2001. doi: doi.org/10.1103/PhysRevE.63.061508.

[25] J. C. Chrispell, R. Cortez, D. B. Khismatullin, and L. J. Fauci. Shape oscillations of a droplet in an Oldroyd-B fluid. *Physica D*, 240:1593–1601, 2011. doi: doi.org/10.1016/j.physd.2011.03.004.

[26] M. Strani and F. Sabetta. Free vibrations of a drop in partial contact with a solid support. *J. Fluid Mech.*, 141:233–247, 1984. doi: doi.org/10.1017/S0022112084000811.

[27] Robert W. Smithwick and Joseph A. M. Boulet. Electrically driven oscillations of a mercury-droplet electrode. *J. Colloid Interf. Sci.*, 150(2):567 – 574, 1992. doi: doi.org/10.1016/0021-9797(92)90225-B.

[28] A. J. B. Milne, B. Defez, M. Cabrerizo-Vílchez, and A. Amirfazli. Understanding (sessile/constrained) bubble and drop oscillations. *Adv. Coll. Int. Sci.*, 203:22–36, 2014. doi: doi.org/10.1016/j.cis.2013.11.006.

[29] Franck Celestini and Richard Kofman. Vibration of submillimeter-size supported droplets. *Phys. Rev. E*, 73:041602, Apr 2006. doi: doi.org/10.1103/PhysRevE.73.041602.

[30] James S. Sharp, David J. Farmer, and James Kelly. Contact angle dependence of the resonant frequency of sessile water droplets. *Langmuir*, 27: 9367–9371, 2011. doi: doi.org/10.1021/la201984y.

[31] Matilda Backholm, Maja Vuckovac, Jan Schreier, Mika Latikka, Michael Hummel, Markus B. Linder, and Robin H. A. Ras. Oscillating ferrofluid droplet microrheology of liquid-immersed sessile droplets. *Langmuir*, 33 (25):6300–6306, 2017. doi: doi.org/10.1021/acs.langmuir.7b01327.

[32] Robert H. Temperton, Michael I. Smith, and James S. Sharp. Mechanical vibrations of pendant liquid droplets. *Eur. Phys. J. E*, 38:79–86, 2015. doi: doi.org/10.1140/epje/i2015-15079-2.

[33] N. D. McMillan, F. E. Feeney, M. J. P. Power, S. M. Kinsella, M. P. Kelly, C. Hammil, K. W. Thompson, and J. P. O'Dea. A qualitative study of fibre drop traces on mechanically excited damped vibrations of drops of pure liquids using FFT analysis. *Instrum. Sci. Technol.*, 22(4):375–395, 1994. doi: doi.org/10.1080/10739149408001196.

[34] Antonio Raudino, Domenica Raciti, and Mario Corti. Anomalous behavior of ultra-low-amplitude capillary waves: A glimpse of the viscoelastic properties of interfacial water? *Langmuir*, 33(25):6439–6448, 2017. doi: doi.org/10.1021/acs.langmuir.7b00895.

[35] G. McHale, S. J. Elliot, M. I. Newton, D. L. Herbertson, and K. Esmer. Levitation-free vibrated droplets: resonant oscillations of liquid marbles. *Langmuir*, 25:529–533, 2009. doi: doi.org/10.1021/la803016f.

[36] Cheuk-Yin. Wong and N. Azziz. Dynamics of nuclear fluid. VI. nuclear giant-resonances as elastic vibrations. *Phys. Rev. C*, 24:2290–2310, 1981. doi: doi.org/10.1103/PhysRevC.24.2290.

[37] F. F. Pollitz. Gravitational viscoelastic postseismic relaxation on a layered spherical earth. *J. Geophys. Res.*, 1021:17921–17941, 1997. doi: doi.org/10.1029/97JB01277.

[38] J. Tromp and J. X. Mitrovica. Surface loading of a viscoelastic earth-I. general theory. *Geophys. J. Int.*, 137:847–855, 1999. doi: doi.org/10.1046/j.1365-246x.1999.00838.x.

[39] S. I. Bastrukov, F. Weber, and D. V. Podgainy. On the stability of global non-radial pulsations of neutron stars. *J. Phys. G.: Nucl. Part. Phys.*, 25: 107–127, 1999. doi: doi.org/10.1088/0954-3899/25/1/010.

[40] F. R. S. Lord Rayleigh. VI. on the capillary phenomena of jets. *Proc. R. Soc. Lond.*, 29:71–97, 1879. doi: doi.org/10.1098/rspl.1879.0015.

[41] Sir Lamb, Horace. *Hydrodynamics*. Cambridge University Press, Cambridge, England, 1895. URL `https://archive.org/details/hydrodynamics00horarich/mode/2up`.

[42] S. Chandrasekhar. The oscillations of a viscous liquid globe. *Proc. Lond. Math. Soc.*, 3-9:141–149, 1959. doi: doi.org/10.1112/plms/s3-9.1.141.

[43] H. Lamb. On the oscillations of a viscous spheroid. *P. Lond. Math. Soc.*, s1-13(1):51–70, 1881. doi: doi.org/10.1112/plms/s1-13.1.51.

[44] D. L. Geng, W. J. Xie, N. Yan, and B. Wei. Vertical vibration and shape oscillation of acoustically levitated water drops. *App. Phys. Lett.*, 105: 104101, 2014. doi: doi.org/10.1063/1.4895580.

[45] I. Egry, H. Giffard, and S. Schneider. The oscillating drop technique revisited. *Meas. Sci. Technol.*, 16:426–431, 2005. doi: doi.org/10.1088/0957-0233/16/2/013.

[46] Ivan Egry, Georg Lohoefer, and Gerd Jacobs. Surface tension of liquid metals: Results from measurements on ground and in space. *Phys. Rev. Lett.*, 75:4043–4046, 1995. doi: doi.org/10.1103/PhysRevLett.75.4043.

[47] Lorena A. Del Castillo, Satomi Ohnishi, Steven L. Carnie, and Roger G. Horn. Variation of local surface properties of an air bubble in water caused by its interaction with another surface. *Langmuir*, 32:7671–7682, 2016. doi: doi.org/10.1021/acs.langmuir.6b01949.

[48] R. H. Temperton and J. S. Sharp. Vibrational modes of elongated sessile droplets. *Langmuir*, 29:4737–4742, 2013. doi: doi.org/10.1021/la304520c.

[49] D. V. Lyubimov, T. P. Lyubimova, and S. V. Shklyaev. Behavior of a drop on an oscillating solid plate. *Phys. Fluids*, 18:012101, 2006. doi: doi.org/10.1063/1.2137358.

[50] S. Mettu and M. K. Chaudhury. Vibration spectroscopy of a sessile drop and its contact line. *Langmuir*, 28:14100–14106, 2012. doi: doi.org/10.1021/la302958m.

[51] X. Noblin, A. Buguin, and F. Brochard-Wyart. Vibrations of sessile drops. *Eur. Phys. J.: Spec. Top.*, 166:7–10, 2009. doi: doi.org/10.1140/epjst/e2009-00869-y.

[52] X. Noblin, A. Buguin, and F. Brochard-Wyart. Vibrated sessile drops: Transition between pinned and mobile contact line oscillations. *Eur. Phys. J.*, 14:395–404, 2004. doi: doi.org/10.1140/epje/i2004-10021-5.

[53] S. T. Milner. Square patterns and secondary instabilities in driven capillary waves. *J. Fluid Mech.*, 225:81–100, 1991. doi: doi.org/10.1017/S0022112091001970.

[54] C. S. Milner and N. N. Dalton Eds. *Glycerol*. Reinhold, 1953.

[55] John Miles. The capillary boundary layer for standing waves. *J. Fluid Mech.*, 222:197–205, 1991. doi: doi.org/10.1017/S0022112091001052.

[56] L. Landau and M. Lifshitz. *Fluid Mechanics, 2nd edition*. Pergamon press, Oxford, England, 1987. URL `https://users-phys.au.dk/~srf/hydro/Landau+Lifschitz.pdf`.

[57] Bo Christiansen, Preben Alstrøm, and Mogens T. Levinsen. Dissipation and ordering in capillary waves at high aspect ratios. *J. Fluid Mech.*, 291: 323–341, 1995. doi: doi.org/10.1017/S0022112095002722.

[58] E. D. Wilkes and O. A. Basaran. Forced-oscillations of pendant (sessile) drops. *Phys. Fluids*, 9:1512–1528, 1997. doi: doi.org/10.1063/1.869276.

[59] Hidemi Akimoto, Katsuhiko Nagai, and Naoki Sakura. Viscosity measurement by the free vibrations of homogeneous viscoelastic sphere. *J. Appl. Mech.*, 79:041002, 2012. doi: doi.org/10.1115/1.4005551.

[60] H. Pleiner, J. L. Harden, and P. Pincus. Surface-modes on a viscoelastic medium. *Europhys. Lett.*, 7:383–387, 1988. doi: doi.org/10.1209/0295-5075/7/5/001.

[61] P.-G. de Gennes. *Scaling Concepts in Polymer Physics*. Cornell University, 1979.

[62] G. Wyllie. Evaporation and surface structure of liquids. *Proc. Roy. Soc. A*, 197:1050, 1949. doi: doi.org/10.1098/rspa.1949.0071. Equation on page 388.

[63] D. Ambrose. Vapour pressure of water at temperatures between 0 and 360°c, 2005. URL `http://www.kayelaby.npl.co.uk/chemistry/3_4/3_4_2.html`.

[64] X. Deng, L. Mammen, H. Butt, and D. Vollmer. Candle soot as a template for a transparent robust superamphiphobic coating. *Science*, 335:67–70, 2012. doi: doi.org/10.1126/science.1207115.

[65] V. C. Harrold, M. Paven, D. Vollmer, and J. S. Sharp. Rheological properties of viscoelastic drops on superamphiphobic substrates. *Langmuir*, 32: 4071–4076, 2016. doi: doi.org/10.1021/acs.langmuir.6b00779.

[66] L. Dong, A. Chaudhury, and M. K. Chaudhury. Lateral vibration of a water drop and its motion on a vibrating surface. *Eur. Phys. J. E*, 21: 231–242, 2006. doi: doi.org/10.1140/epje/i2006-10063-7.

[67] Amin Rahimzadeh and Morteza Eslamian. Experimental study on the evaporation of sessile droplets excited by vertical and horizontal ultrasonic vibration. *Int. J. Heat Mass Transf.*, 114:786–795, 2017. doi: doi.org/10.1016/j.ijheatmasstransfer.2017.06.099.

[68] Liang Hu, Yao Huang, Wenyu Chen, Xin Fu, and Haibo Xie. Pinning effects of wettability contrast on pendant drops on chemically patterned surfaces. *Langmuir*, 32:11780–11788, 2016. doi: doi.org/10.1021/acs.langmuir.6b03318.

[69] Hosub Lim, Anubhav Tripathi, and Jinkee Lee. Dynamics of a capillary invasion in a closed-end capillary. *Langmuir*, 30:9390–9396, 2014. doi: doi.org/10.1021/la501927c.

[70] Zhizhao Che, Teck Neng Wong, Nam-Trung Nguyen, Yit Fatt Yap, and J.C. Chai. Numerical investigation of upstream pressure fluctuation during growth and breakup of pendant drops. *Chem. Eng. Sci.*, 66(21): 5293 – 5300, 2011. doi: doi.org/10.1016/j.ces.2011.07.028.

[71] Alok Kumar, Madhu Ranjan Gunjan, Karan Jakhar, Atul Thakur, and Rishi Raj. Unified framework for mapping shape and stability of pendant drops including the effect of contact angle hysteresis. *Colloids Surf. A: Physicochem. Eng. Asp.*, 597:124619, 2020. doi: doi.org/10.1016/j.colsurfa.2020.124619.

[72] M.W.L. Chee, S. Balaji, G.L. Cuckston, J.R. Davidson, and D.I. Wilson. Pendant drops shed from a liquid lens formed by liquid draining down the inner wall of a wide vertical tube. *Exp. Therm. Fluid Sci.*, 97:364 – 374, 2018. doi: doi.org/10.1016/j.expthermflusci.2018.04.015.

[73] Stephen B. G. M. O'Brien and Ben H. A. A. van den Brule. Shape of a small sessile drop and the determination of contact angle. *J. Chem. Soc., Faraday Trans.*, 87:1579–1583, 1991. doi: doi.org/10.1039/FT9918701579.

[74] Luis P. Thomas, Roberto Gratton, Beatriz M. Marino, and Javier A. Diez. Droplet profiles obtained from the intensity distribution of refraction patterns. *Appl. Opt.*, 34(25):5840–5848, Sep 1995. doi: doi.org/10.1364/AO.34.005840.

[75] R. D. Knight. *Physics for Scientists and Engineers, 2nd Ed.* Pearson Addison-Wesley, 2008.

[76] Clyde E. Stauffer. The measurement of surface tension by the pendant drop technique. *J. Phys. Chem.*, 69:1933–1938, 1965. doi: doi.org/10.1021/j100890a024.

[77] Victoria Harrold and James S. Sharp. Optovibrometry: Tracking changes in the surface tension and viscosity of multicomponent droplets in real-time. *Soft Matter*, 12(42):8790–8797, 2016. doi: doi.org/10.1039/C6SM01901C.

[78] D. P. N. Vlasveld, M. de Jong, H. E. N. Bersee, A. D. Gotsis, and S. J. Picken. The relation between rheological and mechanical properties of PA6 nano- and micro-composites. *Polymer*, 46(23):10279 – 10289, 2005. doi: doi.org/10.1016/j.polymer.2005.08.002.

[79] Peter Hartmann, Mátá Cs. Sándor, Anikó Kovács, and Zoltán Donkó. Static and dynamic viscosity of a single layer dusty plasma. *AIP Conf. Proc.*, 1397(1):146–149, 2011. doi: doi.org/10.1063/1.3659758.

[80] Samiul Amin, Carlos A. Rega, and Hanna Jankevics. Detection of viscoelasticity in aggregating dilute protein solutions through dynamic light scattering-based optical microrheology. *Rheol. Acta*, 51:329–342, 2012. doi: doi.org/10.1007/s00397-011-0606-6.

[81] Pablo Domínguez-García. Brownian disks lab: Simulating time-lapse microscopy experiments for exploring microrheology techniques and colloidal interactions. *Comput. Phys. Commun.*, 252:107123, 2020. doi: doi.org/10.1016/j.cpc.2019.107123.

[82] Samiul Amin, Steven Blake, Rachel C. Kennel, and E. Neil Lewis. Revealing new structural insights from surfactant micelles through DLS, microrheology and raman spectroscopy. *Materials*, 8:3754–3766, 2015. doi: doi.org/10.3390/ma8063754.

[83] Malvern Panalytical. An introduction to DLS microrheology. Technical report, Malvern Instruments Ltd., September 2017. URL `https://www.malvernpanalytical.com/en/learn/knowledge-center/Whitepapers/WP120917IntroDLSMicro.html`.

[84] Malvern Panalytical. Measuring the particle size of small sample volumes using laser diffraction, 2004. URL `https://www.malvernpanalytical.com/en/learn/knowledge-center/application-notes/AN141104MeasSmallVolumesUsingSV.html`.

[85] Malvern Panalytical. *Zetasizer nano accessories guide*, April 2013. URL https://www.cif.iastate.edu/sites/default/files/uploads/Other_Inst/Particle%20Size/Accessories%20and%20Cells%20Guide.pdf.

[86] Thomas G. Mason. Estimating the viscoelastic moduli of complex fluids using the generalized stokes-einstein equation. *Rheol. Acta*, 39:371–378, 2000. doi: doi.org/10.1007/s003970000094.

[87] Thomas G. Mayerhöfer and Jürgen Popp. Electric field standing wave effects in internal reflection and ATR spectroscopy. *Spectrochim. Acta A*, 191:165–171, 2018. doi: doi.org/10.1016/j.saa.2017.10.007.

[88] Gebhard Schramm. *A practical approach to rheology and rheometry*. Gebrueder HAAKE GmbH, Karlsruhe, Germany, 2000.

[89] R. E. Hudson, A. J. Holder, K. M. Hawkins, P. R. Williams, and D. J. Curtis. An enhanced rheometer inertia correction procedure (ERIC) for the study of gelling systems using combined motor-transducer rheometers. *Phys. Fluids*, 29:121602, 2017. doi: doi.org/10.1063/1.4993308.

[90] M. L. Sheely. Glycerol viscosity tables. *Ind. Eng. Chem.*, 24(9):1060–1064, 1932. doi: doi.org/10.1021/ie50273a022.

[91] M.J. Wernke. Glycerol. In Philip Wexler, editor, *Encyclopedia of Toxicology (Third Edition)*, pages 754 – 756. Academic Press, Oxford, third edition edition, 2014. doi: doi.org/10.1016/B978-0-12-386454-3.00510-8.

[92] K. Takamura, H. Fischer, and N. R. Morrow. Physical properties of aqueous glycerol solutions. *J. Petrol. Sci. Eng.*, 98-99(0920-4105):50 – 60, 2012. doi: doi.org/10.1016/j.petrol.2012.09.003.

[93] Glycerine Producers' Association. *Physical properties of glycerine and its solutions*. Glycerine Producers' Association, 1963.

[94] D. M. Henderson and J. W. Miles. Surface-wave damping in a circular cylinder with a fixed contact line. *J. Fluid Mech.*, 275:285–299, 1994. doi: doi.org/10.1017/S0022112094002363.

[95] R. C. Weast (Editor). *Handbook of Chemistry and Physics, 69th Ed.* CRC Press, 1989.

[96] José A. Trejo González, M. Paula Longinotti, and Horacio R. Corti. The viscosity of glycerol-water mixtures including the supercooled region. *J. Chem. Eng. Data*, 56(4):1397–1406, 2011. doi: doi.org/10.1021/je101164q.

[97] Sergey Semenov, Victor M. Starov, Ramon G. Rubio, and Manuel G. Velarde. Computer simulations of evaporation of pinned sessile droplets: Influence of kinetic effects. *Langmuir*, 28(43):15203–15211, 2012. doi: doi.org/10.1021/la303916u.

[98] J. B. Bostwick and P. H. Steen. Capillary oscillations of a constrained liquid drop. *Phys. Fluids*, 21:032108, 2009. doi: doi.org/10.1063/1.3103344.

[99] S. Ramalingam, D. Ramkrishna, and O. A. Basaran. Free vibrations of a spherical drop constrained at an azimuth. *Phys. Fluids*, 24:082102, 2012. doi: doi.org/10.1063/1.4742339.

[100] A. Prosperetti. Linear oscillations of constrained drops, bubbles and plane liquid surfaces. *Phys. Fluids*, 24:032109, 2012. doi: doi.org/10.1063/1.3697796.

[101] T. G. Mason and D. A Weitz. Optical measurements of frequency-dependent linear viscoelastic moduli of complex fluids. *Phys. Rev. Lett.*, 74:1250, 1955. doi: doi.org/10.1103/PhysRevLett.74.1250.

[102] Leslie Nicholson, Christopher Maher, Roger Adams, and Nhan Phan-Thien. Stiffness properties of the human lumbar spine: A lumped parameter model. *Clin. Biomech.*, 16(4):285 – 292, 2001. doi: doi.org/10.1016/S0268-0033(00)00117-0.

[103] T. G. Mason, Hu Gang, and D. A. Weitz. Rheology of complex fluids measured by dynamic light scattering. *J. Mol. Struct.*, 383:81–90, 1996. doi: doi.org/10.1016/S0022-2860(96)09272-1.

[104] I. U. Vakarelski, R. Manica, X. Tang, S. J. O'Shea, G. W. Stevens, F. Grieser, R. R. Dagastine, and D. Y. C. Chan. Dynamic interaction between microbubbles in water. *P. Natl. A. Sci. USA*, 107:11177–11182, 2010. doi: doi.org/10.1073/pnas.1005937107.

[105] Raymond Panneton. Acoustic critical depth and asymptotic absorption of dissipative fluids. *J. Acoust. Soc. Am.*, 145, 2019. doi: doi.org/10.1121/1.5107434.

[106] K. R. Atkins. Third and fourth sound in liquid helium II. *Phys. Rev.*, 113: 962–965, Feb 1959. doi: doi.org/10.1103/PhysRev.113.962.

[107] Zhenglong Chen, Ming Zhong, Yuzhou Luo, Linhong Deng, Zhaoyan Hu, and Yuanlin Song. Determination of rheology and surface tension of airway surface liquid: a review of clinical relevance and measurement techniques. *Respir. Res.*, 20:274, 2019. doi: doi.org/10.1186/s12931-019-1229-1.

[108] Amarin McDonnell, Ji hyun Lee, Eve Makrai, Leslie Y. Yeo, and Laura E. Downie. Tear film extensional viscosity is a novel potential biomarker of dry eye disease. *Invest. Ophth. Vis. Sci.*, 126(8):1196–1198, 2019. doi: doi.org/10.1016/j.ophtha.2019.03.014.

[109] Nuri Erdem Ersoy and Morteza Eslamian. Phenomenological study and comparison of droplet impact dynamics on a dry surface, thin liquid film, liquid film and shallow pool. *Exp. Therm. Fluid Sci.*, 112:109977, 2020. doi: doi.org/10.1016/j.expthermflusci.2019.109977.

[110] Gian Luca Salvagno, Davide Demonte, Giovanni Poli, Emmanuel J. Favaloro, and Giuseppe Lippi. Impact of low volume citrate tubes on results of first-line hemostasis testing. *Int. J. Hematol.*, 41(4):472–477, 2019. doi: doi.org/10.1111/ijlh.13028.

[111] Dorothy M. Adcock, David C. Kressin, and Richard A. Marlar. Minimum specimen volume requirements for routine coagulation testing: Dependence on citrate concentration. *Am. J. Clin. Pathol.*, 109(5):595–599, 1998. doi: doi.org/10.1093/ajcp/109.5.595.

[112] Florian Geyer, Maria D'Acunzi, Azadeh Sharifi-Aghili, Alexander Saal, Nan Gao, Anke Kaltbeitzel, Tim-Frederik Sloot, Rüdiger Berger, Hans-Jürgen Butt, and Doris Vollmer. When and how self-cleaning of superhydrophobic surfaces works. *Sci. Adv.*, 6, 2020. doi: doi.org/10.1126/sciadv.aaw9727.

[113] William S. Y. Wong, Tomas P. Corrales, Abhinav Naga, Philipp Baumli, Anke Kaltbeitzel, Michael Kappl, Periklis Papadopoulos, Doris Vollmer, and Hans-Jürgen Butt. Microdroplet contaminants: When and why superamphiphobic surfaces are not self-cleaning. *ACS Nano.*, 14(4): 3836–3846, 2020. doi: doi.org/10.1021/acsnano.9b08211.

[114] Martin Wild. Introduction to special section on global dimming and brightening. *J. Geophys. Res.: Atmos.*, 115(10):4–1Y,2Y,3Y,4Y, 2010. doi: doi.org/10.1029/2009JD012841. Copyright Blackwell Publishing Ltd. 2010; Last updated - 2015-04-18.

[115] Monika Thakur. *Global Dimming and Global Warming: Dangerous Alliance*, pages 61–70. Springer International Publishing, Cham., 2018. doi: doi.org/10.1007/978-3-319-58415-7_5.

[116] David E. Tambe and Mukul M. Sharma. The effect of colloidal particles on fluid-fluid interfacial properties and emulsion stability. *Adv. Colloid Interface Sci.*, 52:1–63, 1994. doi: doi.org/10.1016/0001-8686(94)80039-1.

[117] Stephen Frazier, Xinyi Jiang, and Justin C. Burton. How to make a giant bubble. *Phys. Rev. Fluids.*, 5:013304, 2020. doi: doi.org/10.1103/PhysRevFluids.5.013304.

[118] Lucie Ducloué, Olivier Pitois, Julie Goyon, Xavier Chateau, and Guillaume Ovarlez. Rheological behaviour of suspensions of bubbles in yield stress fluids. *J. Non-Newton. Fluid*, 215:31–39, 2015. doi: doi.org/10.1016/j.jnnfm.2014.10.003.

[119] Peter Wilde, Alan Mackie, Fiona Husband, Patrick Gunning, and Victor Morris. Proteins and emulsifiers at liquid interfaces. *Adv. Colloid Interface Sci.*, 108-109:63 – 71, 2004. doi: doi.org/10.1016/j.cis.2003.10.011.

[120] M. V. Voinova, M. Rodahl, M. Jonson, and B. Kasemo. Viscoelastic acoustic response of layered polymer films at fluid-solid interfaces: Continuum mechanics approach. *Phys. Scr.*, 59(5):391, 1999. doi: doi.org/10.1238/physica.regular.059a00391.

[121] M.D. Tarn and N. Pamme. Microfluidics. In *Reference Module in Chemistry, Molecular Sciences and Chemical Engineering*. Elsevier, 2014. doi: doi.org/10.1016/B978-0-12-409547-2.05351-8.

[122] Francesca Bragheri, Rebeca Martinez Vazquez, and Roberto Osellame. Chapter 12.3 - microfluidics. In Tommaso Baldacchini, editor, *Three-Dimensional Microfabrication Using Two-photon Polymerization*, Micro and Nano Technologies, pages 310 – 334. William Andrew Publishing, Oxford, 2016. doi: doi.org/10.1016/B978-0-323-35321-2.00016-9.

[123] Maria Laura Coluccio, Gerardo Perozziello, Natalia Malara, Elvira Parrotta, Peng Zhang, Francesco Gentile, Tania Limongi, Pushparani Michael Raj, Gianni Cuda, Patrizio Candeloro, and Enzo Di Fabrizio. Microfluidic platforms for cell cultures and investigations. *Microelectron. Eng.*, 208:14 – 28, 2019. doi: doi.org/10.1016/j.mee.2019.01.004.